No time to waste manure

Citation for published version (APA):
van der Wal, M. (2025). *No time to waste manure: Membrane processes for nutrient separation from manure to increase circularity in tailored fertilization*. [Phd Thesis 1 (Research TU/e / Graduation TU/e), Chemical Engineering and Chemistry]. Eindhoven University of Technology.

Document status and date:
Published: 05/06/2025

Document Version:
Publisher’s PDF, also known as Version of Record (includes final page, issue and volume numbers)

Please check the document version of this publication:

• A submitted manuscript is the version of the article upon submission and before peer-review. There can be important differences between the submitted version and the official published version of record. People interested in the research are advised to contact the author for the final version of the publication, or visit the DOI to the publisher's website.
• The final author version and the galley proof are versions of the publication after peer review.
• The final published version features the final layout of the paper including the volume, issue and page numbers.

Link to publication

General rights
Copyright and moral rights for the publications made accessible in the public portal are retained by the authors and/or other copyright owners and it is a condition of accessing publications that users recognise and abide by the legal requirements associated with these rights.

- Users may download and print one copy of any publication from the public portal for the purpose of private study or research.
- You may not further distribute the material or use it for any profit-making activity or commercial gain
- You may freely distribute the URL identifying the publication in the public portal.

If the publication is distributed under the terms of Article 25fa of the Dutch Copyright Act, indicated by the “Taverne” license above, please follow below link for the End User Agreement:

www.tue.nl/taverne

Take down policy
If you believe that this document breaches copyright please contact us at:

openaccess@tue.nl

providing details and we will investigate your claim.

Download date: 11. jun.. 2025

No time to waste manure

MEMBRANE PROCESSES FOR NUTRIENT SEPARATION FROM MANURE TO INCREASE CIRCULARITY IN TAILORED FERTILIZATION

Marrit van der Wal

PhD Thesis

No time to waste manure

Membrane processes for nutrient separation from manure to increase circularity in tailored fertilization

PROEFSCHRIFT

ter verkrijging van de graad van doctor aan de Technische Universiteit Eindhoven, op gezag van de rector magnificus prof. dr. S.K. Lenaerts, voor een commissie aangewezen door het College voor Promoties, in het openbaar te verdedigen op donderdag 5 juni 2025 om 16:00 uur

door

Marrit van der Wal

geboren te Workum

Dit proefschrift is goedgekeurd door de promotoren en de samenstelling van de promotiecommissie is als volgt:

voorzitter:	prof.dr. A.P.H.J. Schenning
promotoren:	prof.dr.ir. D.C. Nijmeijer dr.ing. Z. Borneman
leden:	prof.dr.ir. E. Meers (Universiteit Gent) prof.dr.ir. C.J.N. Buisman (Wageningen University) prof.dr.ir. R. Tuinier prof.dr.ir J. van der Schaaf
adviseur:	ir. R. van Lijssel (Darling Ingredients International)

Het onderzoek of ontwerp dat in dit proefschrift wordt beschreven is uitgevoerd in overeenstemming met de TU/e Gedragscode Wetenschapsbeoefening.

“Insanity is doing the same thing over and over again

but expecting different results”

- Albert Einstein

This research work was conducted in the Membrane Materials and Processes group at Eindhoven University of Technology, the Netherlands.

This research was part of the project “No Time to Waste” with project number ENPPS.LIFT.019.018 of the research program LIFT. This is (partly) financed by the Dutch Research Council (NWO), Darling ingredients International, Agrifirm, Friesland Campina, Van Drie Group, Agra-Matic B.V., De Heus Voeders B.V., ForFarmers Nederland B.V..

A catalogue record is available from the Eindhoven University of Technology Library

ISBN: 978-90-386-6373-9

Printing: proefschriftspecialist | www.proefschriftspecialist.nl

SUMMARY

Too much nitrogen is released into the air, water and soil in the Netherlands. This is harmful to nature, water and soil quality and biodiversity. Therefore, nitrogen emissions must be reduced. To achieve this, the European Union and Dutch government have set emission limits for agriculture, industry, construction, traffic and transport and are investing in nature restoration. While manure is a valuable source of nutrients for crops, it also poses significant environmental challenges, particularly in terms of nitrogen pollution. Untreated manure releases ammonia (NH_3) into the atmosphere, in addition, when manure is applied to land, excess nitrogen can be converted to ammonium (NH_4^+) and nitrates, which can leach into groundwater and surface waters, leading to eutrophication. The constraints in the agricultural sector are to reduce the environmental impact but this will also result in a significant increase in manure excess over the years, increasing the need for a more efficient and sustainable manure treatment. A manure or digestate treatment plant consists of a solid-liquid separation followed by a polishing step of the solid and liquid fractions, resulting in nutrient-rich streams suitable for tailored fertilization increasing circularity. **Chapter 1** provides information on the origin of manure surpluses and treatment options.

In **Chapter 2**, the flocculation in the solid-liquid separation is studied. Here, the effect of the molecular weight, charge density and branching of reference and commercially available flocculants is investigated by establishing the optimal flocculant dosage and the corresponding maximum organic matter removal. Higher molecular weight flocculants show increased turbidity removal as a result of their long chains corresponding to a higher amount of amide groups and thus adsorption sites. The results presented that polymers with increased cationic charge density values give a moderate and unstable flocculation trend due to unfavorable repulsion between the partially bridged particles. Moreover, a linear high molecular weight flocculant with a nonionic or a low anionic charge density is most effective as it reached the highest organic matter removal at a low dosage.

Chapter 3 focusses on the separation of N and K in the liquid fraction of manure digestate. In this stream, N is present as NH_4^+, which is challenging to separate from K^+ with reverse osmosis (RO) due to their very identical size and charge.

The chapter shows that with smart tuning of the pH to control the NH_3/NH_4^+ equilibrium, nanofiltration (NF) and RO membranes can be used to produce dedicated N and K-rich streams for tailored fertilization as at increased pH, the NH_3/NH_4^+ equilibrium shifts towards neutral NH_3 that permeates much more easy through the membrane than the positively charged NH_4^+ and K^+ ions. Experiments with both artificial NH_4Cl/KCl mixtures as well as real digestate and four different membrane types, ranging from open NF to sea water RO were performed. At neutral pH, none of the membranes showed N/K selectivity, not for single components nor for mixtures. However, when the pH was increased towards alkaline environment, distinct selectivity for N/K was indeed obtained both with model solutions and real digestate. The highest selectivity was reached at pH 12. However, a pH of 10 with >80% of the total ammonia present as NH_3 giving an N/K selectivity of 35 (at a pressure of 20 bar and cross flow velocity of 1.5 m/s) is preferred to guarantee long-term stable membrane operation. Here, the RO membrane for brackish water is the most suitable to separate NH_3 from K^+. The separation is then followed by neutralization of the N-rich permeate to a pH of 6 to allow subsequent concentration of the N fraction. The presented dynamic pH approach proofs that in a two-step RO system both N, and K-enriched fertilizers can be produced from real digestate.

In **Chapter 4**, a promising membrane modification is studied as strategy to enhance the separation of N and K. A three-step modification approach of an ultrafiltration (UF) polyacrylonitrile (PAN) membrane support is investigated to establish ion specific separation. Hydrolysis of the PAN membrane support introduces charged carboxylic acid groups enabling Donnan exclusion with a significant decrease in water flux due to pore swelling. The subsequently applied polyelectrolyte multilayers add size exclusion to the Donnan-exclusion by pore-coverage increasing the retention of monovalent and multivalent ions. This size exclusion can be further enhanced by crosslinking although at some expense of the water flux through the rigid polymer network. The NH_4^+/K^+ separation benefits from this, despite the NH_4^+ and K^+ ions having a similar native size and charge, they differ in dehydration energy. This difference in dehydration energy results in a difference in mobility and thus permeation selectivity through the crosslinked polyelectrolyte layers on the hydrolyzed membranes. Next, the separation of these nutrients can be further improved by increasing the pH of the manure digestate as described in the previous chapter.

Chapter 5 focusses on the on-site production of the required base and acid for the conversion of NH_4^+ and NH_3 for separation and concentration with RO. The chapter investigates the potential of OH^- and H^+ production with in-situ by bipolar membranes, known for their high water dissociation rate. The process becomes more sustainable by saving on transportation, storage and dilution by adding aqueous alkali and acid. For system validation, first a water dissociation experiment was performed in a membrane stack with three compartments fed with a NaCl solution. Follow-up experiments were done with artificial model solutions and co-digested manure digestate. It was found that the NaCl feed and the artificial feed stream showed similar performance for both the OH^- and H^+ production. On the other hand, the real co-digested manure showed an effective OH^- production for the conversion of NH_4^+ to NH_3, which was half of the effective production in the acid compartment. This lower efficiency in the base compartment is due to the presence of other OH^- consuming components in the manure digestate. The surplus in H^+ production can be used as acid for other processes in the manure treatment.

Chapter 6 reflects the results and shows how the research findings of flocculation, nutrient separation at alkaline conditions with RO and bipolar membrane base and acid production can be implemented in existing manure treatment plants and provide insights on economic aspects. Moreover, the chapter provides insights into future research directions. The major goal of manure treatment is to realize circular tailored fertilization using separate nutrient rich streams originating from manure. Hence, the future research directions focusses on improvements to produce these fractions within the scope of the research shown in this dissertation like the removal of phosphate into the solid fraction and additional tuning of the acid-base equilibrium of ammonium.

SAMENVATTING

Te veel stikstof wordt vrijgegeven in de lucht, het water en de bodem in Nederland. Dit is schadelijk voor de natuur, water- en bodemkwaliteit en biodiversiteit. Daarom moeten de stikstofemissies worden verminderd. Om dit te bereiken, hebben de Europese Unie en de Nederlandse overheid emissiegrenzen vastgesteld voor de landbouw, industrie, bouw, verkeer en transport en investeren ze in natuurherstel. Hoewel mest een waardevolle bron van nutriënten is voor gewassen, brengt het ook aanzienlijke milieuproblemen met zich mee, vooral op het gebied van stikstofvervuiling. Onbehandelde mest stoot ammoniak (NH_3) uit in de atmosfeer. Bovendien kan overtollige stikstof, wanneer mest op het land wordt aangebracht, worden omgezet in ammonium (NH_4^+) en nitraten, die in het grondwater en oppervlaktewater kunnen uitspoelen, wat leidt tot eutrofiëring. De restricties in de landbouwsector zijn er om de milieueffecten te verminderen, maar dit zal ook resulteren in een aanzienlijke toename van het mestoverschot in de loop der jaren, waardoor de behoefte aan een efficiëntere en duurzamere mestbehandeling toeneemt. Een mest- of digestaatbehandelingsinstallatie bestaat uit een vast-vloeistofscheiding, gevolgd door een polijststap voor de vaste en vloeibare fracties, resulterend in nutriëntenrijke stromen die geschikt zijn voor bemesting op maat om de circulariteit te vergroten. **Hoofdstuk 1** geeft informatie over de oorsprong van mestoverschotten en behandelingsopties.

In **Hoofdstuk 2** wordt de flocculatie in de vast-vloeistofscheiding bestudeerd. Hier wordt het effect van het molecuulgewicht, de ladingsdichtheid en vertakking van referentie- en commercieel beschikbare flocculanten onderzocht door de optimale flocculantdosis en de bijbehorende maximale verwijdering van organisch materiaal vast te stellen. Flocculanten met een hoger molecuulgewicht laten een verhoogde troebelheidsverwijdering zien als gevolg van hun lange ketens met daardoor een groter aantal amidegroepen en dus adsorptieplaatsen. De resultaten toonden aan dat polymeren met verhoogde kationische ladingsdichtheidswaarden een matige en onstabiele flocculatietrend vertonen vanwege ongunstige afstoting tussen de gedeeltelijk gelinkte deeltjes. Bovendien is een lineaire flocculant met een hoog molecuulgewicht en een niet-ionische of lage anionische ladingsdichtheid het meest effectief, gezien het de hoogste verwijdering van organisch materiaal bereikte bij een lage dosering.

Hoofdstuk 3 richt zich op de scheiding van N en K in de vloeibare fractie van mestdigestaat. In deze stroom is N aanwezig als NH_4^+, wat moeilijk te scheiden is van K^+ met omgekeerde osmose (RO) vanwege hun zeer identieke grootte en lading. Het hoofdstuk toont aan dat met afstemming van de pH om het NH_3/NH_4^+ evenwicht te regelen, nanofiltratie (NF) en RO-membranen kunnen worden gebruikt om toegewijde N- en K-rijke stromen te produceren voor bemesting op maat, aangezien bij verhoogde pH het NH_3/NH_4^+ evenwicht verschuift naar neutrale NH_3 dat veel gemakkelijker door het membraan kan doordringen dan de positief geladen NH_4^+ en K^+ ionen. Experimenten met zowel kunstmatige NH_4Cl/KCl mengsels als echte digestaat en vier verschillende membraantypes, variërend van open NF tot zeewater RO, werden uitgevoerd. Bij neutrale pH vertoonde geen van de membranen N/K selectiviteit, voor zowel de kunstmatige oplossing als echte digestaat. Echter, wanneer de pH werd verhoogd naar een alkalische waardes, werd er inderdaad een duidelijke selectiviteit voor N/K verkregen, zowel met kunstmatige oplossingen als echte digestaat. De hoogste selectiviteit werd bereikt bij pH 12. Echter, een pH van 10 met >80% van de totale ammoniak aanwezig als NH_3, wat een N/K selectiviteit van 35 geeft (bij een druk van 20 bar en een stroomsnelheid van 1.5 m/s), heeft de voorkeur om een langdurige stabiele membraanwerking te garanderen. Het RO-membraan voor brak water is het meest geschikt om NH_3 van K^+ te scheiden. De scheiding kan vervolgens worden gevolgd door neutralisatie van het N-rijke permeaat naar een pH van 6 om de concentratie van de N-fractie mogelijk te maken. De gepresenteerde dynamische pH-benadering bewijst dat in een twee staps RO-systeem zowel N- als K-rijke meststoffen kunnen worden geproduceerd uit echte digestaat.

In **Hoofdstuk 4** wordt een veelbelovende membraanmodificatie bestudeerd als strategie om de scheiding van N en K te verbeteren. Een drie staps modificatiebenadering van een ultrafiltratie (UF) polyacrylonitril (PAN) membraansupport wordt onderzocht om ion-specifieke scheiding te realiseren. Hydrolyse van de PAN-membraansupport introduceert geladen carboxylzuur-groepen die Donnan-uitsluiting mogelijk maken met een significante afname van de waterflux als gevolg van poriezwelling. De daaropvolgende aangebrachte polyelektrolyt-multilagen voegen grootte-uitsluiting toe aan de Donnan-uitsluiting door poriebedekking, waardoor de retentie van monovalente en multivalente ionen toeneemt. Deze grootte-uitsluiting kan verder worden verbeterd door crosslinking, hoewel dit ten koste gaat van de waterflux door het rigide polymeernetwerk. De NH_4^+/K^+ scheiding profiteert hiervan, ondanks dat de NH_4^+ en K^+ ionen vergelijkbare grootte en lading hebben, verschillen ze namelijk in dehydratie-energie. Dit verschil in dehydratie-energie resulteert in een verschil in mobiliteit en dus permeatieselectiviteit door de gecrosslinkte polyelektrolyt-lagen op de gehydrolyseerde membranen. Vervolgens kan de scheiding van deze nutriënten verder worden verbeterd door de pH van het mestdigestaat te verhogen zoals beschreven in het vorige hoofdstuk.

Hoofdstuk 5 richt zich op de productie van de benodigde base en zuur op locatie voor de omzetting van NH_4^+ en NH_3 voor scheiding en concentratie met RO. Het hoofdstuk onderzoekt de potentie van OH^- en H^+ productie in-situ met bipolaire membranen, bekend om hun hoge waterdissociatiesnelheid. Het proces wordt duurzamer door te besparen op transport, opslag en verdunning door toevoeging van waterige base en zuur. Voor systeemvalidatie werd eerst een waterdissociatie-experiment uitgevoerd in een membraanstack met drie compartimenten gevoed met een NaCl-oplossing. Vervolgexperimenten werden uitgevoerd met kunstmatige modeloplossingen en co-vergiste mestdigestaat. Het bleek dat de NaCl-voeding en de kunstmatige voedingsstroom vergelijkbare prestaties vertoonden voor zowel de OH^- als H^+ productie. Aan de andere kant toonde de echte co-vergiste mest een gehalveerde effectieve OH^- productie voor de omzetting van NH_4^+ naar NH_3 in vergelijk met de effectieve productie in het zuurcompartiment. Deze lagere efficiëntie van het basecompartiment is te wijten aan de aanwezigheid van andere OH^- consumerende componenten in mestdigestaat. Het overschot aan H^+ productie kan worden gebruikt als zuur voor andere processen in de mestbehandeling.

Hoofdstuk 6 reflecteert op de resultaten en toont hoe de onderzoeksresultaten van flocculatie, nutriëntenscheiding bij alkalische omstandigheden met RO en bipolaire membraan base- en zuurproductie kunnen worden geïmplementeerd in bestaande mestbehandelingsinstallaties en geeft inzichten in economische aspecten. Daarnaast geeft het hoofdstuk inzichten in toekomstige onderzoeks-richtingen. Het belangrijkste doel van mestbehandeling is om circulaire bemesting op maat te realiseren met behulp van afzonderlijke nutriëntenrijke stromen afkomstig van mest. Daarom ligt de focus op verbeteringen in de productie van deze fracties binnen de scope van het onderzoek zoals getoond in dit proefschrift, zoals de verwijdering van fosfaat naar de vaste fractie en extra afstemming van het zuur-base evenwicht van ammonium.

TABLE OF CONTENTS

CHAPTER 1

Introduction

1.1 Dutch agriculture

The growing human population is ever increasing the footprint on planet earth. The emissions from the human needs pollute the atmosphere. This pollution originates from greenhouse gas emissions from energy production, industry, transport, waste management and agriculture of which the majority of greenhouse gas emissions, in terms of CO_2 equivalents, originate from energy production. Agriculture is responsible for approximately 11% of the total greenhouse gas emissions, in CO_2 equivalents, of which the agricultural sector produces the majority of the overall emitted methane and nitrogen oxides [1]. Moreover, the increasing population and thus growing food needs have resulted in depleting nutrient sources [2]. Hence, to lower our impact on earth, all aforementioned sectors have to reduce their emissions and changes towards more circular approaches are crucial. For example, recently, the government has been ordered in the lawsuit between the government and Greenpeace to hasten the reduction of nitrogen emissions to reach the goals set for 2030 [3]. Important steps towards a more sustainable agriculture have been made in the past years. In the Netherlands, 90% of the for agriculture available land is in use. Only 6% of this land is used for horticulture whereas the majority is used for livestock [4]. This correlates to the high livestock density in the Netherlands when compared to other European countries. Fig. 1.1 shows that almost all provinces in the Netherlands have more than 1.4 unit of livestock per utilized agricultural land [5]. Hence, it is not surprising that the Netherlands is the second largest agri-food exporter in the world after the US [6].

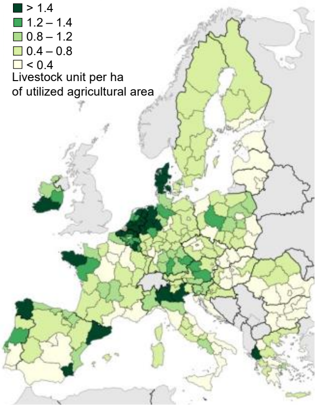

Fig. 1.1: Livestock density in Europe presented as livestock unit per hectare of utilized agricultural area [5].

A significant part of the exports come from livestock. The majority of the livestock in the Netherlands consists of poultry followed by swine and cattle, as shown in Fig. 1.2a [7]. This large number of livestock produces also a large amount of manure. For example, one cow produces 29 kg of manure per day and one chicken produces 0.08 kg [8]. Overall, 74.6 million tons of manure were produced in the Netherlands in 2023 [9]. Fig. 1.2b shows that cattle has the largest contribution to the manure production followed by pigs and chickens, based on the number of animals and their respective manure production.

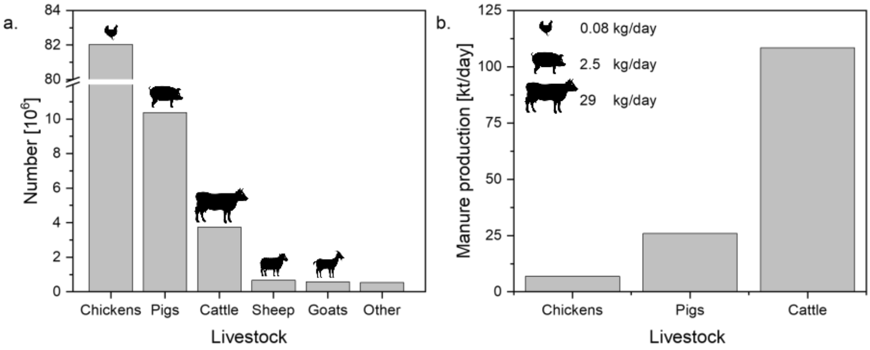

Fig. 1.2: a. The number of animals per livestock type in December 2023 in the Netherlands [7]. b. The daily manure production of each livestock type [8].

Even though manure contains multiple valuable components, it also causes environmental issues. One of the main issues is the emission of methane and nitrogen oxides that contribute to our overall greenhouse gas emissions. Moreover, the emission of ammonia results in deposition of nutrients in vulnerable areas. These emissions occur in stables, during storage and spreading of manure on land as fertilizer [10]. Over the years, much research has been conducted on how to reduce these emissions. For example, emission-reduced stables, short term storage before processing and improved spreading techniques [10]. Nevertheless, the spreading of manure leads to more environmental issues next to emissions. The nutrients phosphate and nitrate tend to leach into the surface water resulting in eutrophication [10]. Eutrophication induces a chain reaction and is followed by the excessive growth of simple organisms like algae due to a high amount of nutrients that subsequently leads to depletion of oxygen and thus death of organisms in water bodies. Hence, the European union and the Dutch government aim to reduce emissions and nutrient leaching to improve climate and environment.

1.1.1 *Manure management*

Following from the high emissions and leaching, the European union and Dutch government implemented constraints in the agricultural sector. These constraints follow from several frameworks, mainly concerning nitrogen emissions, like the well-known nitrates directive [11]. The Dutch government introduced several laws regarding livestock and manure management as well. This starts with the management of livestock numbers per business, for example via phosphate rights [12]. The limitation in livestock number should ensure that the manure production stays below the established production ceilings. These ceilings limit the production of phosphate and nitrogen from manure, where the Dutch phosphate ceiling is 172.9 million kg per year and for nitrogen 504.4 million kg per year. The production of these nutrients is distributed between the different livestock types resulting in specific ceilings for dairy cattle, pigs and poultry as shown in Fig. 1.3 [12]. However, in 2025 these ceilings are lowered by 10% [13].

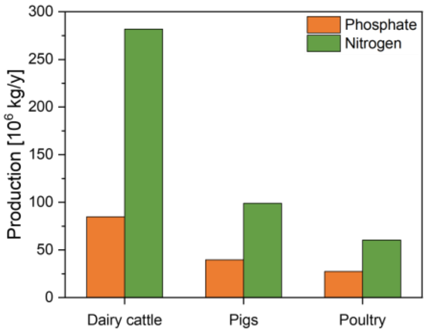

Fig. 1.3: The production ceiling of phosphate and nitrogen in 10^6 kg per year for dairy cattle, pigs and poultry [12].

Next to the aim to reduce manure production, the government asks for nitrogen emission reductions. Where in some regions the aimed reduction is below 12% in other regions, a very significant reduction of over 95% is needed, as shown in Fig. 1.4. The more pressing areas that require a significant reduction are the so-called Natura-2000 areas, areas that are based on the 1979 Birds directive, and are considered vulnerable to high nitrogen emissions [14], [15]. As mentioned before, this reduction should predominantly be reached by lowering the livestock number, improved stable design and fertilization limitations [16].

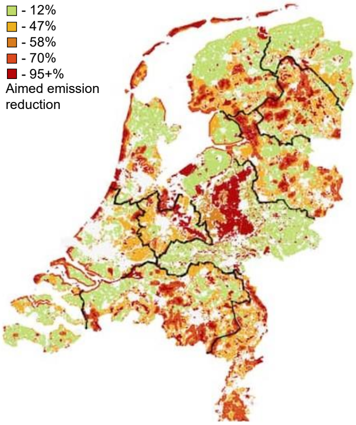

Fig. 1.4: Aimed nitrogen reduction per region in the Netherlands [17].

The emission reduction from agriculture is partially reached by fertilization limitations reducing emission and nutrient leaching into the water bodies. The use of manure for fertilization is restricted by a prohibition of application during certain periods. Moreover, application/spreading methods are improved over the years to ensure limited emissions [16]. Since 2024, the so-called buffer regions are implemented where fertilization is prohibited within 5 meters from the water body [18]. In addition, Dutch legislation limits the amount of nutrients from manure and fertilizer that can be applied on different types of land based on the 1991 European nitrogen directive. For phosphate the amount from manure and/or fertilizers is limited to 75 kg/ha for grassland and 40 kg/ha for other farmland. On the other hand, for nitrogen a distinction is made between fertilization with manure and artificial fertilizer. A maximum of 170 kg of nitrogen per hectare can originate from manure whereas an additional amount of nitrogen from fertilizer depends on the crop, the harvest, ecology and the surrounding water. Moreover, the derogation rule provided some farmers with the opportunity to surpass the 170 kg nitrogen per hectare in cases where there was no imminent effect on the environment. However, this derogation rule will be diminished over time starting in 2024 [19]. This will result in a significant increase in manure excess over the years starting with an excess of approximately 25 million tons of manure in 2026 [20]. This excess manure must be exported or treated. Hence, in the coming years the necessity for efficient and sustainable manure treatment will grow.

1.2 Manure treatment

Over the past years, manure treatment has grown as a result of the aforementioned restrictions and thus growing manure excess. The main focus has been to recover resources like bioenergy and nutrients from manure, whereas the treatment also has potential for the reduction of the environmental impact [21]. Various manure management systems are in use nowadays that are either on-farm or centralized. The choice between on-farm or centralization requires various considerations like the type of manure, arable land availability, scale, transportation, use of potential products and social variables like the compliance of farmers [22].

Different processes can be considered for manure treatment. These processes can be biological, chemical or mechanical, all contributing to energy, nutrient and water recovery to different extents. A current treatment plant typically consists of solid-liquid separation of manure or manure digestate followed by eventual polishing of the solid and liquid fractions resulting in nutrient recovery [23], [24]. An overview of treatment processes is shown in Fig. 1.5.

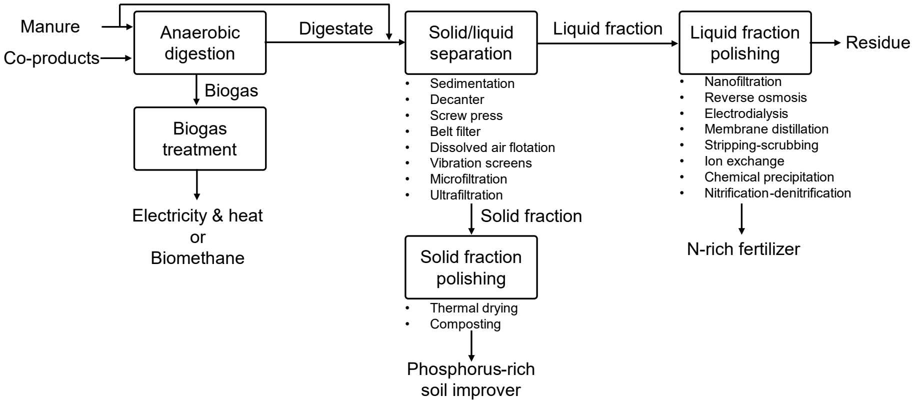

Fig. 1.5: A schematic overview of a manure treatment process with several options showing different products that can be produced [23], [24].

1.2.1 Biogas production

Anaerobic digestion is one of the biological processes often encountered in a manure treatment process to produce biogas that can be converted into either energy and heat or into biomethane. In this process a part of the organic matter is converted into biomethane in several steps. First, hydrolysis breaks down complex organic matter like cellulose, starch and proteins. The produced dissolved organic molecules are then broken down via acidogenesis into alcohols, volatile fatty acids, H_2 and CO_2. Next acetogenesis produces acetic acid whereas meanwhile in the last stage methanogenesis produces methane from the available H_2 and CO_2 [25]. This symbiotic biological system requires a specific temperature, pH and time and is highly impacted by toxic components present like NH_3 and H_2S. To improve the performance of the system several adaptations are possible. For example, co-digestion where next to manure, organic waste is added to the digestor in order to increase the carbon to nitrogen ratio to improve the nutrient balance for the bacteria and limit the production of NH_3 and increase in pH [25], [26]. Also, additives like iron can be added to reduce the amount of toxic H_2S [27]. The use of co-products, additives and the overall performance of the bacteria leads to the production of complex digestate streams. The complexity in terms of content, species and their concentrations can result in the requirement of additional or different treatment process steps to reach suitable products from digestate.

1.2.2 Solid-liquid separation

The digestate stream produced in the anaerobic digestion is a source of valuable nutrients and organic matter, similar to manure, which can be valorized with additional treatment steps [28]. The solid content and type of solids present in the digestate are important for the solid-liquid separation step that typically follows as first treatment step. This step often consists of more than one step starting with the removal of the course materials. This can be done with a relatively simple sedimentation process or with mechanical systems like a sieve belt, decanter or screw press. Additional steps are often installed to remove the smaller particles that are left behind in the liquid stream. For this, processes like dissolved air flotation (DAF), a drum filter, filter paper or ultrafiltration can be used. All steps either employing gravity, centrifugal or mechanical driving forces for separation [23], [29]. To improve these processes, additives are often used to increase both weight and size of the particles to enhance separation. Such additives are either coagulants like metal salts or polymer-based flocculants like polyacrylamide. The use of coagulants and flocculants requires precise dosing as too little of the additives does not provide adequate removal whereas too much can lead to lower agglomeration efficiencies and processing problems later in the treatment system [23], [30]. For example, processes like reverse osmosis (RO) suffer from dissolved polymers as these foul the membrane surface. Moreover, the type of coagulant or flocculant most suitable can change with, for example different co-products added for biogas production [23], [31]. Hence, monitoring of the additive performance is essential for optimal treatment and safekeeping of additional treatment steps.

1.2.2.1 Flocculation

Flocculation is used to enhance the removal of solids during treatment steps by the formation of agglomerates with flocculants. These flocculants are typically long polymers with molecular weights ranging between a thousand and millions g/mol that can eventually also have positively or negatively charged groups [32], [33]. Depending on their affinity and their length they interact with the solid material present via electrostatic, hydrogen and/or hydrophobic interactions [32]. Overall, the addition of flocculants results in agglomerates either by forcing particles together by altering the attraction and repulsion between the particles or by actively binding particles [33]. Finding the most suitable polymer and dosage requires experimental determination to improve large scale usage of flocculation [30].

So far, research regarding the use of flocculants for manure digestate is limited. Hjorth has extensively studied the effect of the typical flocculant polymer polyacrylamide and investigated the effect of charge and polymer structure on the removal of solids from manure [30], [34]. Moreover, an extensive literature review showed the effect of coagulants, flocculants and the combination of both for manure slurries [35]. Vanotti et al. and Riaño and García-González et al. showed the use of PAM as flocculant on large scale for enhancement of solid-liquid separation of manure streams [36], [37]. Also, some flocculation performance studies were performed for manure digestate. Luo et al. showed that several combinations of polyacrylamide with coagulants can lead to superior removal of solids [38]. Similarly, Salud Camilleri-Rumbau et al. showed the improvement from flocculation combined with coagulation on the performance of membranes in terms of reducing fouling on tubular ultrafiltration membranes [39]. Nevertheless, these studies provide little information regarding the range of charge and the optimal dosage for especially manure digestate, which has a different composition in comparison to manure.

1.2.3 Nutrient recovery from liquid fraction

The liquid fraction produced in the solid-liquid separation step contains valuable nutrients like nitrogen (N) and potassium (K) [23], [31]. This liquid fraction is often polished to ensure a high-quality stream suitable for fertilization. There are several treatment options used for this step like RO, stripping-scrubbing, struvite production, electrochemical treatment and biological processes like nitrification-denitrification [23]. Depending on the goal of the polishing step, nutrients can either be recovered or removed. For example, nitrification-denitrification is applied to remove N as this nutrient results in emissions of ammonia and nitrogen oxides and is therefore a limiting factor for disposal [40]. However, N is also a valuable nutrient that is currently partially applied on land as artificial fertilizer. These artificial N fertilizers are typically produced with the Haber-Bosch process that produces ammonium salts from the N in the air using large amounts of (fossil-based) energy while simultaneously emitting significant amounts of carbon dioxide [41]. Hence, a more sustainable, circular approach is the use of the N-rich concentrate obtained from manure treatment as fertilizer. Unfortunately, there are strict regulations for the production of manure-based fertilizers that are allowed for use on land [31]. However, legislation is currently under development to allow the so-called Renure, REcovered Nitrogen from manURE, products for the replacement of artificial fertilizers up to a certain amount [24]. The Renure legislation allows only RO, stripping-scrubbing and struvite precipitation for the production of such nutrient-rich products. Renure products have to meet certain criteria as presented in Table 1.1 to ensure safe application on land [42].

Table 1.1: Final product criteria for manure-based fertilizers Renure [42].

Category	Criteria
Technology	Physical, chemical and/or biological process step
Nitrogen ratio	Nitrogen: Total Nitrogen ≥90% or
	Total Organic Carbon: Total Nitrogen ≤3
	Corrected for N not originating from manure
Metals	Cu ≤300 mg / kg dry matter
	Zn ≤800 mg / kg dry matter
Micro-organisms	Salmonella spp. 0 colony forming units (CFU) in 25 ml
	Escherichia coli or Enterococcaceae ≤1 000 CFU in 1 ml

RO is a relevant technology for large scale (centralized) treatment as it allows the recovery of water next to the production of a concentrated mineral stream containing N and K. Stripping-scrubbing, an alternative approach for N-removal from manure in the form of ammonium sulphate or ammonium nitrate, is more suitable for small scale (on-farm) treatment as in that case, water is not removed from the treated liquid fraction increasing product volumes and with that transportation costs [22], [23], [43]. The production of struvite,

$MgNH_4PO_4 \cdot 6H_2O$, provides challenges in terms of the quality of the final product due to the presence of for example heavy metals making this option less interesting for immediate application on large scale [40].

1.2.3.1 *Reverse osmosis in manure treatment*

RO is a membrane process already extensively used in manure treatment for the recovery of clean water, as in RO even small ions like the nutrients NH_4^+ and K^+ are retained in the so-called mineral concentrate [44], [45]. This rejection stems from the relatively dense selective layer of the membrane. As this layer has a relatively high resistance to permeation, combined with the high osmotic pressures of the feed solutions, RO operates at high pressures when compared to other available membrane techniques like micro-, ultra- and nanofiltration as shown in Fig. 1.6 [46], [47]. Depending on the type of membrane, the application and the specific stream to be treated pressures up to 80 - 100 bar are employed [46], [47].

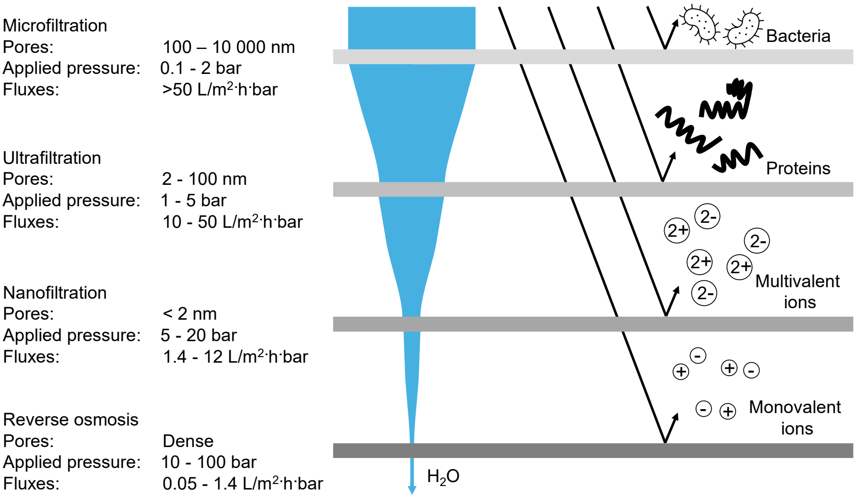

Fig. 1.6: Schematic overview of different membrane techniques indicating their pore size, applied pressure, flux and species typically retained [46], [47].

In manure treatment, micro- and ultrafiltration are sometimes used for, for example, as pre-treatment steps for RO to lower the presence of organic matter to reduce the fouling tendency of the solution [23], [45]. The larger pores present in the selective layer of these membranes provide a higher water flux at lower pressures while retaining for example organic matter, bacteria, proteins and suspended solids while ions like ammonium and potassium permeate [46],

[47]. Also nanofiltration can be used for manure treatment, however, the monovalent salt rejection of nanofiltration membranes is low in comparison to RO due to the more open selective layer, resulting in a permeate stream contaminated with monovalent ions, which thus does not allow direct discharge to surface water [23], [45], [48]. The rejection of these types of membranes originates from several exclusion mechanisms providing selectivity by differences in size and/or charge. Exclusion by size plays a crucial role in the rejection achieved with porous membranes: solutes with a larger size than the pore size of the membrane are retained and solutes with a smaller are sterically hindered [46], [47], [49]. The exclusion by charge originates from electrostatic repulsion or Donnan exclusion between the fixed charges of the membrane and similarly charged species (co-ions) in the feed solution. Salt retention occurs when the repulsive forces between the co-ion and membrane exceed the attractive forces between membrane charges and oppositely charged counter-ions as electroneutrality has to be maintained [46], [47], [49]. Moreover, also dielectric exclusion contributes to retention and is caused by the presence of a solvation energy barrier due to the difference in dielectric constant of the bulk solution and the solvent in the membrane resulting in a difference in permeation resistance depending on the dehydration energy of the ion [49], [50]. However, the use of membrane technology for manure treatment has as drawback that severe fouling occurs over time due to the presence of organic matter and scaling components [23]. Hence, often alkaline, acidic and surfactant containing solutions are used to restore the performance of the membranes [46], [47], although compromising membrane lifetime. Nowadays, the production of base and acid can be achieved simultaneously with so-called bipolar membranes which reach several million times faster water dissociation rates compared to dissociation in aqueous solutions [51]. The bipolar membranes show potential in electrodialysis systems for integrated production of base and acid for amongst the recovery of ammonium [52]–[56].

Mainly RO is applied for the concentration of N and K to produce a mineral concentrate, this concentrate can serve as green N-K fertilizer substitute for artificial fertilizer, while clean water is recovered reducing transport and storage costs [24], [45], [57]–[60]. Over the past years several studies have shown the potential of RO for the production of a mineral concentrate on large scale [29], [31], [61], [62]. However, the production of separate concentrated N and K streams is a prerequisite for true circular processes and tailored fertilization [41], [63]. Zarebska et al. suggests the separation of N and K with nanofiltration at high pH as this converts ammonium to ammonia and thus enhances the permeation of ammonia while potassium ions are retained [23]. Masse et al. measured that at a high pH more N in the form of ammonia permeates the membrane confirming the potential to separate N from K at a high pH [64]. Overall, the manure treatment can be further improved to increase sustainability in terms of emission reduction by the formation of separate nutrient-rich fractions suitable to replace artificial fertilizers and thus increasing circularity.

1.3 Dissertation overview

The aim of this dissertation is to address several aspects in manure digestate treatment that led to an improvement in current processes used to valorize manure and increase circularity in the agricultural sector. In the previous sections the urgency of manure treatment is elaborated and the implementation of current manure treatment is discussed. It also indicated several aspects that require improvement like the flocculation in the solid-liquid separation, the urge to separate N from K to increase the value of the products and the necessity of base and acid on manure treatment plants. The chapters in this dissertation further investigate these treatment aspects in order to enhance the separation of nutrients into separate fractions to increase circularity in the agricultural sector.

In **Chapter 2**, flocculation in the solid-liquid separation pre-treatment process step for manure digestate is investigated. Different flocculants and dosages are systematically researched in order to get insights on the organic matter removal efficiency and thus into which flocculant type is most suitable for manure digestate and how the optimal dosage can be established further optimizing the solid-liquid separation.

Chapter 3 focusses on the separation of N and K with RO using commercial membranes. Here, the addition of base and acid is employed to tune the solution pH as tool to utilize the ammonium/ammonia equilibrium in order to enhance N permeation in the form of ammonia through the membrane while retaining potassium ions. This research focusses on both artificial and real liquid manure digestate and compares dead-end to crossflow filtration to determine the separation performance and efficiency.

Following the separation of N and K using commercial membranes, **Chapter 4** investigates the modification of membranes with the aim of further improving the N/K separation performance. In this chapter, an ultrafiltration polyacrylonitrile membrane is used as substrate for modification in three subsequent steps: hydrolysis, polyelectrolyte layer formation and crosslinking. The performance changes induced by the modification steps are monitored by investigating the retention of various salt solutions including artificial and real liquid manure digestate.

In **Chapter 5** the use of bipolar membrane electrodialysis for the on-site production of base and acid for N and K separation with RO is studied. This chapter investigates an integrated process consisting of a bipolar membrane electrodialysis (BMED) stack producing base and acid, which adjust the pH of the digestate solutions, integrated with N and K separation with RO as investigated in **Chapter 3**. The produced base creates an alkaline environment for the manure digestate stream to reach high amounts of ammonia permeating through the RO membrane, whereas the acid produced is used to concentrate the N in the permeate stream with a subsequent RO in the form of ammonium. In this approach, hydroxide ions and protons are released directly into the liquid manure digestate and the N-rich stream from the separation using artificial solutions and real liquid manure digestate reducing the addition of water with aqueous base and acid.

Chapter 6 provides the main conclusions of the dissertation and gives insights into the possible implementation. Moreover, it provides suggestions for future research directions.

1.4 References

[1] L. van der Net, N. Staats, P.W.H.G. Coenen, J.D. Rienstra, P.J. Zijlema, E.J.M.M. Arets, K. Baas, S.A. van Baren, R. Dröge, K. Geertjes, E. Honig, B. Huet, R.A.B. te Molder, J.A. Montefoort, T.C. van der Zee and M.C. van Zanten, “National Inventory Report 2024 - Greenhouse gas emissions in the Netherlands 1990-2022.” pp. 1–442, 2024.

[2] M.A. Sutton, A. Bleeker, C.M. Howard, M. Bekunda, B. Grizzetti, W. de Vries, H.J.M. Grinsven, Y.P. Abrol, T.K. Adhya, G. Billen, E.A. Davidson, A. Datta, R. Diaz, J.W. Erisman, X.J. Liu, O. Oenema, C. Palm, N. Raghuram, S. Reis, R.W. Scholz, T. Sims, H. Westhoek en F.S. Zhang, *Our Nutrient World: The challenge to produce more food and energy with less pollution*. 2013.

[3] NOS nieuws, “Greenpeace wint zaak tegen Staat, rechter dwingt kabinet meer haast te maken met stikstofaanpak,” Jan. 22, 2025.

[4] CBS, “Agriculture; crops, livestock and land use by general farm type, region,” 2024. https://www.cbs.nl/en-gb/figures/detail/80783eng#LandUseTotal_2, Accessed November 2024.

[5] Eurostat, “Agri-environmental indicator - livestock patterns,” 2024. https://ec.europa.eu/eurostat/statistics-explained/index.php?title=Agri-environmental_indicator_-_livestock_patterns#Livestock_density_at_EU_level_in_2020, Accessed November 2024.

[6] WUR, “State of Agriculture and Food: Stable trends in the agricultural sector,” 2022. https://www.wur.nl/en/research-results/research-institutes/economic-research/show-wecr/state-of-agriculture-and-food-stable-trends-in-the-agricultural-sector.htm, Accessed November 2024.

[7] CBS, “Livestock on agricultural holdings: reference date 1 April and 1 December,” 2024. https://www.cbs.nl/en-gb/figures/detail/84952ENG?dl=59C2E, Accessed November 2024.

[8] CBS, “Standardised calculation methods for animal manure and nutrients,” 2012.

[9] Ministerie van Landbouw Natuur en Voedselkwaliteit, “Rapportage

Nederlands mestbeleid 2023," 2024.

[10] O. Oenema *et al.*, "Nitrogen in current European policies," in *The European nitrogen assessment*, Cambridge University Press, 2011, pp. 62–81.

[11] European Commission, *COUNCIL DIRECTIVE of 12 December 1991 concerning the protection of waters against pollution caused by nitrates from agricultural sources*, no. 12 December 1991.

[12] Rijksoverheid, *Meststoffenwet*. The Netherlands, 2024.

[13] Staten-Generaal, *Wijziging van de Meststoffenwet in verband met de voorwaarden over de maximale mestproductie in de derogatiebeschikking 2022-2025 (Wet wijziging Meststoffenwet in verband met de maximale mestproductie)*. 2024, pp. 1–36.

[14] European Commission, *Council Directive of 2 April 1979 on the conservation of wild birds*. 2010.

[15] Ministerie van Landbouw Natuur en Voedselkwaliteit, "Startnotitie Nationaal Programma Landelijk Gebied," pp. 1–78, 2022.

[16] W. de Vries, L. Schulte-Uebbing, H. Kros, J.C. Voogd, and G. Louwagie, "Spatially explicit boundaries for agricultural nitrogen inputs in the European Union to meet air and water quality targets," *Sci. Total Environ.*, vol. 786, p. 147283, 2021, doi: 10.1016/j.scitotenv.2021.147283.

[17] L. van Beest, "De feiten op een rij: wat is stikstof eigenlijk, en wat is nou het probleem?," 2022.

[18] Rijksdienst voor ondernemend Nederland, "Bufferstroken 2024," 2024. https://www.rvo.nl/onderwerpen/bufferstroken-2024, Accessed November 2024.

[19] Rijksdienst voor ondernemend Nederland, "Derogatie," 2024. https://www.rvo.nl/onderwerpen/mest/derogatie, Accessed November 2024.

[20] J. Roefs and R. Van Noort, "Ontwikkeling stikstofbalans tot 2030 per provincie," 2024. [Online]. Available:

https://www.mestverwaarding.nl/storage/article/files/2024/06/667d4b7f6cc3f.pdf.

[21] C.J. Glover, A. McDonnell, K.S. Rollins, S.R. Hiibel, and P.K. Cornejo, “Assessing the environmental impact of resource recovery from dairy manure,” *J. Environ. Manage.*, vol. 330, no. January, p. 117150, 2023, doi: 10.1016/j.jenvman.2022.117150.

[22] X. Flotats, A. Bonmatí, B. Fernández, and A. Magrí, “Manure treatment technologies: On-farm versus centralized strategies. NE Spain as case study,” *Bioresour. Technol.*, vol. 100, no. 22, pp. 5519–5526, 2009, doi: 10.1016/j.biortech.2008.12.050.

[23] A. Zarebska, D. Romero Nieto, K.V. Christensen, L. Fjerbæk Søtoft, and B. Norddahl, “Ammonium fertilizers production from manure: A critical review,” *Crit. Rev. Environ. Sci. Technol.*, vol. 45, no. 14, pp. 1469–1521, 2015, doi: 10.1080/10643389.2014.955630.

[24] R. Vingerhoets, M. Spiller, O. Schoumans, S.E. Vlaeminck, J. Buysse, and E. Meers, “Economic potential for nutrient recovery from manure in the European union,” *Resour. Conserv. Recycl.*, vol. 215, no. May 2024, p. 108079, 2025, doi: 10.1016/j.resconrec.2024.108079.

[25] A. Jasińska, A. Grosser, and E. Meers, “Possibilities and Limitations of Anaerobic Co-Digestion of Animal Manure—A Critical Review,” *Energies*, vol. 16, no. 9, pp. 1–30, 2023, doi: 10.3390/en16093885.

[26] L.A. Akamine, R. Passini, S. Sousa, and A. Fernandes, “Anaerobic Co-Digestion of Cattle Manure and Brewer’s Residual Yeast : Process Stability and Methane and Hydrogen Sulfide Production,” 2023.

[27] M. Farghali, F.J. Andriamanohiarisoamanana, M.M. Ahmed, S. Kotb, Y. Yumamoto, M. Iwasaki, T. Yamashiro and K. Umetsu, “Prospects for biogas production and H_2S control from the anaerobic digestion of cattle manure : The influence of microscale waste iron powder and iron oxide nanoparticles,” *Waste Manag.*, vol. 101, pp. 141–149, 2020, doi: 10.1016/j.wasman.2019.10.003.

[28] R. Rodríguez-alegre, J. Zapata-jiménez, X. You, S. Sanchis, and J. García-montaño, “Science of the Total Environment Nutrient recovery and valorisation from pig slurry liquid fraction with membrane

technologies," vol. 874, no. December, 2023, doi: 10.1016/j.scitotenv.2023.162548.

[29] P. Hoeksma, F.E. de Buisonjé, and A.J.A. Aarnink, "Full-scale production of mineral concentrates from pig slurry using reverse osmosis," *9th Int. Livest. Environ. Symp.*, p. 6, 2012.

[30] M. Hjorth, M.L. Christensen, and P.V. Christensen, "Flocculation, coagulation, and precipitation of manure affecting three separation techniques," *Bioresour. Technol.*, vol. 99, no. 18, pp. 8598–8604, 2008, doi: 10.1016/j.biortech.2008.04.009.

[31] P. Hoeksma, H. Schmitt, H.P. Komleh, and P. Ehlert, "Composition of mineral concentrates," 2020. doi: https://doi.org/10.18174/541577.

[32] J. Gregory and S. Barany, "Adsorption and flocculation by polymers and polymer mixtures," *Adv. Colloid Interface Sci.*, vol. 169, no. 1, pp. 1–12, 2011, doi: 10.1016/j.cis.011.06.004.

[33] E.S. Tarleton and R. J. Wakeman, "Pretreatment of suspensions," *Solid/Liquid Sep.*, pp. 126–151, 2007, doi: 10.1016/b978-185617421-3/50003-1.

[34] M. Hjorth and B.U. Jørgensen, "Polymer flocculation mechanism in animal slurry established by charge neutralization," *Water Res.*, vol. 46, no. 4, pp. 1045–1051, 2011, doi: 10.1016/j.watres.2011.11.078.

[35] M. Hjorth, K.V. Christensen, M.L. Christensen, and S.G. Sommer, "Solid-liquid separation of animal slurry in theory and practice," *Sustain. Agric.*, vol. 2, pp. 953–986, 2009, doi: 10.1007/978-94-007-0394-0_43.

[36] M.B. Vanotti, A.A. Szogi, P.G. Hunt, P.D. Millner, and F.J. Humenik, "Development of environmentally superior treatment system to replace anaerobic swine lagoons in the USA," *Bioresour. Technol.*, vol. 98, no. 17, pp. 3184–3194, 2007, doi: 10.1016/j.biortech.2006.07.009.

[37] B. Riaño and M.C. García-González, "On-farm treatment of swine manure based on solid-liquid separation and biological nitrification-denitrification of the liquid fraction," *J. Environ. Manage.*, vol. 132, pp. 87–93, 2014, doi: 10.1016/j.jenvman.2013.10.014.

[38] H. Luo, T. Lyu, A. Muhmood, Y. Xue, H. Wu, E. Meers, R. Dong and S.

Wu, “Effect of flocculation pre-treatment on membrane nutrient recovery of digested chicken slurry: Mitigating suspended solids and retaining nutrients,” *Chem. Eng. J.*, vol. 352, no. July, pp. 855–862, 2018, doi: 10.1016/j.cej.2018.07.097.

[39] M.S. Camilleri-Rumbau *et al.*, “Ultrafiltration of separated digestate by tubular membranes: Influence of feed pretreatment on hydraulic performance and heavy metals removal,” *J. Environ. Manage.*, vol. 250, no. August, p. 109404, 2019, doi: 10.1016/j.jenvman.2019.109404.

[40] B. Pandey and L. Chen, “Technologies to recover nitrogen from livestock manure - A review,” *Sci. Total Environ.*, vol. 784, p. 147098, 2021, doi: 10.1016/j.scitotenv.2021.147098.

[41] C. Vaneeckhaute, E. Meers, E. Michels, J. Buysse, and F. M. G. Tack, “Ecological and economic benefits of the application of bio-based mineral fertilizers in modern agriculture,” *Biomass and Bioenergy*, vol. 49, pp. 239–248, 2013, doi: 10.1016/j.biombioe.2012.12.036.

[42] European Comission, *Annex to the comission directive amending council directive 91/676/EEC as regards the use of certain fertilising materials from livestock manure*. 2024.

[43] J. Bousek, D. Scroccaro, J. Sima, N. Weissenbacher, and W. Fuchs, “Bioresource Technology Influence of the gas composition on the efficiency of ammonia stripping of biogas digestate,” *Bioresour. Technol.*, vol. 203, pp. 259–266, 2016, doi: 10.1016/j.biortech.2015.12.046.

[44] P. Hoeksma and F.E. de Buisonjé, “Production of mineral concentrates from animal manure using reverse osmosis Monitoring of pilot plants in 2012-2014,” 2015, [Online]. Available: www.wageningenUR.nl/livestockresearch.

[45] L. Masse, D.I. Massé, and Y. Pellerin, “The use of membranes for the treatment of manure: a critical literature review,” *Biosyst. Eng.*, vol. 98, no. 4, pp. 371–380, 2007, doi: 10.1016/j.biosystemseng.2007.09.003.

[46] R.W. Baker, *MEMBRANE TECHNOLOGY*, 2th ed. John Wiley & Sons, Ltd., 2004.

[47] M. Mulder, *Basic Principles of Membrane Technology*. Dordrecht, Boston, London: Kluwer academic publishers, 1996.

[48] P. Samanta, H.M. Schönettin, H. Horn, and F. Saravia, “MF – NF Treatment Train for Pig Manure : Nutrient Recovery and Reuse of Product Water,” *Membranes (Basel).*, 2022, doi: https://doi.org/10.3390/membranes12020165 Academic.

[49] R. Epsztein, E. Shaulsky, N. Dizge, D.M. Warsinger, and M. Elimelech, “Role of Ionic Charge Density in Donnan Exclusion of Monovalent Anions by Nanofiltration,” *Environ. Sci. Technol.*, vol. 52, no. 7, pp. 4108–4116, 2018, doi: 10.1021/acs.est.7b06400.

[50] O.A. Kazi, W. chen, J.G. Eatman, F. Gao, Y. Liu, Y. Wang, A. Xia and S.B. Darling, “Material Design Strategies for Recovery of Critical Resources from Water,” *Adv. Mater.*, vol. 35, no. 36, pp. 1–34, 2023, doi: 10.1002/adma.202300913.

[51] H. Strathmann, J.J. Krol, H.J. Rapp, and G. Eigenberger, “Limiting current density and water dissociation in bipolar membranes,” *J. Memb. Sci.*, vol. 125, no. 1, pp. 123–142, 1997, doi: 10.1016/S0376-7388(96)00185-8.

[52] M. A. Ben Ali, M. Rakib, S. Laborie, P. Viers, and G. Durand, “Coupling of bipolar membrane electrodialysis and ammonia stripping for direct treatment of wastewaters containing ammonium nitrate,” vol. 244, pp. 89–96, 2004, doi: 10.1016/j.memsci.2004.07.007.

[53] F. Ferrari, M. Pijuan, S. Molenaar, N. Duinslaeger, T. Sleutels, P. Kunte and J. Redjenovic, “Ammonia recovery from anaerobic digester centrate using onsite pilot scale bipolar membrane electrodialysis coupled to membrane stripping,” *Water Res.*, vol. 218, no. April, 2022, doi: 10.1016/j.watres.2022.118504.

[54] M. Rodrigues, A. Paradkar, T. Sleutels, A. ter Heijne, C.J.N. Buisman, H.V.M. Hamelers and P. Kunte, “Donnan Dialysis for scaling mitigation during electrochemical ammonium recovery from complex wastewater,” *Water Res.*, vol. 201, no. February, 2021, doi: 10.1016/j.watres.2021.117260.

[55] M. Rodrigues, T.T. de Mattos, T. Sleutels, A. ter Heijne, H.V.M.

Hamelers, C.J.N. Buisman and P. Kunte, “Minimal Bipolar Membrane Cell Configuration for Scaling Up Ammonium Recovery,” *ACS Sustainable Chem. Eng.*, vol. 8, pp. 17359-17367, 2020, doi: 10.1021/acssuschemeng.0c05043.

[56] D. Saabas and J. Lee, “Recovery of ammonia from simulated membrane contactor effluent using bipolar membrane electrodialysis,” *J. Memb. Sci.*, vol. 644, no. August 2021, p. 120081, 2022, doi: 10.1016/j.memsci.2021.120081.

[57] M.S. Camilleri-Rumbau, K. Briceño, L.F. Søtoft, K.V. Christensen, M.C. Roda-Serrat, M. Errico and B. Norddahl, “Treatment of manure and digestate liquid fractions using membranes: Opportunities and challenges,” *Int. J. Environ. Res. Public Health*, vol. 18, no. 6, pp. 1–30, 2021, doi: 10.3390/ijerph18063107.

[58] J. de Vrieze, G. Colica, C. Pintucci, J. Sarli, C. Pedizzi, G. Willeghems, A. Bral, S. Varga, D. Prat, L. Peng, M. Spiller, J. Buysse, J. Colsen, O. Benito, M. Carballa and S.E. Vlaeminck, “Resource recovery from pig manure via an integrated approach : A technical and economic assessment for full-scale applications,” *Bioresour. Technol.*, vol. 272, no. October, pp. 582–593, 2019, doi: 10.1016/j.biortech.2018.10.024.

[59] D. Bolzonella, F. Fatone, M. Gottardo, and N. Frison, “Nutrients recovery from anaerobic digestate of agro-waste : Techno-economic assessment of full scale applications,” *J. Environ. Manage.*, vol. 216, pp. 111–119, 2018, doi: 10.1016/j.jenvman.2017.08.026.

[60] C. Vaneeckhaute, V. Lebuf, E. Michels, E. Belia, P.A. Vanrolleghem, F.M.G. Tack and E. Meers, “Nutrient Recovery from Digestate : Systematic Technology Review and Product Classification,” *Waste and biomass valorization*, pp. 21–40, 2017, doi: 10.1007/s12649-016-9642-x.

[61] G. L. Velthof, “Mineral concentrate from processed manure as fertiliser,” 2015, Available: https://edepot.wur.nl/352930.

[62] P. Hoeksma and F.E. de Buisonjé, “Production of mineral concentrates from animal manure using reverse osmosis,” 2015. [Online]. Available: https://edepot.wur.nl/364053.

[63] O.F. Schoumans, W.H. Rulkens, O. Oenema, and P.A.I. Ehlert, “Phosphorus recovery from animal manure; Technical opportunities and agro-economical perspectives,” *Alterra Rep.*, vol. 2158, p. 110, 2010.

[64] L. Masse, D.I. Massé, and Y. Pellerin, “The effect of pH on the separation of manure nutrients with reverse osmosis membranes,” *J. Memb. Sci.*, vol. 325, no. 2, pp. 914–919, 2008, doi: 10.1016/j.memsci.2008.09.017.

CHAPTER 2

Optimizing flocculation of digestate to increase circularity in manure treatment

Abstract

The flocculation of (co-)digested cattle and pig manure has rarely been investigated, leading to a rather intuitive use of flocculants in manure digestate treatment processes, resulting in overdosing and increasing costs. Here, the effect of molecular weight, charge density and branching of reference and commercially available flocculants is investigated by establishing the optimal flocculant dosage and the corresponding maximum organic matter removal. Higher molecular weight flocculants show increased turbidity removal as result of their long chains corresponding to a higher amount adsorption sites. Results presented show that polymers with an increased cationic charge density give moderate and unstable flocculation due to the low amounts of non-charged parts essential for the hydrophobic interactions and hydrogen bonding. Further, the results show that a linear high molecular weight flocculant with a nonionic or a low anionic charge density is the most effective as it reached the highest organic matter removal at a low dosage.

This chapter is published as:

M. van der Wal, Z. Borneman, K. Nijmeijer, Optimizing flocculation of digestate to increase circularity in manure treatment, *Bioresource Technology Reports,* 23, **2023**

2.1 Introduction

Manure surplus is a well-known challenge for the agricultural sector due to more strict legislation on the utilization of manure in Europe and particularly in the Netherlands [1]. The Netherlands aims to lower the agricultural nitrogen emission by farm housing, nutrition and manure production by 10 kt/yr in 2030 to protect the so-called Nature 2000 areas through an “integrated approach to nitrogen” plan (Programma Aanpak Stikstof, PAS) [2]. As stated in these regulations, manure processing is becoming increasingly important. Most of all, the pig industry has difficulties to meet the legislation as they often do not own land for crops and thus lack the convenience of direct manure application for fertilization. This increases the need for manure treatment. Therefore, this sector aims for the valorization of pig manure into separate nutrient-rich fractions for tailored fertilization while limiting the emission of nitrogen in the form of ammonia and nitrogen oxide and (climate-driven) CO_2 to meet the imminent legislation [1], [3], [4]. The valorization treatment, see Fig. 2.1 for a schematic overview, often involves co-digestion of manure, various mechanical and membrane separation technologies and polishing steps to produce biogas, dischargeable water and nutrient-rich fractions [3]–[5].

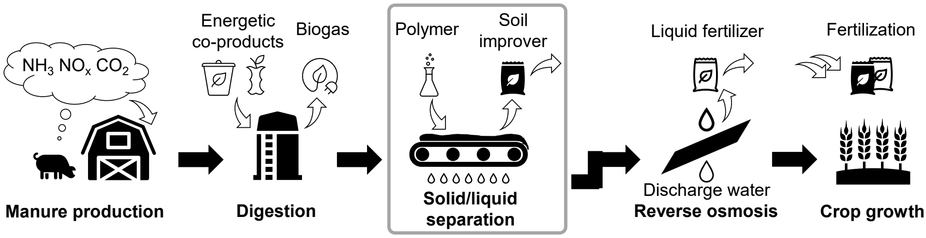

Fig. 2.1: A schematic overview of general manure treatment for fertilizer production.

A typical manure treatment process starts with the digestion of manure in combination with energetic co-products like food and agricultural waste and can be enhanced by the addition of glycerol to increase the production of biogas [6]. The digestion leaves a residual stream known as digestate. This stream contains a large amount of water and nutrients like phosphorus, nitrogen and potassium useful for crop growth. Hence, the digestate is separated into a phosphor-rich solid fraction and a liquid stream with techniques like a sieve belt press and/or dissolved air flotation. Further separation is applied to the liquid streams by extraction of water using reverse osmosis (RO) installations to produce a mineral concentrate and dischargeable water, which simultaneously lowers the transportation costs of the nutrient-rich mineral stream. The solid fraction rich in phosphorus and the mineral concentrate containing nitrogen and potassium are used as basic fertilizers in fertilization where the nutrient ratio is adjusted for the specific crop.

The mechanical solid-liquid separation step is often improved by addition of polymeric flocculants to enhance the dewatering of the manure slurry and to increase the organic matter removal efficiency. This simultaneously increases the recovery of the phosphorus-rich solid fraction [4], [7]. The liquid fraction is subsequently cleaned from the suspended particles, after which a high-quality liquid stream containing nitrogen and potassium species is obtained that is further treated by reverse osmosis [4]. However, so far particularly this dosage of the polymeric flocculant in the digestate solid-liquid separation step is not well studied. Dosing is done rather intuitively in the current treatment facilities. When the flocculation does not perform well, more is added. As removal of added flocculant is not possible this intuitive dosage often results in an overdosage of the polymeric flocculant. This unnecessarily increases the costs and the amount of chemicals used and has even an opposite effect on the intended solid-liquid separation.

Moreover, the excess polymer accumulates in the treatment system due to the recycle loops present in the installation and inevitably ends up in the RO system. The presence of polymer in the RO system results in fouling of the membranes and increases the operational costs [7]. Hence, the importance to design an accessible method to find a suitable flocculant and determine its optimal dosage to increase the efficiency in the solid-liquid separation.

In this chapter, the effect of the molecular weight (MW), charge density (CD) and branching of polymeric flocculants on the flocculation performance of co-digested manure digestate is investigated. Polyacrylamide (PAM) is also selected for this study as this type of polymer is frequently used as flocculant in manure and digestate treatment because of its settling performance and low production costs [8], [9]. PAM polymers with a similar chemical structure but different charged or noncharged functional groups are used to investigate the influence of MW and CD. In addition, linear and branched chemical structures are compared.

2.1.1 Background

As mentioned, to increase the efficiency of solid-liquid separations often flocculation with polymers or coagulation is used. The characteristics of the polymers, mainly MW and CD, influence the flocculation performance in terms of floc formation which leads to a certain turbidity removal from the liquid stream and corresponding flocculant dosage. Flocculants are known for their high Mw ranging from 10^4 to 10^8 g/mol [10]. Based on charge, flocculants are divided into two subclasses 1) anionic and non-ionic flocculants containing often a negative carboxylic group and 2) cationic flocculants containing a positive ammonium functionality [10]. Table 2.1 indicates the classification of the flocculants in terms of structure, MW and CD.

Table 2.1: Classification of flocculants based on structure, MW and CD [11], [12].

Characteristic	**Category**	
Structure	Linear	
	Branched	
Molecular weight [g/mol]	Low	$<3 \cdot 10^6$
	Medium	$3\text{-}6 \cdot 10^6$
	Standard	$6\text{-}10 \cdot 10^6$
	High	$10\text{-}15 \cdot 10^6$
	Very high	$>15 \cdot 10^6$
Charge class	Non-ionic	
	Anionic	
	Cationic	
Charge density [%]	Low	<10
	Medium	10-40
	High	40-80
	Very high	>80

The formation of flocs is based on charge neutralization, patching and/or polymer bridging as shown in Fig. 2.2. The neutralization of charged particles is generally referred to as coagulation and often achieved by the addition of metal salts like iron (III) sulphate/chloride or aluminum chloride. The highly charged metal ions interfere with the stable colloidal particles according to the DLVO theory [12]–[14]. This theory states that the double layer of counter ions, measured as the zeta potential, around the colloid determines whether the particles are attracted to or repelled from each other. The presence of metal ions destabilizes this double layer which leads to lower repulsion forces (V_r) compared to the attractive forces (V_A) between the particles. As a result of the decrease in repulsion, the distribution of the forces shifts, lowering the energy barrier for the particles to overcome for interaction with one another and therefore increasing the flocculation potential. Hence, small flocs are formed which typically form a good foundation for additional flocculation to produce larger flocs [13], [15], [16].

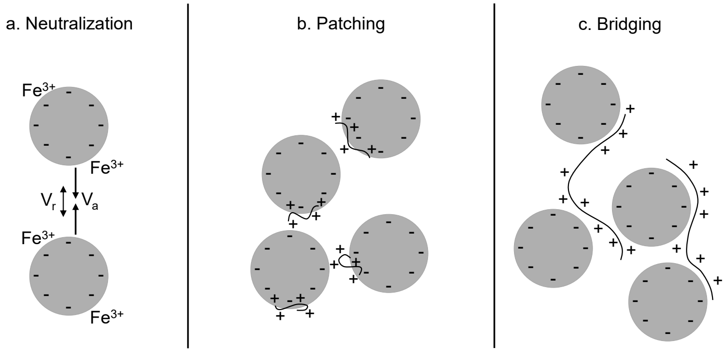

Fig. 2.2: Various flocculation mechanisms, a. neutralization (coagulation), b. patching and c. bridging are shown schematically for negatively charged particles (representing organic matter) and positively charged flocculants.

Another way to increase the attraction between the particles is by the addition and subsequent attachment of relatively short high CD polymers. These polymer chains adsorb patchwise onto the negatively charged particles to form areas of opposite charge [12], [17]. This gives the required attractive interaction between the particles to induce agglomeration which occurs when areas of opposite charge align and coincide. The positive and negative sites on two or more different particles induce a large attraction force to form strong bonds between the particles. This subsequently results in floc formation [8], [15], [17].

High MW polymers on the other hand can form bridges between the particles by adsorption of one polymer chain onto several particles simultaneously. This results in strong flocs capable of withstanding the agitation often used in manure treatment [10]. The long chains contain tails and a substantial amounts of adsorption sites that are able to form loops on the surfaces. When such loops and tails extend further than the electrical double layer around the particle, multiple particles can be actively adsorbed on one long polymer chain. Increasing the MW of the polymer increases the number of adsorption sites and flocculation opportunities and thus usually results in higher efficiencies [8], [16],

[18]. However, this bridging flocculation depends on the particle surface coverage and thus on the polymer concentration [10].

The attractive interactions required for the formation of aggregates are defined by the physical chemical surface interactions. The interactions are based on charge, dipole moments and the free energy of particles and polymers [14]. These driving forces will result in electrostatic or hydrophobic interactions or hydrogen bond formation facilitating the aggregate development [14], [17].

The relatively strong hydrophobic interactions can occur between hydrophobic segments of polymers onto hydrophobic parts of particles [17]. This interaction is driven by the entropy and the free energy of water surrounding the components in the system. The hydrophobic interactions result in an aggregate of non-polar particles in polar solvents [14]. However, the organic matter particles in digestate are often more hydrophilic components like humic acids and proteins that rather form hydrogen bonds in the polar solvent [16].

Hydrogen bonds are a result of attractive interactions between a partially positively charged hydrogen, attached to an electronegative element, and an electronegative element from another component. These elements are typically oxygen and nitrogen. However, negatively charged species might also contribute to the hydrogen bonding. This interaction is considered a contact like interaction which dominates other intermolecular interactions like van der Waals interactions [14]. These hydrogen bonds are often observed for bridging flocculation as the organic matter particles contain the electronegative elements and the long bridging polymers generally contain amide bonds suitable for this hydrogen bond formation [12], [17].

Looking further into the bridging flocculation, high MW polymers with a positive charge are often used to aggregate negatively charged organic matter typically present in digestate [9], [19]. Polymers with a high CD easily attach to the negative sites of the particles, forming strong bridges and flocs. However, the amount of charge added with the polymers should be aligned with the charge present on the particles in solution to prevent charge overcompensation [17], [20], [21]. Such overcompensation occurs in case e.g. the polymer contains significantly more charges compared to the bound particles, resulting in an excess of positive charges attached to the particles. This excess charge from the polymers induce repulsive forces between the partially bridged particles, preventing the formation of additional bridges for the formation of large flocs as presented in Fig. 2.3 [20]. Therefore, for low to non-charged particles the addition of low or non-charged polymers is favorable to induce floc formation by bridging through several loops and tails based on the physical chemical interactions and especially hydrogen bonding rather than on strong electrostatic interactions [17].

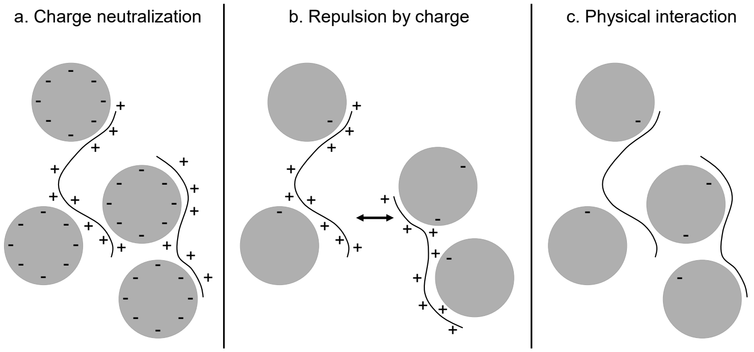

Fig. 2.3: A schematic drawing of the flocculation mechanisms for a. highly charged particles and polymers, b. charge repulsion present for low charged particles combined with highly charged polymers c. and uncharged polymer for low/non-charged particles.

Next to the MW and CD, the chemical structure of a polymeric flocculant plays a significant role in the flocculation efficiency as well. Flocculants are polymers with a linear or branched chemical structure. Large amounts of branches result in steric hindrance during floc formation, which lowers the efficiency [12], [16]. This steric hinderance between the polymers reduces the ability of the polymer adsorption sites to reach the particle surface, preventing attachment. Consequently, a higher dosage is required to reach the same organic matter removal as for linear polymers [12], [15]. Nevertheless, branching can be favorable in case the polymer side chains have certain functionalities like a specific charge or increased hydrophobicity that changes the flocculation interactions [12]. The charged functional side chain is used to bind particles through charge neutralization to form strong flocs. Flocculation polymers can also be modified by adding hydrophobic groups for hydrophobic interactions and to improve dewatering of the flocs [12]. In this chapter, the focus is on the investigation on the interplay of MW, CD and linear or branched structures of various commercial flocculants.

2.2 Materials and methods

2.2.1 Chemicals and materials

Nonionic polyacrylamide (nPAM) with MWs of $2.5 \cdot 10^4$, $1.5 \cdot 10^5$ and $2.5 \cdot 10^6$ g/mol (Sigma Aldrich, Germany), with a medium to standard MW (Table 1), were used to investigate the effect of MW. Commercially available cationic PAM (cPAM) with an MW of 10^6 g/mol and CD values of +0.18, +0.43 and +1.57 meq/g (SNF Floerger, France), corresponding to the low to medium CD range for flocculants, were investigated for the effect of cationic charge. Additionally, synthetic polymers 5CL, 12AB and 8AL (MW $^*10^6$ g/mol, Cationic/Anionic, Linear/Branched) were used for the performance evaluation of commercial flocculants typically applied in manure treatment processes. The bulk composition of the flocculants consists of polyacrylamide. However, due to the use of commercial products, the exact composition of the monomers of the flocculants is unknown. The MW of the commercial flocculants was measured using a 1 M sodium chloride (Akzonobel, Denmark) (currently Nouryon), citric acid (VWR, USA) and sodium phosphate dibasic (Sigma Aldrich, Germany) buffer of pH 7. The CD of the polymers was determined using N/400 potassium polyvinyl sulphate (PVSK) and polydiallyldimethyl ammonium chloride (PDAD) solutions (Fujifilm Wako Chemicals, USA) with pH adjustment by addition of 1 M hydrochloric acid (Sigma Aldrich, Germany) and 1 M sodium hydroxide (Sigma Aldrich, Germany).

2.2.2 Digestate preparation

Real co-digestate was collected after the hygenisation step from the manure treatment processing plant Duurzaam Landleven Bernheze, Heeswijk-Dinther (the Netherlands). Before transport the co-digestate was filtered through a screen with a 4 mm mesh to remove coarse impurities. The average characteristics and ion composition of the digestate from three different days over the range of 5 months are shown in Table 2.2.

The amount of dry matter (DM) in the digestate was measured by weight after water evaporation for 24 hours at 105 °C under a nitrogen flow. The turbidity values of the digestate before treatment and of the liquid fraction were measured, after a dilution of 200 times using water, with a turbidity meter (Eutech TN-100, Thermo scientific, USA).

Table 2.2: The average characteristics and ion composition of the co-digested manure.

Characteristic		**Ion composition**	
DM feed	85 g/kg		
Turbidity digestate	16 500 NTU	Sodium	2.30 g/L
Turbidity liquid fraction	6 000 NTU	Ammonium	5.47 g/L
Particle size	100 to 2000 nm	Potassium	5.17 g/L
pH	8.5	Chloride	3.40 g/L
Conductivity	35 mS/cm	Phosphate	1.86 g/L
Zeta potential	-32 mV	Sulphate	0.07 g/L
Surface charge density	-32 meq/kg digestate		

The particle size of the digestate was measured with an Antonpaar Litesizer 500 with an angle of 175 °, 12 to 30 runs at 20 °C repeated three times. This resulted in particle size distribution up to 2000 nm for sample 2 and 3 as visualized in Fig. S2.1. The particle size distribution of sample 1 deviates a little since it also contains some bigger particles. The Litesizer 500 was also used for the zeta potential measurements of 100 runs repeated three times at 20 °C using the Smoluchowski method to calculate the zeta potential of the liquid fractions after flocculation and resulted in a value of -32 mV for the manure digestate. Zeta potential measurements were also performed after titration of the digestate with polycation solution ($2.5\cdot10^{-4}$ mol/mL PDAD solution with 1 eq/mol charge) to find the surface charge density of the digestate [19], [22]. For the pH and conductivity, a pH meter (pocket pro+ multi 2, Hach, France) and a conductivity meter (GMH 3400, Greisinger, Germany) were used. The ion composition was measured with a Thermo Fisher Integrion-Aquion ion chromatography system (Thermo Fisher, Breda, the Netherlands) using an CS12A cation column with a methyl sulfonic acid eluent and an AS12A anion column with a sodium carbonate/sodium bicarbonate eluent.

2.2.3 Flocculation procedure

A jar tester flocculator system (Velp scientifica, Italy) was used with six simultaneously stirring paddles. Beakers with 250 grams of homogenous digestate at room temperature were used for the flocculation. In the first step the digestate was rapidly pre-mixed at 300 rpm for one minute after which flocculant in mg/g dry matter (DM) was added. The solution was mixed for another minute. The flocculation proceeded with five minutes of slow stirring at 50 rpm for floc formation. The solid-liquid separation was simulated by a centrifuge (Sigma 2-16 KL, Salm en Kipp, the Netherlands) running 45 mL of the flocculation mixtures at 12,000 rpm for ten minutes. Next 10 mL of supernatant was removed to represent the liquid fraction. The turbidity of the liquid fraction was measured after a dilution of 200 times with demineralized water [23]. Water was used as the effect of salt concentration from a dilution with a salt solution (neutral pH) on the turbidity was within the error of the measurement, as was tested with NaCl solutions with a conductivity range of 0.005 to 31.5 mS/cm, of which the highest is comparable to the conductivity of the original digestate.

2.2.4 Polymer structure characterization

The general structure of the commercial flocculants 5CL, 12AB and 8AL were compared to nPAM (MW 10^6 g/mol) through ATR FT-IR (Varian, the Netherlands) and solid-solid NMR (MW of the polymers was too high for liquid NMR). A Varian-cary 3100 FT-IR spectrometer with a golden gate attenuated total reflectance (ATR) was used to produce spectra (resolution 4 cm^{-1} and 50 scans) of the synthetic polymers at room temperature. The solid-state MAS NMR (Magic Angle Spinning Nuclear Magnetic Resonance) spectra were obtained using an 11.7 T AVANCE NEO Bruker NMR spectrometer operating at 500 MHz, and 125 MHz for ^1H and ^{13}C respectively. ^1H and ^{13}C MAS NMR experiments were performed using a Bruker triple channel 4 mm MAS probe head spinning at a rate of 8 kHz. A Hahn echo pulse sequence p_1-τ_1-p_2-τ_2-aq with a 90° pulse p_1=5 μs and a 180° pulse p_2=10 μsec was used for ^1H NMR spectra with an interscan delay of 5 sec. ^{13}C spectra were measured using a CPMAS pulse sequence with a 2 ms contact time and 5 s interscan delay. NMR shift calibrations of ^1H and ^{13}C were done using tetramethyl silane and solid adamantane, respectively.

2.2.5 Molecular weight and charge density calculations

The MW was calculated with the Mark-Houwink equation and constants for PAM which involved the intrinsic viscosity as shown in Eq. 2.1 [10]. The reduced viscosity of several polymer solutions with various concentration in a buffer of pH 7 was determined with a 532 10 Ubbelohde viscometer (SI analytics, Germany) in a water bath of 30 °C. The intrinsic viscosity ($\eta_{intrinsic}$) was extrapolated as the intersection with the y-axis after plotting the reduced viscosity (dL/g) against the polymer concentration (g/dL).

$$\eta_{intrinsic} = 3.73 \cdot 10^{-4} \cdot MW^{0.66} \qquad \textit{Eq. 2.1}$$

Direct and indirect colloidal titration were used to establish the *CD* (meq/g) in acidic and alkaline conditions according to Eq. 2.2. The cationic and anionic titration required the addition of PVSK and PDAD solution with a concentration of $2.5 \cdot 10^{-3}$ M ($M_{titrant}$) and molar equivalent of 1 eq/mol ($Eq_{titrant}$). The amount of PVSK or PDAD in terms of volume in liters ($V_{titrant}$) required for the color change of toluidine from blue to purple violet was determined. The results were used to calculate the equivalent charge per $0.5 \cdot 10^{-3}$ gram of polymer ($m_{polymer}$) [24].

$$CD = \frac{V_{titrant} \cdot M_{titrant} \cdot Eq_{titrant}}{m_{polymer}} \qquad \text{Eq. 2.2}$$

2.3 Results and discussion

2.3.1 The effect of molecular weight and cationic charge density

The effect of MW on the flocculation performance is investigated using several nPAM polymers with different MWs (respectively 10^4, 10^5 and 10^6 g/mol) as flocculants and measuring the turbidity over a range of polymer dosages (Fig. 2.4).

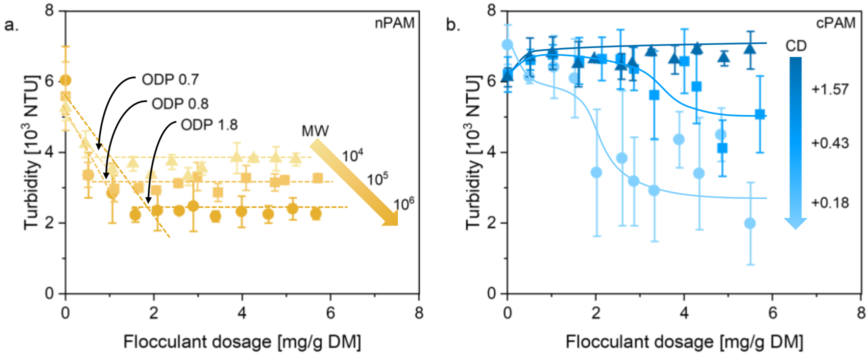

Fig. 2.4: The turbidity [10^3 NTU] of the remaining liquid fraction after flocculant treatment over a range of flocculant dosages [mg/g DM] for a. nPAM with an MW of respectively 10^4, 10^5 and 10^6 g/mol and b. cPAM with an MW of 10^6 g/mol and CDs of +0.18, +0.41 and +1.57 meq/g. Lines are provided to guide the eye.

Fig. 2.4a shows that initially the turbidity of the supernatant decreases with increasing nPAM dosage. This proves that a higher polymer dosage results in an increased amount of sedimented aggregated particles during floc formation resulting in a lower turbidity [8], [15]. However, after a certain dosage point, referred to as the optimal dosage point (ODP), no additional turbidity removal and thus particle attachments, occurs as indicated by the plateau value. At this point, steric stabilization occurs as a result of the high polymer concentration [12]. This high concentration of polymer adsorbs onto the particles which gives hinderance for bridging formation and thus reaches a maximum removal. That is in agreement with previous findings with bentonite (Gregory and Barany et al.) and kaolinite (Nasser and James et al.) particles [8], [17]. Moreover, the addition of high polymer dosages above the ODP results in an excess of polymer that is unbound to the particles which can even slightly increase the turbidity again. Such overdosages will lower the manure treatment performance in the long-term due buildup of polymer in the process [17]. Dosages just below the ODP are thus preferred giving fractional surface covering of flocculant (Gregory and Barany et al.) [17].

Fig. 2.4a shows that the plateau region for high MW polymers is reached at lower turbidity values. This lower turbidity correlates to increased organic matter removal and thus higher flocculation efficiency. This efficiency corresponds to the number of aggregates that is formed during flocculation as the removal of aggregates in solid-liquid separation is more efficient compared to particles [15]. The formation of these aggregates is for nPAM based on the number of bridges that are formed between the particles and polymers [17]. This amount is higher for long chain high MW polymers as these contain a larger amount of amide groups that can adsorb onto the particles through hydrogen bonding [8], [17], [25].

Alongside the MW of the polymers, the CD of the flocculant plays a significant role in the flocculation of negatively charged organic matter. This flocculation occurs when electrostatic interactions are made when the particles contain negative charges or dipole moments (partial charges) and the polymers contain positive charges. The interaction is based on the coulombic potential energy of interaction between the particle and polymer. The potential energy between a charge and dipole moment reaches zero much faster with increasing distance between the particle and polymer compared to the interaction energy between two charges [14]. Therefore, the interaction chance for charged particles to form an ionic interaction is much higher compared to partially charged particles forming a van der Waals interaction, which would be the case for patching flocculation [10].

To understand the flocculation of digestate in more detail, the effect of the amount of cationic charge is investigated by using cPAM with CD values of respectively +0.18, +0.43 and +1.57 meq/g and an MW of respectively

10^6 g/mol (best performing polymer from Fig. 2.4a). The turbidity of the remaining liquid fraction against the flocculant dosage for cPAM with various CD values is shown in Fig. 2.4b. The results demonstrate that cationically charged PAMs are not able to reach the same flocculation efficiencies as neutral nPAM for the flocculation of digestate to enhance solid-liquid separation. The graph shows some flocculation for the lower CD values while no floc formation is observed for the polymer with a high CD value of +1.57 meq/L. The flocculation with low CD polymers reaches the plateau region at a dosage comparable to nPAM. However, in comparison, this polymer removes less organic matter and gives unstable flocculation behavior as shown by significant deviations over the whole dosage range. The charge compensation from the cationically charged polymers would be up to 3% based on the surface charge density of the digestate and polymers [22]. However, no organic matter removal is observed at this charge compensation of 3% whereas at 0.3% charge compensation a significant drop of turbidity was measured. This indicates that electrostatic interactions are of minor importance compared to hydrogen bonding and hydrophobic interactions at low flocculant dosages. The removal of turbidity at low cationic CD suggests that the organic matter removed had a low number of negative charges compared to the high surface charge density of -32 meq/kg of the digestate. In contradiction, as reported in literature, typically a lower surface charge density of around -4 meq/kg manure is found, where the use of cationically charged polymers results in significant organic matter removal indicating the removal of negative charges [15], [19], [22]. For co-digested manure, it was found that flocculants with a low cationic charge are more effective compared to high cationically charged polymers, showing that the removed organic matter from digestate contains low amounts of negatively charged particles [9]. This further indicates the importance of hydrogen bonding and hydrophobic interactions for the flocculation of digestate. In contradiction, the study from Sievers et al., shows successful flocculation experiments of digested manure with high cationically charged polymers, nevertheless at high optimal dosage values of 150 mg/g DM. However, in their study, the digested manure was diluted with tap water before flocculation whereas here undiluted manure is used, being more efficient and in line with reality as added water gives additional costs as it has to be removed and cleaned again before it can be discharged [26].

In this research, more insight was gained with zeta potential measurements which is often used in research concerning model solutions containing e.g.

kaolin where the negative kaolin particles are removed with positively charged polymer resulting in increasing zeta potential values with increasing flocculant dosages [8]. The zeta potentials of the liquid fractions after flocculation with the cationically charged PAMs showed no significant change over the dosage range as for example for the low cationically charged polymer no addition of cPAM resulted in a zeta potential of -40 mV and dosages of 2.6 (approximately the ODP) and 5.2 mg/g DM resulted in zeta potentials values of -40.9 and -42.1 mV. Also, the use of high charge density cPAM resulted in a similar zeta potential at the highest dosage of -41.8 mV as the amount of charge compensated would not result in significant zeta potential change. However, as a change in turbidity was observed for the low CD flocculant, the zeta potential measurements confirmed that bridging flocculation based on hydrophobic interactions and hydrogen bonding is dominant and electrostatic interactions are of minor importance in this dosage range. For the low CD flocculant, the polymer chain has sufficient non-charged parts for these interactions. Increasing the CD resulted in less change in turbidity as more charge groups would result in less polymer chain suitable for non-electrostatic interactions. As a result, the influence of the high concentration of ions present in the digestate (Table 2.2) on the flocculation interaction is limited. Typically, the ions influence electrostatic interaction whereas the bridging flocculation mechanism based on the hydrophobic interactions and hydrogen bonding in the digestate is insensitive to the ionic strength of the solution [27].

2.3.2 Efficiency of commercial flocculants

2.3.2.1 Characterization of commercial flocculants

Typically, commercial flocculants are PAM based polymers, nPAM as used in this study, is thus used as a reference material to assess commercial flocculants 5CL, 12AB and 8AL typically used for manure treatment processes [8], [9]. First, the characteristics of the commercial flocculants were determined before investigating their flocculation performance. The functional groups and structure of the polymer combined with the MW and CD provide important information on the flocculation performance [8].

The functional groups of the commercial polymers are assigned through ATR FT-IR spectra (see Fig. S2.2). The FT-IR shows that all bonds from the functional groups of nPAM are also present in the spectra of the commercial flocculants. The peaks found in the spectra are assigned to the carbon backbone and the amide group of nPAM [28]–[30]. The peak at 1100 cm^{-1}, presenting the C-O acyl bond, is more intense in the 5CL spectrum compared to the spectrum of nPAM. The higher intensity suggests the presences of charged groups close to this bond as typically present in amine-based charged flocculants [31], [32].

The solid-state NMR (see Fig. S2.3a and b) shows that the polymer base of all commercial flocculants consists of PAM as the peaks corresponding to the protons and carbons of PAM are found for all flocculants. The additional information from the NMR spectra suggests the presence of charged groups and branching, which can influence the flocculation performance of the polymer. For 5CL an additional peak is found in the ^{13}C spectra at 162 ppm, as shown by the blue dotted line, which represents the presence of a charged group changing the chemical shift of the amide group [33]. The ^{13}C NMR spectrum for 8AL shows a small additional peak at 53 ppm, presented by the red dotted line, which indicates the presence of a methoxy group indicating that small amounts of electron negative groups are present [33], [34]. The ^{1}H NMR spectrum of 12AB shows an additional peak in the downfield at 0.1 ppm, as shown by the green dotted line, which indicates the presence of CH_3 at a low chemical shift as a result of alkane branching [35].

The flocculation performance of the polymers is largely devoted to the MW and CD of the commercial flocculants [16]. The molecular weight of these synthetic polymers, given in Table 2.3, show a significant difference between the polymers ranging from $4.9 \cdot 10^6$ to $12 \cdot 10^6$ g/mol which are standard values for bridging flocculation [12]. These measurements indicate that 5CL contains a low cationic charge whereas very low anionic charge densities for the high molecular weight flocculants 12AB and 8AL compared to nPAM. Literature indicates that high MW polymers with a low anionic CD stretch because of repulsion within the polymer coil. The extension of the polymer increases the formation of loops and leads to higher flocculation efficiencies [8], [16].

Table 2.3: Experimentally determined characteristics for nPAM (reference), 5CL, 12AB and 8AL.

Flocculant	nPAM	5CL	12AB	8AL
Molecular weight [$\cdot 10^6$ g/mol]	2.5	4.9	12	8.1
Charge density [meq/g]	0	+0.09	-0.02	-0.03
Structure	Linear	Linear	Branched	Linear

2.3.2.2 *Flocculation performance*

Next, the flocculation behavior of the commercial polymers is investigated and compared to that of nPAM (Fig. 2.5). All flocculants show the same removal trend where the turbidity lowers with increasing flocculant dosage until a plateau is reached, similar to the performance results of nPAM. Again, the minimum turbidity value is established from the plateau region which correlates to the maximum organic matter removal. The start of the plateau region is the corresponds to the optimal dosage point (ODP). This value can be quantified from the intersection of the stable part of the linear declining slope with the asymptotic line, as presented by the dashed lines drawn in Fig. 2.5.

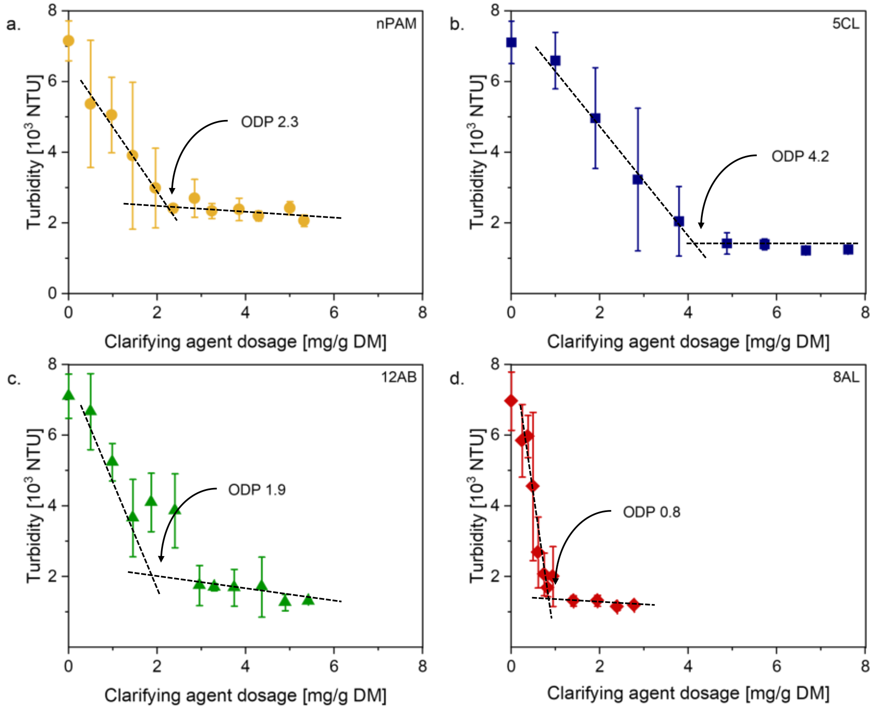

Fig. 2.5: The liquid fraction turbidity [10^3 NTU] versus the flocculant dosage [mg/g DM] of a. nPAM and commercially available flocculants b. 5CL, c. 12AB and d. 8AL.

This shows that a minimum turbidity of approximately 1200 NTU is reached for the commercially available polymers while a value of only 2200 NTU is obtained for reference polymer nPAM. This confirms that the high MW of all commercial polymers results in lower turbidity values and thus increased organic matter removal. However, the various commercially available flocculants do show different ODP values due to their characteristics influencing the efficiency of the bridging flocculation. These ODP values are significantly lower than those found in literature for digestate (15.8 mg/g DM) and manure (10 mg/g DM) [9], [15]. However, in that case, the initial amount of DM in the digestate and manure was approximately 33 and 56 g/kg and their flocculation procedures were different than the methods used in our study, involving a filter press and gravitational drainage. This makes it thus difficult to directly compare their results with the ones found in our study where a feed with a DM of 84 g/kg is used and a procedure using a centrifuge [9], [15]. The reference nPAM required an optimal dosage of 2.3 mg/g DM, slightly higher than the ODP value found in the MW investigation as a result of the difference between the digestate batches. 5CL has the highest ODP value (4.2 mg/g DM) due to its low cationic CD and lower MW compared to the other flocculants. The branched high MW flocculant 12AB reaches the minimum turbidity at an ODP value of 1.9 mg/g DM, which is lower compared to the reference nPAM due to its higher MW. Moreover, 8AL required a much lower dosage (0.8 mg/g DM) leading to a high flocculation efficiency as a result of its high MW and linear chemical structure.

The performance of the commercial flocculants also shows a different behavior in terms of flocculation stability. Based on the CD results for cPAM, it was expected that more repulsion would occur for the low positively charged 5CL as schematically shown in Fig. 2.3b. Though, only a larger deviation (in terms of larger error bars) is found up to the plateau region, most likely induced by some repulsion before stable flocculation is achieved at the high ODP value. Moreover, 5CL shows a plateau with a small deviation while 12AB gives varying flocculation performances over the whole dosage range. This is explained by the branching of 12AB interfering with the hydrophobic interactions and hydrogen bonding resulting in polymer adsorption on the particles. This steric hindrance lowers the overall performance of the high MW polymer in terms of stability [12], [15]. The high MW and very low anionic charge of 8AL results in stable and efficient flocculation, as a low dosage is enough to reach the minimum turbidity. Literature confirms that the flocculation performance for linear polymers with a high MW is high due to the large amount of adsorption sites and thus increased bridging capacity [16], [17]. In addition, following the studies of Dayarathne et al. and Nasser and James et al. that state that the small anionic charge of 8AL can result in repulsion within the polymer, leading to stretching of the long chain depending on the ion composition of the solution, it is hypothesized that a low ion concentration potentially leads to more repulsion between the charges in the polymer chain and thus stretching which would be favorable for the bridging flocculation as shown in Fig. 2.2c [8], [16]. This further increases the amount of adsorption sites and therefore improves the efficiency. The overall results show that a high MW flocculant increases the organic matter removal wherein using a low CD anionic flocculant further increases turbidity removal even at a lower dosage.

2.4 Conclusion

Various flocculants were investigated to determine the effect of polymer characteristics on the flocculation of manure digestate. Turbidity determinations provide insight into the flocculant efficiency and usage in organic matter removal. Cationic high CD flocculants provide moderate and unstable floc formation resulting in lower turbidity removal as the majority of the flocculation interactions are hydrophobic interactions and hydrogen bonding. The best turbidity removal was obtained with linear high MW low CD anionic flocculants. This flocculant reached the lowest turbidity values at small flocculant dosages lowering use of chemicals and costs.

2.5 References

[1] Y. Hou, “Towards improving the manure management chain,” 2016, doi:0.18174/392808.

[2] M. de Heer, F. Roozen, and R. Maas, “The Integrated Approach to Nitrogen in the Netherlands: A preliminary review from a societal, scientific, juridical and practical perspective,” *J. Nat. Conserv.*, vol. 35, pp. 101–111, 2017, doi: 10.1016/j.jnc.2016.11.006.

[3] G.L. Velthof, “Mineral concentrate from processed manure as fertiliser,” 2015. [Online]. Available: https://edepot.wur.nl/352930.

[4] H. Aguirre-Villegas, R.A. Larson, and M.D. Ruark, “Solid-Liquid Separation of Manure and Effects on Greenhouse Gas and Ammonia Emissions,” 2017.

[5] P. Hoeksma and F.E. de Buisonjé, “Production of mineral concentrates from animal manure using reverse osmosis,” 2015. [Online]. Available: https://edepot.wur.nl/364053.

[6] S. Astals, V. Nolla-ardèvol, and J. Mata-alvarez, “Bioresource Technology Anaerobic co-digestion of pig manure and crude glycerol at mesophilic conditions : Biogas and digestate,” *Bioresour. Technol.*, vol. 110, pp. 63–70, 2012, doi: 10.1016/j.biortech.2012.01.080.

[7] H. Luo, T. Lyu, A. Muhmood, Y. Xue, H. Wu, E. Meers, R. Dong and S. Wu, “Effect of flocculation pre-treatment on membrane nutrient recovery of digested chicken slurry: Mitigating suspended solids and retaining nutrients,” *Chem. Eng. J.*, vol. 352, no. July, pp. 855–862, 2018, doi: 10.1016/j.cej.2018.07.097.

[8] M.S. Nasser and A.E. James, “The effect of polyacrylamide charge density and molecular weight on the flocculation and sedimentation behaviour of kaolinite suspensions,” *Sep. Purif. Technol.*, vol. 52, no. 2, pp. 241–252, 2006, doi: 10.1016/j.seppur.2006.04.005.

[9] S. Heviánková, R. Souček, M. Kyncl, and N. Surovcová, “Contribution To The Study Of Flocculation Of Digestate,” *Geosci. Eng.*, vol. 61, no. 3, pp. 37–44, 2018, doi: 10.1515/gse-2015-0021.

[10] SNF Floerger, “Water soluble polymers,” 2014. https://us.snf.com/wp-

content/uploads/2014/08/Water-Soluble-Polymers-E.pdf, Accessed November 2022.

[11] C.S. Lee, J. Robinson, and M.F. Chong, “A review on application of flocculants in wastewater treatment,” *Process Saf. Environ. Prot.*, vol. 92, no. 6, pp. 489–508, 2014, doi: 10.1016/j.psep.2014.04.010.

[12] M. Hyrycz, M. Ochowiak, A. Krupińska, S. Włodarczak, and M. Matuszak, “A review of flocculants as an efficient method for increasing the efficiency of municipal sludge dewatering: Mechanisms, performances, influencing factors and perspectives,” *Sci. Total Environ.*, vol. 820, 2022, doi: 10.1016/j.scitotenv.2022.153328.

[13] J. Duan and J. Gregory, “Coagulation by hydrolysing metal salts,” *Adv. Colloid Interface Sci.*, vol. 100–102, pp. 475–502, 2003, doi: 10.1016/S0001-8686(02)00067-2.

[14] P. Atkins and J. de Paula, *Physical chemistry*, 10th ed. Oxford University PRess, 2014.

[15] M. Hjorth, M.L. Christensen, and P.V. Christensen, “Flocculation, coagulation, and precipitation of manure affecting three separation techniques,” *Bioresour. Technol.*, vol. 99, no. 18, pp. 8598–8604, 2008, doi: 10.1016/j.biortech.2008.04.009.

[16] H.N.P. Dayarathne, M.J. Angove, R. Aryal, H. Abuel-Naga, and B. Mainali, “Removal of natural organic matter from source water: Review on coagulants, dual coagulation, alternative coagulants, and mechanisms,” *J. Water Process Eng.*, vol. 40, no. November 2020, p. 101820, 2021, doi: 10.1016/j.jwpe.2020.101820.

[17] J. Gregory and S. Barany, “Adsorption and flocculation by polymers and polymer mixtures,” *Adv. Colloid Interface Sci.*, vol. 169, no. 1, pp. 1–12, 2011, doi: 10.1016/j.cis.2011.06.004.

[18] G. Petzold, M. Mende, K. Lunkwitz, S. Schwarz, and H. Buchhammer, “Higher efficiency in the flocculation of clay suspensions by using combinations of oppositely charged polyelectrolytes,” *Colloids Surfaces A Physicochem. Eng. Asp.*, vol. 218, pp. 47–57, 2003, doi: 10.1016/S0927-7757(02)00584-8.

[19] M.L. Christensen, M. Hjorth, and K. Keiding, “Characterization of pig slurry with reference to flocculation and separation,” *Water Res.*, vol. 43, no. 3, pp. 773–783, 2009, doi: 10.1016/j.watres.2008.11.010.

[20] N.G. Hoogeveen, M.A. Cohen Stuart and G.J. Fleer, “Can charged (block co)polymers act as stabilisers and flocculants of oxides?,” *Colloids Surfaces A Physicochem. Eng. Asp.*, vol. 117, no. 1–2, pp. 77–88, 1996, doi: 10.1016/0927-7757(96)03699-0.

[21] Y. Shin, J.E. Roberts, and M.M. Santore, “The relationship between polymer/substrate charge density and charge overcompensation by adsorbed polyelectrolyte layers,” *J. Colloid Interface Sci.*, vol. 247, no. 1, pp. 220–230, 2002, doi: 10.1006/jcis.2001.8100.

[22] M. Hjorth and B. U. Jørgensen, “Polymer flocculation mechanism in animal slurry established by charge neutralization,” *Water Res.*, vol. 46, no. 4, pp. 1045–1051, 2011, doi: 10.1016/j.watres.2011.11.078.

[23] C.F. Lenhart, K.N. Brooks, D. Heneley, and J.A. Magner, “Spatial and temporal variation in suspended sediment, organic matter, and turbidity in a Minnesota prairie river: Implications for TMDLs,” *Environ. Monit. Assess.*, vol. 165, no. 1–4, pp. 435–447, 2010, doi: 10.1007/s10661-009-0957-y.

[24] S.K. Kam and J. Gregory, “The interaction of humic substances with cationic polyelectrolytes,” *Water Res.*, vol. 35, no. 15, pp. 3557–3566, 2001, doi: 10.1016/S0043-1354(01)00092-6.

[25] S. Biggs, M. Habgood, G.J. Jameson, and Y. Yan, “Aggregate structures formed via a bridging flocculation mechanism,” *Chem. Eng. J.*, vol. 80, pp. 13–22, 2000, doi: https://doi.org/10.1016/S1383-5866(00)00072-1.

[26] D.M. Sievers, M.W. Jenner, and M. Hanna, “Treatment of dilute manure wastewaters by chemical coagulation,” *Am. Soc. Agric. Eng.*, vol. 37, pp. 597–601, 1994.

[27] Y. Huang and Y. Lapitsky, “Monovalent Salt Enhances Colloidal Stability during the Formation of Chitosan/Tripolyphosphate Microgels,” *Langmuir*, pp. 10392–10399, 2011.

[28] E. Arinaitwe and M. Pawlik, “A method for measuring the degree of anionicity of polyacrylamide-based flocculants,” *Int. J. Miner. Process.*, vol. 91, no. 1–2, pp. 50–54, 2009, doi: 10.1016/j.minpro.2008.12.002.

[29] L.T. Chiem, L. Huynh, J. Ralston, and D.A. Beattie, “An in situ ATR-FTIR study of polyacrylamide adsorption at the talc surface,” *J. Colloid Interface Sci.*, vol. 297, no. 1, pp. 54–61, 2006, doi: 10.1016/j.jcis.2005.10.037.

[30] W.M. Kulicke, R. Kniewske, and J. Klein, “Preparation, characterization, solution properties and rheological behaviour of polyacrylamide,” *Prog. Polym. Sci.*, vol. 8, pp. 373–468, 1982, doi: https://doi.org/10.1016/0079-6700(82)90004-1.

[31] W. Sun, G. Zhang, H. Cao, and H. Li, “Synthesis and flocculation properties of star-shaped cationic polyacrylamide,” *Int. J. Polym. Sci.*, vol. 25, no. 14, pp. 7835–7839, 2013, doi: 10.14233/ajchem.2013.14649.

[32] F. Lin, Y. You, X. Yang, Q. Lu, T. Wang, B. Huang and B. Lu, “Microwave-assisted facile synthesis of TEMPO-oxidized cellulose beads with high adsorption capacity for organic dyes,” *Cellulose*, vol. 24, no. 11, pp. 5025–5040, 2017, doi: 10.1007/s10570-017-1473-9.

[33] J.R. Garbow, L.M. Ferrantello, and R.E. Stark, “13C nuclear magnetic resonance study of suberized potato cell wall,” *Plant Physiol.*, vol. 90, no. 3, pp. 783–787, 1989, doi: 10.1104/pp.90.3.783.

[34] C.P. Neto, J. Rocha, A. Gil, N. Cordeiro, A.P. Esculcas, S. Rocha, I. Delgadillo, J.D. Pedrosa de Jesus and A.J. Ferrer Correia, “13C solid-state nuclear magnetic resonance and Fourier transform infrared studies of the thermal decomposition of cork,” *Solid State Nucl. Magn. Reson.*, vol. 4, no. 3, pp. 143–151, 1995, doi: 10.1016/0926-2040(94)00039-F.

[35] P. Beauchamp, *Advanced Organic Spectroscopy Tools for Beginning Organic Spectroscopists*. 2016.

S2 Supplementary information

S2.1 Particle size distribution

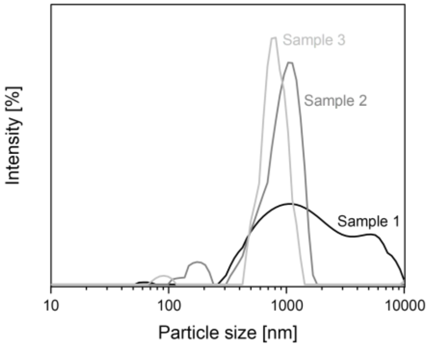

Fig. S2.1: The particle size distribution measured with dynamic light scattering of three digestate samples taken in December, January and April shown as the intensity at different particles sizes on a logarithmic scale in nm.

S2.2. ATR FT-IR

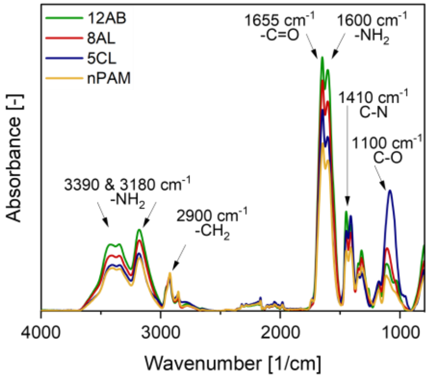

Fig. S2.2: FTIR spectra of the reference nPAM and the commercially available flocculants 5CL, 12AB and 8AL.

S2.3 Solid state proton and carbon NMR

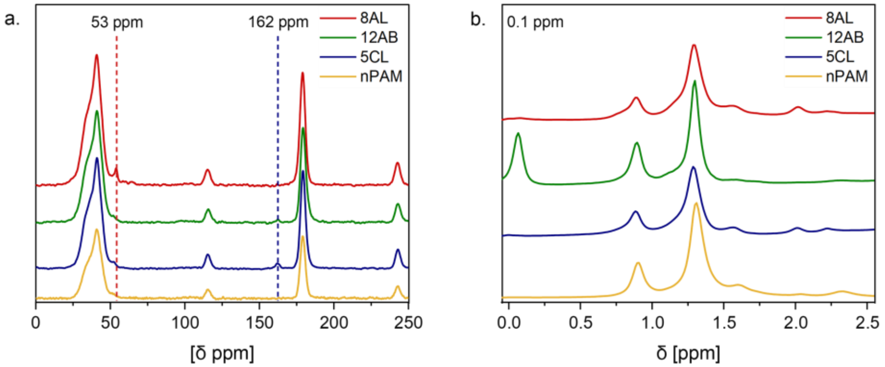

Fig. S2.3: a. The solid-state proton NMR of nPAM, 5CL, 12AB and 8AL and in b. the solid-state carbon NMR.

CHAPTER 3

Dynamic ammonium retention for nutrient separation from manure digestate

Abstract

Typically, manure digestate is mechanically separated into a solid phosphorous-rich fraction and a liquid fraction containing both NH_4^+ and K. These ions are difficult to separate due to their very identical size and charge. This chapter shows that with smart tuning of the pH to control the NH_3/NH_4^+ equilibrium, membranes can produce dedicated N and K-rich streams. The increased pH switches the equilibrium towards the neutrally charged solute NH_3 that permeates more easily through the membrane than charged NH_4^+ and K^+ ions. Experiments with both artificial NH_4Cl/KCl mixtures as well as real liquid digestate and four different membrane types, ranging from open nanofiltration (NF) to sea water reverse osmosis (RO) membranes were performed. At neutral pH, no N/K selectivity was observed, not for single components nor for mixtures. When the pH was increased towards alkaline environment, distinct selectivity for N/K was obtained both with model solutions and real liquid digestate. At a suitable pH of 10, with >80% of the total ammonia present as NH_3, the RO BW membrane showed a high N/K selectivity of 35 in the crossflow system. Additional RO steps at low pH allows subsequent concentration of the formed NH_4^+ and K^+ fractions. The presented dynamic pH approach proofs that in a two-step RO system both N, and K-enriched fertilizers can be produced from real liquid digestate.

This chapter is published as:

M. van der Wal, J. van Alphen, K. Nijmeijer, Z. Borneman, Dynamic ammonium retention for nutrients separation from manure, *Waste management,* 190, **2024**

3.1 Introduction

Tailored fertilization of N, P and K combined with limited nitrogen and greenhouse gas emissions is an essential aspect of a sustainable agricultural sector. This tailored fertilization typically covers various fertilization parameters, amongst these nutrient supply, absorption uptake rates, soil and weather conditions. In general, it is based on the amount of nutrients present in the soil, the nutrient balance (e.g. N/K ratio) in the soil and the specific crop needs. For example, grass typically requires a relatively high amount of N, while the soil provides sufficient P and K. Tomatoes and other vegetables need additional P and K for their flowering while flowering bulbs flourish with a high P-amount for healthy roots [1].

For example, computer simulations and mathematical models are used to increase or level agricultural productivity but at lower operation costs. Such models support farmers in taking systematic decisions based on e.g. weather conditions, crop species needs, fertilizer and soil characteristics [2]. In addition, this approach lowers the use of agricultural machinery as its use and transport routes are also optimized [3]. These models would benefit from separate nutrient streams to tailor the nutrient ratio per crop per season on different types of soil.

A major contribution towards sustainable agriculture must come from the valorization of manure though. The agricultural sector puts much effort in the development of technologies to valorize manure producing separate individual nutrient-rich fractions that can be used for tailored fertilization while limiting N and CO_2 emissions [3]. Moreover, the combination of tailored fertilization with an improved soil ecosystem results in an additional reduction of greenhouse gas emissions as enhanced cultivation of the soil increases its abilities for carbon storage [3]. The degree of greenhouse gas emission reduction also depends on the type of fertilizer used for tailored application of nutrients. Typically, the production of N-containing fertilizers is done with the Haber-Bosch process where N from the air is converted into ammonium (NH_4^+). This process has a high fossil energy demand (29 GJ/t N-fertilizer) and associated CO_2 emissions as it requires high temperatures and pressures [4], [5]. Hence, using manure digestate (often considered waste) as a nutrient resource combined with a treatment procedure with a low environmental impact will sustainabilize the agricultural sector and has a positive impact on the environment as N and CO_2 emissions are reduced. The strict regulations often forbidding direct manure application and the economic benefits compared to artificial fertilizer are other drivers [5], [6].

Adequate valorization treatment technologies do not exist yet and the above clearly stresses the need for technology that can produce separate nutrient-rich fractions that each individually can be used for tailored fertilization in terms of crop type and requirements, seasonal variations, soil characteristics etc..

Due to stricter regulations towards N emissions, the focus of many current technological approaches is often on the removal of N (ammonia) only, to meet these regulations and lower the environmental impact [6]. Company et al. shows, for example, the use of nitrification-denitrification biological pretreatment to lower the N-content for the recovery of K-rich struvite ($MgKPO_4 \cdot 6H_2O$) [6]. However, struvite typically precipitates as $NH_4MgPO_4 \cdot 6H_2O$, which thus results in the removal of both N and simultaneously P [7].

Often current manure treatment installations also involve the production of biogas by (co-)digestion of the manure. In such cases, manure is first treated in a digestor to produce biogas after which the remaining digestate undergoes a multistep fractionation and separation process. After mechanical separation of the digestate in a solid phosphorous-rich fraction and a liquid fraction containing the original amounts of N and K, this liquid fraction is further treated with a reverse osmosis (RO) membrane process to produce a mineral concentrate [8]. Especially, the N and K present in this liquid fraction are difficult to separate: N is mainly present in the form of ammonium ions (NH_4^+) that have a similar charge, valency, radius, hydration number and molar Gibbs energy of hydration as K^+ (Table 3.1).

Table 3.1: The characteristics of K^+ and NH_4^+.

Specie	**Valency**	**Radius hydrated[a] [Å]**	**Radius Stokes[a] [Å]**	**Hydration number[b]**	**Molar Gibbs energy of hydration[c] [kJ/mol]**	**Diffusion coefficient in water[d] [m^2/s]**
K^+	1+	3.31	1.25	6.8	-295	$1.96 \cdot 10^{-9}$
NH_4^+	1+	3.31	1.25	5.2	-285	$1.95 \cdot 10^{-9}$

[a] Nightingale et al. [9], [b] Aydin et al. [10], [c] Marcus et al. [11], [d] Tomczak et al. [12]

However, NH_4^+ forms an equilibrium with NH_3: Where NH_4^+ is highly retained by most RO membranes, the neutral molecule NH_3 (molecular size 3.26 Å) can easily permeate the membrane (diffusion coefficient in water $2.1 \cdot 10^{-9}$ m^2/s [13]), due to the absence of charge and thus Donnan (charge) exclusion [14]–[16]. The NH_4^+/NH_3 equilibrium is pH-sensitive, and the pH can thus be used to tune the degree of retention of the total ammonium N (TAN) relative to the retention of K-species [14]. At a high pH the acid-base equilibrium shifts towards NH_3 while at low pH mostly NH_4^+ is present as shown in Fig. 3.1a.

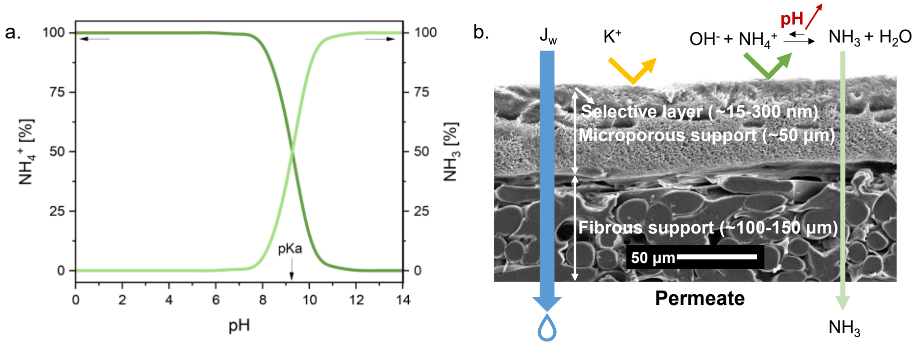

Fig. 3.1: a. The acid-base equilibrium of NH_4^+ and NH_3 is shown as the percentage of the component versus the pH. b. A schematic overview of the pH influence on the retention or permeation of K and N species through a NF or RO membrane presented by a SEM cross section picture of a NF90 membrane (500x magnification). Thickness indication from Yang et al. [17]

Some techniques use this NH_4^+/NH_3 equilibrium combined with the high vapor pressure of NH_3 to separate the gaseous N with distillation, stripping-scrubbing or gas permeable membranes where the NH_3-vapor is captured in low pH solutions [7]. Also, membrane processes, such as nanofiltration NF and RO are often combined with a pH change to capture the N [18]

However, in the end, these technologies produce an acidic solution or create a mineral concentrate in which both N and K are present not allowing tailored fertilization of e.g. N-rich or K-rich fractions. Clearly, tailored fertilization requires the use of single nutrient rich streams to facilitate the tunability of the ratio between the different main nutrients and to match the pH conditions of the targeted crop. Hence, the above approaches are insufficient.

In this research, it is proposed to use the pH sensitivity of the NH_4^+/NH_3 equilibrium to control the permeation of N-species through a NF or RO membrane (Fig. 3.1b) thus steering the ultimate retentate and permeate compositions resulting in an N-rich and a K-rich fraction applicable for tailored fertilization. To prevent nutrient leaching and to avoid the high transport costs of undiluted manure/digestate, the digestate fraction is already concentrated by default. The process proposed here is only a minor modification to the current technology, so the additional costs are limited. It is expected that at high pH, N is predominantly present as NH_3 (next to the presence of K^+). In a membrane process, K^+ is retained by the membrane, while neutral NH_3 molecules do permeate the membrane. At low pH on the other hand, N is present as NH_4^+ and both NH_4^+ and K^+ are retained by the membrane. When applied in a membrane cascade this approach results in a permeate stream rich in N which for example is suitable as a versatile fertilizer in the agriculture [19]. Moreover, the retentate stream enriched in K is of value as fertilizer for K-demanding crops like maize and potatoes [20]. In this chapter, the value of this concept is investigated using both artificial NH_4^+/K^+ feed mixtures as well as real liquid digestate samples at different pH's both in a stirred dead end filtration cell and a crossflow system. By increasing the pH, the neutralized N-molecule can permeate the membrane while the charged K-ion is permanently retained by the membrane thereby separating the nutrients, resulting in two fractions. A concentrated mineral digestate fraction that is enriched in K/N and a diluted permeate fraction that contains almost pure N, which increases the application of this mineral fertilizer.

3.2 Materials and methods

3.2.1 Chemicals and materials

For the salt solutions, sodium chloride (Sanal® P, pharmaceutical grade) was kindly supplied by Akzonobel (currently Nouryon) and ammonium chloride (purity 98+%) and potassium chloride (purity 99+%) by Thermo Scientific, the Netherlands. For pH adjustments 1 M sodium hydroxide and 1 M hydrochloric acid from Honeywell Fluka, USA were purchased, sulfuric acid (98%) from VWR Chemicals, USA and 0.1 M potassium hydroxide from Supelco, Switzerland. The solutions were prepared with demineralized water and the pH was measured with a WTW plus Inolab® pH meter, Germany. Real feed measurements were conducted with liquid manure digestate from a co-digestion system collected after pre-treatment by a sieve belt, dissolved air flotation and pre-filtered over an 80 µm filter cloth kindly provided by Duurzaam Landleven Bernheze, the Netherlands. The pretreated liquid manure digestate is a complex stream due to the use of varying co-products during digestion and amongst organic matter, metals and humic acid next to the ions, the ions composition is presented in Table S3.1.

The extensively investigated NF270 and NF90 thin film composite membranes were used from Dupont FilmTec™, Germany. In addition, in manure treatment facilities used, thin film nanocomposite membranes LG BW 400 R G2 (RO BW) and LG SW 400 R G2 (RO SW) were kindly provided by LG Chem, South Korea. The membrane characteristics from the provided datasheets are mentioned in Table S3.2. The characteristics show that the more open NF membranes have a high multivalent ion retention compared to monovalent ion retention whereas the RO membranes almost retain all ions present due to their denser selective layer [15].

3.2.2 Surface charge

The surface charge of the membranes over a pH range of 2 to 12 was measured in terms of zeta potential using a 5 mM KCl solution adjusted in pH using HCl and KOH. The zeta potential was determined with the electrokinetic analyzer SurPASS^{TM}3 from Anton Paar, Austria, and calculated from the measured streaming potential using the Helmholtz-Smoluchowski equation.

3.2.3 Dead-end cell filtration

The membrane performance using different solutions was established using a HP4750X stirred dead-end filtration cell from Sterlitech, USA. Nitrogen gas was used to adjust the transmembrane pressure, the pressure was set using a Tescom™ pressure regulator (maximum pressure of 60 bar). The cell was continuously stirred at 500 rpm to minimize the boundary layer effects, the accumulation of ions above the membrane surface, at the membrane surface using a stirring plate from Velp scientific, Italy.

3.2.3.1 Pure water permeability

All permeation measurements were carried out in triplicate with new membranes, providing a standard deviation, at room temperature for 10 minutes after a stabilization time of 2 minutes using 100 mL feed solution and for every measurement a new membrane was used with an area of $1.5 \cdot 10^{-3}$ m^2 that had been conditioned in demineralized water for at least 12 hours. The permeation was measured over a pressure range up to 50% of the maximum allowable trans membrane pressure. Moreover, for the RO SW low fluxes were observed up to 20 bar, hence higher transmembrane pressures up to 40 bar present more accurate results. The pure water permeability was calculated using Eq. 3.1 with the weight of the permeate, W_P, in g measured, the density ρ of demineralized water (997 g/L), the effective membrane area A in m^2, time t in h and the starting pressure P applied in bar.

$$Pure\ water\ permeability = \frac{W_P/\rho}{A \cdot t \cdot P} \qquad \text{Eq. 3.1}$$

3.2.3.2 Retention measurements

The single salt retention, indicating the percentage of a solute that is retained by the membrane, was measured in triplicate with new membranes providing a standard deviation over the same pressure range using a model single salt solution containing 8.9 g/L NaCl. Additionally, NH_4Cl and KCl single salt solutions were used containing 3.5 g/L NH_4^+ or K^+, which is similar to the concentration in pre-treated liquid manure digestate. The concentrations of the salt and species in the solutions used for retention measurements are presented in Table 3.2 along with the theoretical and measured osmotic pressure. The theoretical osmotic pressure for pre-treated liquid digestate was based on the ionic composition presented in Table S3.1. The ion composition shows a gap in terms of electroneutrality as the hydroxide ions, metals, humic acids and other organic species were not measured. The measured osmotic pressures were calculated from the Osmolality as measured with the Osmomat 3000, from Gonotec Germany.

Table 3.2: The solution composition in terms of concentration [g/L] along with the measured and theoretical osmotic pressure [bar], conc. stands for concentration.

Solution	**Salt conc.** [g/L]	**NH_4^+ conc.** [g/L]	**K^+ conc.** [g/L]	**Theoretical osmotic pressure** [bar]	**Measured osmotic pressure** [bar]
NaCl	8.9	-	-	7.3	6.9
NH_4Cl	10.4	3.5	-	9.5	8.7
KCl	6.7	-	3.5	4.4	4.0
NH_4Cl/KCl	10.4/6.7	3.5	3.5	13.9	15.9
Pre-treated liquid digestate	-	3.7	3.2	12.1	12.7

The observed retention R_{obs} was calculated, as shown in Eq. 3.2, using the concentration ratio of the permeate collected C_P and the average of the feed and retentate values $C_{F,avg}$, to correct for changes in the concentration. In this case, these values were measured as conductivity values in mS/cm using a Hach pocket pro conductivity meter, USA. In addition the flux in L/m^2·h was calculated using the measured weight of the permeate W_P in gram, the density ρ in g/L, membrane area A in m^2 and the time t in h as shown in Eq. 3.3.

$$R_{obs} = \left(1 - \frac{C_p}{C_{F,avg}}\right) \cdot 100\% \qquad \textit{Eq. 3.2}$$

$$Flux = \frac{W_P/\rho}{A \cdot t} \qquad \textit{Eq. 3.3}$$

To determine the occurrence of any interaction between the ions, the same experiment was conducted using a solution containing both NH_4Cl and KCl (10.4 and 6.7 g/L). As the permeate collected contains both NH_4^+ and K^+ ions, the permeate was analyzed with ion chromatography to determine the concentration of the individual species after an appropriate dilution. For ion chromatography analysis a Thermo Fisher Aquion and Integrion ion chromatography system from Thermo Fisher, the Netherlands, was used, using an Ionpac CS12A cation and Dionex Ionpac AS11 anion column, and methyl sulfonic acid and KOH eluents. The measured concentrations of NH_4^+ and K^+ were used to calculate the observed retention using Eq. 3.2 and the flux was calculated as explained previously. The same approach was used to investigate the effect of the pH in the range 6 to 12 on both the retention and flux at a pressure of approximately 20 bar. This pH range was investigated for the artificial NH_4Cl/KCl solution and pre-treated liquid manure digestate. The pH of the artificial solution was adjusted by dosing 1 M NaOH whereas the real feed with an initial pH of 8.3 was acidified using H_2SO_4 and brought to alkaline conditions using NaOH. Moreover, the permeate was collected in 1 M HCl to prevent evaporation of NH_3. The flux and retention were measured as described before.

3.2.4 Crossflow filtration

To mimic a commercial large scale crossflow system, the MMS triple system from MMS AG Membrane Systems, Switzerland, was used to investigate the performance in terms of the flux and the separation of N and K. The system allows to simultaneously test three membranes ($2.8 \cdot 10^{-3}$ m^2) as triplicate to include the standard deviation. To convert the NH_4^+ to NH_3, the pH was adjusted to 10 by using 1 M NaOH and the flow velocity was varied between 0.75 to 1.5 m/s during the measurements. After a stable flux was obtained, permeate samples were collected during 30 min at room temperature. The permeate was collected in 1 M HCl to prevent NH_3 evaporation. The resulting fluxes and observed retentions were calculated as shown in Eq. 3.1 and Eq. 3.2. As there are two solutes in an aqueous stream the selectivity of N over K was expressed as the ratio of the two species in the permeate over the ratio of the species in the feed in terms of concentration *c* in g/L as shown in Eq. 3.4 [21].

$$Selectivity_{N/K} = \frac{c_{N,P} \,/\, c_{K,P}}{c_{N,F}/c_{K,F}} \qquad \textit{Eq. 3.4}$$

3.3 Results and discussion

3.3.1 Typical membrane filtration performance

Looking into the surface charge, it is observed that all zeta potentials measured were slightly negative as shown in Table S3.3. For example, -29 mV for the NF 270 and -17 mV for the NF 90 at pH 6. Moreover, the apparent zeta potential values over a pH range of 2 to 12 are shown in Fig. S3.2 presenting a negative surface charge for all membranes for the in this research investigated pH range of 6 to 12. This indicates that due to the negative charge, anion rejection based on charge can be expected followed by rejection of cations to maintain electroneutrality, which is in addition to size exclusion. Over this pH range, the negative surface charge is found as a result of dissociation of the different carboxylic acid groups as their pKa values are 5.3 and 9.0 according to a study from Coronell et al. [22]. However, we observe a clear difference between the zeta potential of the RO BW (-32 mV) and RO SW (-3.4 mV) membranes which indicates a difference in the chemical composition of the components used in the interfacial polymerization step when forming the selective polyamide layer on top of the membrane support.

The membrane filtration performance depends on the charge, the chemistry and the morphology of the selective layers. Both the NF and RO membranes investigated contain a selective layer of polyamide where NF270 consists of semi aromatic polymers while the other membranes are composed of fully aromatic polymers [23], [24]. The NF270 membrane is prepared through an interfacial polymerization reaction of benzenetricarbonyl trichloride and piperazine on a non-woven polyester reinforced polysulfone microporous support [25]. For the NF90 membrane benzenetricarbonyl trichloride is also used as the acid chloride but now 1,3-phenylene diamine is applied to form the selective interfacial polymerization polyamide layer [25]. The RO membranes are fabricated in a similar manner as the NF90 with additional embedding of nanoparticles to improve the flux without compromising the salt retention. Moreover, these membranes are covered with an antifouling layer [26].

A clear difference between the membranes is observed for the pure water permeability as shown in Fig. 3.2a. The NF270 membrane is known for its loose structure creating less resistance to permeation and therefore shows a high pure water permeability of 14.5 L/m²·h·bar [15], [27], [28]. On the other hand, the NF90 membrane has a lower pure water permeability compared to NF270 due to a more dense fully aromatic top layer [23]. The NF90 membrane is classified as a tight NF-membrane. This NF90 reaches similar pure water permeabilities as the RO BW membranes that have values of respectively 8.2 and 6.6 L/m²·h·bar. For the RO SW membrane a low pure water permeability of 2.1 L/m²·h·bar was found compared to the RO BW membrane. The RO BW is typically used for desalination of brackish water (2-5 g/L) which means that less stringent requirements can be imposed on mechanical strength and salt retention as the applied pressures exerted on this membrane are much lower. In comparison, the RO SW membranes are designed for seawater (32-40 g salt/L) desalination requiring more pressure to demonstrate water permeation and to show resistance against both salt permeation and the high osmotic pressure created by the sea water, hence the RO SW membrane is denser [15].

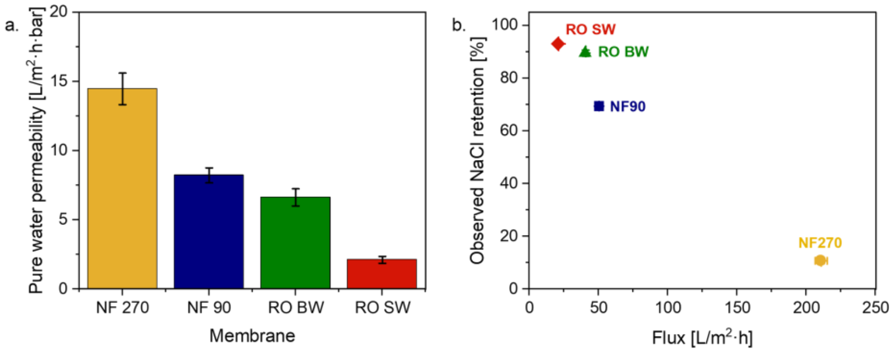

Fig. 3.2: a. The pure water permeability [L/m²·h·bar] and b. the single salt NaCl retention [%] versus the flux [L/m²·h] at 20 bar applied pressure for NF270, NF90, RO BW and RO SW measured in triplicate in the dead-end filtration set-up using demineralized water and a 8.9 g/L NaCl feed solution.

Moreover, a similar trend for the flux, which represents the permeate stream production rate, is observed with an NaCl feed solution, further confirming the increase in density of the active top layer from the NF270 to the RO SW membrane. Usually, a trade-off relationship exists between the flux and retention of membranes. A denser structure ensures that less solutes can permeate through the membrane, resulting in a higher retention at the expense of the permeate flux. For example the RO membranes show, when operated at 20 bars, NaCl retentions higher than 90% and fluxes of 21 and 41 L/m^2·h, as presented in Fig. 3.2b, while the NF membranes show lower retentions and higher flux values. At these conditions, the NF90 membrane reaches a NaCl retention of 69% at a flux of 50 L/m^2·h indicating that the NF90 filtration performance is comparable with the “loose” RO BW membrane. At the bottom of the trade-off line is the NF270 that shows a 10 times higher flux, but this is at the expense of the NaCl retention, which only reached 11%. The measured salt retentions deviate slightly from the manufacturer’s datasheets as given in Table S3.2. This is due to differences in the experimental conditions; effective pressure, concentrations and hydrodynamic conditions used. To be able to properly compare the membranes with each other we used for all membranes a monovalent NaCl test solution containing 8.9 g NaCl/L and an applied pressure of 20 bar. Nevertheless, the measured retention and flux values represent the trade-off and thus the expected difference in the density of the selective layer of the membranes [15].

3.3.2 *Retention of NH_4^+ and K^+*

To determine the difference in retention between NH_4^+ and K^+, retention of single salt solutions and a mixture of salts was measured with the dead-end filtration cell over a pressure range as shown in Fig. 3.3. Opposite to the other membranes, for the RO SW membrane a higher pressure range is measured. This pressure range was chosen in order to allow comparison between single salt and mixed salt permeation. The measured osmotic pressure of the mixed salt solutions is 15.9 bars which indicates a high osmotic pressure difference. This high osmotic pressure remains for RO SW membrane as due to its high salt retention the osmotic pressure difference over the membrane is (almost) equal to the osmotic pressure of the feed solution. This requires a high applied pressure in order to create a water flux through the membrane. This effect is further enhanced by the accumulation of salt in the boundary layer of the mixed salt solution above the membrane. For this reason, all measurements for the

RO BW and NF90 membranes were carried out from 10 to 20 bar while for the RO SW membrane a pressure range from 15 to 40 bar was chosen.

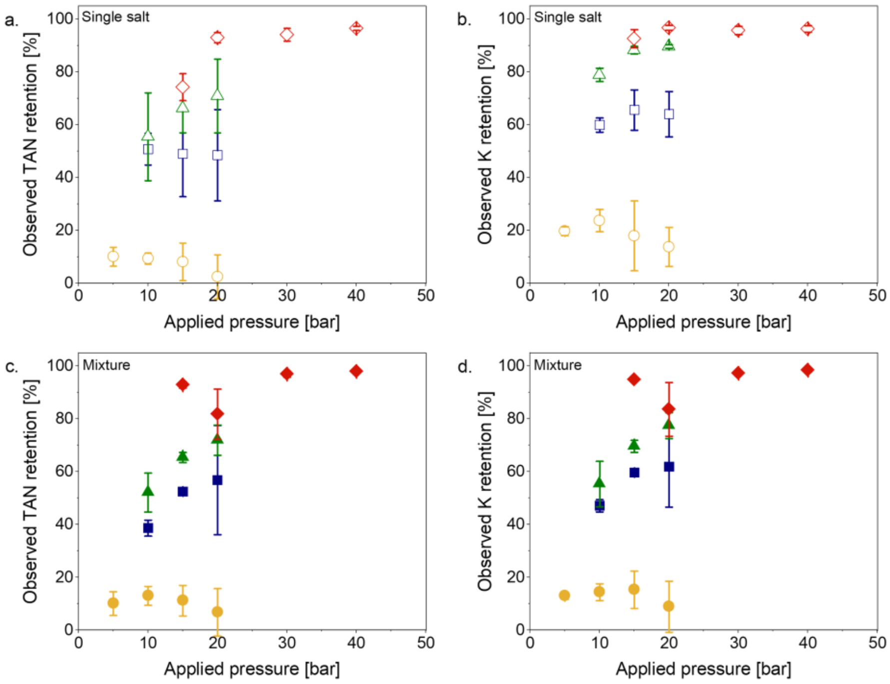

Fig. 3.3: a. The single salt TAN retention [%] and b. the K retention [%] versus the applied pressure for the NF270 (yellow circle), NF90 (blue square), RO BW (green triangle) and RO SW (red diamond) membranes at approximately pH 5-5.5 in the dead-end filtration set-up using single salt solutions (10.4 and 6.7 g/L). c. The TAN and d. the K retention [%] against the applied pressure for the mixture of salts for the NF270 (yellow circle), NF90 (blue square), RO BW (green triangle) and RO SW (red diamond) membranes at a pH of 5.2 measured with the dead-end filtration set-up using a NH_4Cl/KCl solution (10.4 and 6.7 g/L).

Typically, an increase in effective pressure results in an increase in retention as the water flux is convective and thus increases with pressure while the salt flux is diffusion controlled and therefore remains relatively constant [15]. In agreement with this, for example an increase in the water flux for the RO BW membrane from 21 to 57 L/m^2·h was found while increasing the transmembrane pressure from 10 to 20 bar whereas the KCl permeation flux only slightly increases from 16 to 22 g/m^2·h resulting in an increasing retention with increasing pressure (Fig. S3.3). For the single salt solutions, this behavior is also observed for the RO SW membrane where the retention increases from 75 to approximately 97% for both TAN and K when the applied pressure increases from 15 to 40 bars.

Moreover, both nutrients N and K were present as their monovalent cations, NH_4^+ and K^+: As the solutions used for these experiments had pH values below 6 and the pK_a value of ammonia is 9.25 [29], >99.9% of the N was present as NH_4^+ and almost no non-charged NH_3 was present. Therefore, based on the similarity in physical properties of these two cations (Table 3.1), similar retentions are expected for TAN and K in the individual and mixed solutions.

Oppositely, for single salt solutions at 20 bar, the RO BW membrane reaches a retention of 71% for TAN and 90% for the K^+-ions. This difference in retention can be attributed to lower water flux of the NH_4Cl solution induced by the lower effective transmembrane pressure of the NH_4Cl solution. Although both single salt solutions contain 3.5 g cation/L, comparable to the digestate concentration, due to the difference in the molecular weight of the salts the osmotic pressure are measured to be 8.7 and 4.0 bar (Table 3.2), for the NH_4Cl and KCl solutions respectively. In addition, the hydration number and hydration energy of NH_4^+ are slightly lower than those of K^+ (Table 3.1), hence the permeation of NH_4^+ through pores with sizes similar to those of the NH_4^+ and K^+ ions requires less energy, allowing easier permeation [10]. For the NF90 a relatively constant retention is observed with increasing pressure for TAN and K instead of the expected increase with flux and thus applied pressure as is observed for the RO membranes. Moreover, for the NF270 membrane, the retention observed for both TAN and K remains low at a more or less constant value due to the largely convection-controlled transport and therefore almost a pressure-independent retention.

A mixture of both 3.5 g cations/L of NH_4Cl and KCl was measured in the same way to define any competition between NH_4^+ and K^+. Again, the more open NF270 membrane shows a low and almost a pressure-independent retention due to its open character. For the NF90 membrane the typical increase in retention with increasing effective pressure is observed due to the increased water flux at higher pressure, while the salt flux is pressure independent due to its diffusive character. In agreement with the single salt experiments also the RO membranes show increased retentions at higher pressures, but do show a difference in the values of NH_4^+ and K^+ retention when compared with the single salt mixtures. This is caused by the different osmotic pressure of the solutions.

In the case of a mixture, both ions are in the same solution and therefore experience the same osmotic pressure. As expected, since both ions have the same characteristics (Table 3.1) they show the exact same retention behavior. However, the slight difference in hydration number and a 10 kJ/mol lower NH_4^+ dehydration energy of implies that for NH_4^+ it is easier to migrate through the nanopores of the membrane [10]. This difference is so small that it does not result in a noticeable increase in N/K selectivity. Therefore, next the use of pH adjustment is investigated to separate NH_4^+ from K^+.

3.3.3 Tuning N/K selectivity with pH

The separation of the N and K relies on the acid-base equilibrium of the ammonium typically present in manure digestate. In an alkaline environment the equilibrium shifts from the monovalent cation NH_4^+ to the neutral NH_3 (Fig. 3.1) that, because it is uncharged, permeates more easily through the membrane as it is not affected by the Donnan exclusion mechanism [15], [18]. In Fig. 3.4 the retention is shown when filtrating a mixture of TAN and K^+ in the pH range from 6 to 12 at an applied pressure of 20 bar using the dead-end filtration set-up.

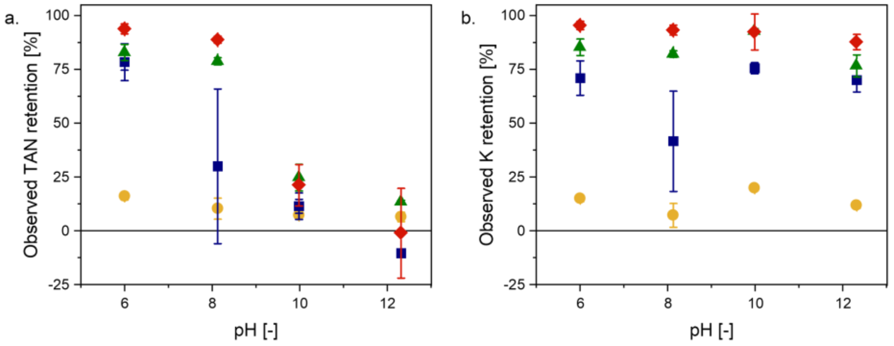

Fig. 3.4: The retention of a. TAN and b. K [%] as function of the pH for a mixture of NH_4Cl and KCl (10.4 and 6.7 g/L) at 20 bar pressure in the dead-end filtration set-up for the NF270 (yellow circle), NF90 (blue square), RO BW (green triangle) and RO SW (red diamond) membranes.

For the TAN retention a clear decrease in retention for all membranes is observed when the equilibrium shifts more towards neutral NH_3 (higher pH). At pH 6 the retention of both TAN and K is similar for each membrane as N is for >99% present as NH_4^+, see Fig. 3.1a. Moreover, at pH 12 the TAN is present for >99% as neutral NH_3, which results in much lower retentions approaching zero and even below that. The negative retentions are the result of the high NH_3 flux through the membrane in proportion to the water flux as the osmotic pressure created over the membrane acts as driving force for the diffusion of NH_3 through the membrane [15]. On the other hand, the retention of K^+ remains constant and high regardless of the change in pH for these membranes. A plausible reason for this is that in the case of the positively charged K^+ the osmotic pressure difference cannot be compensated, due to electroneutrality restrictions by K^+ transport only. There is only a slight drop in retention when the pH exceeds 10 because the high OH^- ion concentration results in some permeation of these ions, as OH^- ions (diffusion coefficient in water $4.5 \cdot 10^{-9}$ m^2/s [30]) permeate more easily through the membrane than Cl^- ions (diffusion coefficient in water $2.2 \cdot 10^{-9}$ m^2/s [31]) and are accompanied by K^+ ions to ensure electroneutrality. For the NF270 membrane low retentions are observed for both TAN and K^+ making NF270 not suitable for this application. The NF90 membrane reaches a relatively high retention for K^+ although it also shows slight instability at for example pH 8. This instability in performance might be related to the response of the NF90 membrane to the pH: Imbrogno et al. (2018) found a 1.65 fold increase in pure water flux when increasing the pH from 6 to 8 while in the range from 2 till 6 the pure water flux was decreasing with a factor 1.2 [32]. A well-recognized explanation for this flux increase is the swelling of the membrane in alkaline environment that results in an increased pore size [33].

The biggest difference in retention between N and K can be reached by increasing the pH above 8. The fully aromatic membranes used in this study are suitable for pH’s up to 11 (Table S3.2). Even though the highest separation efficiency is achieved at pH 12, a feed solution with a pH below 11 is recommended to avoid membrane damage and ensure long-term operation. The biggest difference in retention is achieved with the RO SW membrane due to its excellent monovalent salt retention creating the highest osmotic pressure difference as driving force for the NH_3 to diffuse towards the permeate. As a consequence of the trade-off between retention and flux, the flux of the RO SW membrane is found to be the lowest under these conditions (Fig. S3.5). To produce a compelling amount of the N-rich stream, the RO BW membrane is recommended for this process as the flux with 31 $L/m^2 \cdot h$ when operated at 20 bars is about two fold that of the RO SW membrane while the difference in permeation between TAN and K^+ is similar for both membranes.

3.3.4 Performance with real feed stream

Next, the performance of pH tuning using real liquid manure digestate feed streams was investigated. This pre-treated liquid manure digestate has TAN and K^+ concentrations of approximately 3.7 and 3.2 g/L (Table 3.2). The retention of TAN and K^+ for this real feed stream was measured with the dead-end filtration set-up at 20 bar pressure over a pH range from 6 to 12 (Fig. 3.5).

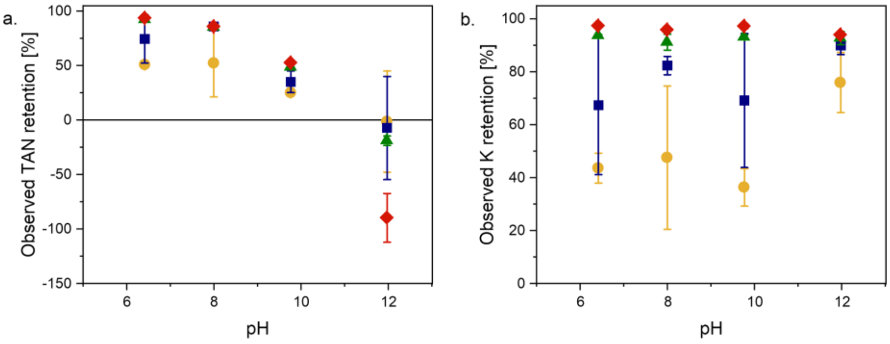

Fig. 3.5: The retention of a. TAN and b. K [%] versus the pH for pre-treated real liquid manure digestate at a pressure of 20 bar in the dead-end filtration set-up for the NF270 (yellow circle), NF90 (blue square), RO BW (green triangle) and RO SW (red diamond) membranes.

The results show the effect of the sensitivity of the NH_3/NH_4^+ equilibrium for pH as also for the pre-treated real liquid manure digestate a large separation is observed when the equilibrium is switched to neutral NH_3 which easily permeates while K^+ is retained. When comparing the retention values of TAN and K^+ for the real liquid digestate feed with the values for the artificial solutions, a difference is observed at pH 10 where the retention of TAN is higher for the real feed and at pH 12 where the retention for the real feed is lower in comparison to the artificial feed. Also, a clear decrease in flux is observed when real feed is used as shown in Fig. S3.6. The organic matter still present in the pre-treated liquid manure digestate fouls the membrane surface resulting in the formation of an additional resistance layer on the membrane that covers the pores and increases the permeation resistance. Moreover, this layer shields the membrane charge. Hence, until a pH of about 10, a retention of approximately 50% is observed for the NF270 membrane, which is a large increase compared to the retention obtained with this membrane for the artificial solutions. Moreover, the NF90 membrane shows instable results for both TAN and K^+ retentions, which is hypothesized to be the result of the pH as mentioned before. In comparison, both RO membranes show stable results and only a slight decrease in flux most likely due to less severe fouling due to their antifouling layer as they showed visually less fouling after measurements in comparison to the NF membranes. Another difference between the real feed and the artificial mixture is the difference in osmotic pressure. The osmotic pressure of the real feed stream is experimentally determined at 12.7 bar. This is lower than the measured osmotic pressure of 15.9 bar for artificial feed (Table 3.2) and presumed to be the result of the presence of divalent counter ions and other organic components in the real feed (ion composition is presented in Table S3.1), giving a lower amount of particles contributing to the osmotic pressure. Typically, a higher effective pressure (applied pressure – osmotic pressure) increases the water flux but the effect on solutes is less, thus lowering the concentration of solutes in the permeate. In contrast, membrane fouling caused by the organic matter present in the feed counteracts this increase in water flux. Hence, both the effective pressure and the organic matter present affect the water permeation and subsequently the retention. Most important, the RO membranes show the same clear trend in TAN permeation at higher pH values as the mixed component system. Overall, a maximum difference between the retention of TAN and K is reached for the RO SW membrane at a pH of 12. However, as addressed earlier, a pH of 12 reduces the membrane lifetime. To circumvent this effect, a pH of 10 is therefore recommended, also because the adverse effect on NH_3 permeation is limited because also at pH 10 more than 80% of the TAN is still present as NH_3. Overall, the consumption of base remains low due to the already alkaline pH of the liquid digestate of approximately 8. At these process conditions the RO BW reaches a flux of 11 $L/m^2{\cdot}h$ with an N enriched permeate stream that contains 1.4 g/L of N and 0.4 g/L of K suitable as agricultural fertilizer. After neutralization, this permeate stream can be concentrated with an additional RO-step to increase the economic value through broader applicability and reduction of transportation costs. Moreover, the acidification of the NH_3 containing permeate stream requires less acid due to the lowered buffer capacity since organic biomolecules and carbonates are retained together with the potassium and are left behind in the retentate fraction of the first RO step. The acidification of this stream benefits the fertilization performance at around neutral pH and prevents evaporation of ammonia after application on land. For the acidification, sulfuric acid or nitric acid are recommended as these are commonly used for the production of fertilizers like ammonium sulphate and ammonium nitrate. Overall, using this dynamic approach, an N enriched permeate stream can be produced while as by-catch a K enriched retentate stream is obtained. At a recovery of 50% the K concentration in this retentate stream is doubled reaching TAN and K concentrations of 4.0 and 5.4 g/L. This stream would be suitable in for example application on maize and potato crops [20].

3.3.5 Influence of the crossflow velocity on the performance

The dead-end system provides valuable information about the membrane performance. To gain more information about the filtration process, laboratory-scale crossflow experiments were carried out as this better mimics the flow conditions in membrane modules in large-scale membrane systems [15]. Moreover, crossflow allows to create better defined turbulence in the feed channels above the membrane surface that reduces the boundary layer effects and the fouling sensitivity. To verify this, first the permeation behavior of a 8.9 g/L NaCl solution at 20 bar applied pressure was carried out using the RO BW membrane in both the dead end and crossflow system. In agreement with the above, a higher retention of 97.5% is observed with the crossflow setup in comparison to a retention of only 89.5% in the dead-end cell. The flux measured with the crossflow setup was approximately 10% higher explaining the higher retention and permeate production rate. Hence, the lab scale crossflow system was also used to investigate the separation of TAN and K with the RO BW membrane, as that is more comparable to industrial systems. Fig. 3.6a presents the retention of TAN and K against the different crossflow velocities at a pH 10 and a pressure of 20 bar. At this pH, TAN is mostly present as NH_3.

The graph shows TAN and K retentions of 14 to 18% and 96 to 98% respectively, slightly increasing with increasing crossflow velocity. Also, the flux increases slightly with increasing crossflow velocity from 23 to 29 $L/m^2 \cdot h$. This small change indicates that there is some concentration polarization but that the higher crossflow velocity lowers concentration polarization and boundary layer effects resulting in a lower osmotic pressure of the feed just above the membrane. This lower osmotic pressure increases the effective pressure applied and thus the water flux. Since the flux of the salt ions is mostly diffusion controlled and thus less effected by the applied pressure, also the retention increases [15].

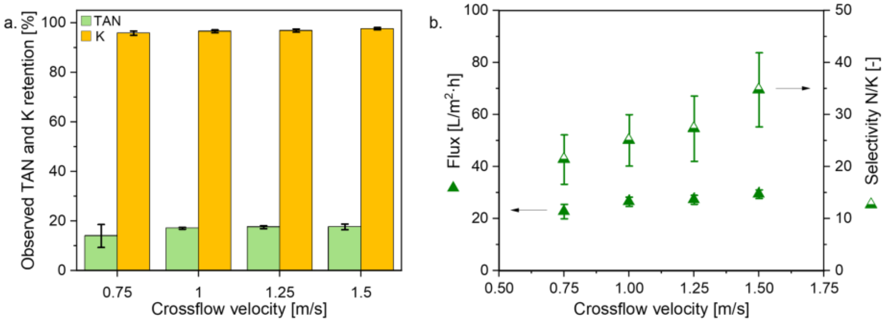

Fig. 3.6: a. The retention of TAN and K [%] of a NH_4Cl/KCl mixture (10.4 and 6.7 g/L) for different crossflow velocities [m/s] at pH 10 and 20 bar pressure in the crossflow system with the RO BW membrane. b. The flux in L/m^2·h and the selectivity of N/K for the RO BW membrane versus the crossflow velocities [m/s].

Moreover, the RO BW when operated at 1.5 m/s, pH 10, and a transmembrane pressure of 20 bar reaches a high selectivity of N/K of approximately 35 (Fig. 3.6b), which means a permeate stream of 29 L/m^2·h with a much higher N/K ratio. This obtained N/K selectivity with the crossflow cell is higher when compared with the N/K selectivity of 3 obtained with the dead-end cell. This N/K selectivity increase is not a result of the boundary layer alone. The difference in N/K selectivity is also due to the much higher amount of NH_3 in the permeate in comparison to K and thus the N/K ratio in the permeate. This higher NH_3 permeation is likely the result of permeation over the length of the membrane in the crossflow cell. Due to this length, there is a longer residence time during which more NH_4^+ dissociates into NH_3 and a proton to compensate for the shift in the NH_4^+/NH_3 equilibrium caused by the initial NH_3 permeation, whereas in the dead-end cell a continuous supply of NH_4^+ is caused by the stirring [18]. Overall, the stage cut for each crossflow velocity was below 1% which means no significant change in salt concentration above the membrane between the inlet and outlet. Nevertheless, a decline in concentration difference was observed for the K at higher crossflow velocities due to the small decrease in the observed retention whereas the N concentration was less affected due to the higher permeation rate of NH_3 resulting in less pronounced boundary layer effects.

3.4 Conclusion

As the agricultural sector aims to valorize manure, the potential of pH to tune the retention of solutes was investigated for the separation of N and K to produce separate nutrient rich fractions for further use in tailored fertilization. Four different membranes (NF270, NF90, RO BW and RO SW) were investigated where the more open NF270 gave the lowest retentions and the RO SW the highest. Each membrane shows no difference between the TAN and K retention at a pH of 6 over pressure range of approximately 5 to 40 bar indicating that separation at pH 6 cannot be achieved. By increasing the pH it is shown that membrane separation can successfully separate TAN from K. The N/K selectivity was achieved as a result of the shift in the NH_4^+/NH_3 equilibrium where the neutral solute NH_3 permeates the membrane while K^+ rejected remained unchanged and high up to a pH of 10. While a pH of 12 provides the highest N/K selectivity it exceeds the typical maximum pH for long-term membrane operation, hence a pH of 10 is recommended. The principle was confirmed with pre-treated real liquid manure digestate where the RO BW provided a N/K selectivity of 3 with a flux of 11 $L/m^2 \cdot h$ at a pH of 10. In conclusion, by dynamically tuning the pH to 10 a permeate stream containing approximately 1.4 g/L of N and 0.4 g/L of K can be produced. To subsequently concentrate the N-containing stream, a second RO step at a pH of 6 can easily be performed. The translation to large scale membrane separation of N and K was proven by the high N/K selectivity of 35 reached in the crossflow system at a pH of 10 with the RO BW membrane. Overall, the tunability of the N retention by pH is easily incorporated in RO systems of existing manure treatment plants. This shows the potential of this dynamic process for manure valorization to produce a separate N rich stream and a K enriched retentate stream suitable as fertilizer.

3.5 References

[1] B.W. Hariyadi, F. Nizak, I.R. Nurmalasari, and Y. Kogoya, “Effect of Dose And Time of Npk Fertilizer Application on The Growth And Yield of Tomato Plants (Lycopersicum Esculentum Mill),” *Agric. Sci.*, 2019, [Online]. Available: https://eprints.unmerbaya.ac.id/id/eprint/208/.

[2] C. Chen, J. Pan, and S. Kee, “A review of precision fertilization research,” *Environ. Earth Sci.*, pp. 4073–4080, 2014, doi: 10.1007/s12665-013-2792-2.

[3] A. Balafoutis, B. Beck, S. Fountas, T. van der Wal, I. Soto, M. Gómez-Barbero, A. Barnes and V. Eory, “Precision agriculture technologies positively contributing to ghg emissions mitigation, farm productivity and economics,” *Sustain.*, vol. 9, no. 8, pp. 1–28, 2017, doi: 10.3390/su9081339.

[4] C. Vaneeckhaute, E. Meers, E. Michels, J. Buysse, and F. M. G. Tack, “Ecological and economic benefits of the application of bio-based mineral fertilizers in modern agriculture,” *Biomass and Bioenergy*, vol. 49, pp. 239–248, 2013, doi: 10.1016/j.biombioe.2012.12.036.

[5] J. De Vrieze, G. Colica, C. Pintucci, J. Sarli, C. Pedizzi, G. Willeghems, A. Bral, S. Varga, D. Prat, L. Peng, M. Spiller, J. Buysse, J. Colsen, O. Benito, M. Carballa and S.E. Vlaeminck, “Resource recovery from pig manure via an integrated approach : A technical and economic assessment for full-scale applications,” *Bioresour. Technol.*, vol. 272, no. October 2018, pp. 582–593, 2019, doi: 10.1016/j.biortech.2018.10.024.

[6] E. Company, M. Farrés, J. Colprim, and A. Magrí, “Exploring the recovery of potassium-rich struvite after a nitrification- denitrification process in pig slurry treatment,” *Sci. Total Environ.*, vol. 847, no. July, 2022, doi: 10.1016/j.scitotenv.2022.157574.

[7] B. Pandey and L. Chen, “Science of the Total Environment Technologies to recover nitrogen from livestock manure - A review,” *Sci. Total Environ.*, vol. 784, p. 147098, 2021, doi: 10.1016/j.scitotenv.2021.147098.

[8] P. Hoeksma, H. Schmitt, H.P. Komleh, and P. Ehlert, “Composition of mineral concentrates,” 2020. doi: https://doi.org/10.18174/541577.

[9] E.R. Nightingale, “Phenomenological theory of ion solvation. Effective radii of hydrated ions,” *J. Phys. Chem.*, vol. 63, no. 9, pp. 1381–1387, 1959, doi: 10.1021/j150579a011.

[10] F. Aydin, C. Zhan, C. Ritt, R. Epsztein, M. Elimelech, E. Schwegler and T.A. Pham., “Similarities and differences between potassium and ammonium ions in liquid water: A first-principles study,” *Phys. Chem.*, vol. 22, no. 4, pp. 2540–2548, 2020, doi: 10.1039/c9cp06163k.

[11] Y. Marcus, “Thermodynamics of Solvation of Ions,” *J. Chem. Soc., Faraday Trans.*, vol. 89, no. 4, pp. 713–718, 1993.

[12] W. Tomczak, “The Application of the Nanofiltration Membrane NF270 for Separation of Fermentation Broths,” *Membranes.*, vol. 12, no. 12, 2022, doi: 10.3390/membranes12121263.

[13] D. Leaist, “Proton-Coupled Transport of Ammonia in Aqueous Hydrochloric Acid,” *Aust. J. Chem.*, vol. 38, no. 2, p. 249, 1985, doi: 10.1071/ch9850249.

[14] L. Masse, D.I. Massé, and Y. Pellerin, “The use of membranes for the treatment of manure: a critical literature review,” *Biosyst. Eng.*, vol. 98, no. 4, pp. 371–380, 2007, doi: 10.1016/j.biosystemseng.2007.09.003.

[15] R.W. Baker, *MEMBRANE TECHNOLOGY*, 2th ed. John Wiley & Sons, Ltd., 2004.

[16] N. Sharma, P. Srinivasan, S. Kumar, J.B. Balaguru Rayappan, and K. Kailasam, “Heptazine based organic framework as a chemiresistive sensor for ammonia detection at room temperature,” *J. Mater. Chem. A*, vol. 6, no. 38, pp. 18389–18395, 2018, doi: 10.1039/c8ta06937a.

[17] S. Yang, Y. Wen, C. Duan, H. Zhang, X. Liu, and Y. Ni, “Poly dimethyl diallyl ammonium chloride assisted cellulase pretreatment for pulp refining efficiency enhancement,” *Carbohydr. Polym.*, vol. 203, no. August 2018, pp. 342–348, 2019, doi: 10.1016/j.carbpol.2018.09.079.

[18] L. Masse, D.I. Massé, and Y. Pellerin, “The effect of pH on the separation of manure nutrients with reverse osmosis membranes,” *J. Memb. Sci.*, vol. 325, no. 2, pp. 914–919, 2008, doi: 10.1016/j.memsci.2008.09.017.

[19] European Commission, “Fertiliser input estimates in farms,” 2021. [Online]. Available: https://ec.europa.eu/info/food-farming-fisheries/farming/facts-and-figures/performance-agricultural-policy/studies-and-reports/economic-analyses-and-briefs/agricultural-and-farm-economics, Accessed November 2023.

[20] C. Zörb, M. Senbayram, and E. Peiter, “Potassium in agriculture - Status and perspectives,” *J. Plant Physiol.*, vol. 171, no. 9, pp. 656–669, 2014, doi: 10.1016/j.jplph.2013.08.008.

[21] M. Mulder, *Basic Principles of Membrane Technology*. Dordrecht: Kluwer acadamic publishers, 1996.

[22] O. Coronell, B.J. Marinas, X. Zhang, and D.G. Gahill, “Quantification of Functional Groups and Modeling of Their Ionization Behavior in the Active Layer of FT30 Reverse Osmosis Membrane,” *Environ. Sci. Technol.*, vol. 42, no. 14, pp. 5260–5266, 2008.

[23] S.S. Wadekar and R.D. Vidic, “Influence of Active Layer on Separation Potentials of Nanofiltration Membranes for Inorganic Ions,” *Environ. Sci. Technol.*, vol. 51, no. 10, pp. 5658–5665, 2017, doi: 10.1021/acs.est.6b05973.

[24] V. Freger, J. Gilron, and S. Belfer, “TFC polyamide membranes modified by grafting of hydrophilic polymers : an FT-IR / AFM / TEM study,” *J. Memb. Sci.*, vol. 209, pp. 283–292, 2002.

[25] M. Gryta, J. Bastrzyk, and D. Lech, “Evaluation of fouling potential of nanofiltration membranes based on the dynamic contact angle measurements,” *Polish J. Chem. Technol.*, vol. 14, no. 3, pp. 97–104, 2012, doi: 10.2478/v10026-012-0091-4.

[26] C.J. Kurth, J.A. Koehler, M. Zhou, B. Anderson Holmberg, and R.L. Burk, “Improved hybrid TFC RO membranes with nitrogen additives,” WO 2011/008549 A2, 2011.

[27] R. Wang and S. Lin, “Pore model for nanofiltration: History, theoretical framework, key predictions, limitations, and prospects,” *J. Memb. Sci.*, vol. 620, no. July 2020, p. 118809, 2021, doi: 10.1016/j.memsci.2020.118809.

[28] R. Epsztein, E. Shaulsky, N. Dizge, D.M. Warsinger, and M. Elimelech, “Role of Ionic Charge Density in Donnan Exclusion of Monovalent Anions by

Nanofiltration,” *Environ. Sci. Technol.*, vol. 52, no. 7, pp. 4108–4116, 2018, doi: 10.1021/acs.est.7b06400.

[29] M.L. Gerardo, N.H.M. Aljohani, D.L. Oatley-radcliffe, and R.W. Lovitt, “Moving towards sustainable resources : Recovery and fractionation of nutrients from dairy manure digestate using membranes,” *Water Res.*, vol. 80, pp. 80–89, 2015, doi: 10.1016/j.watres.2015.05.016.

[30] G.K.H. Wiberg and M. Arenz, “On the influence of hydronium and hydroxide ion diffusion on the hydrogen and oxygen evolution reactions in aqueous media,” *Electrochim. Acta*, vol. 158, pp. 13–17, 2015, doi: 10.1016/j.electacta.2015.01.109.

[31] J.R. Jones, D.L.G. Rowlands, and C.B. Monk, “Diffusion coefficient of water in water and in some alkaline earth chloride solutions at 25°C,” *Trans. Faraday Soc.*, vol. 61, pp. 1384–1388, 1965, doi: 10.1039/TF9656101384.

[32] A. Imbrogno, A. Tiraferri, S. Abbenante, S. Wyand, R. Schwaiger, T. Luxbacher and A.I. Schäfer, “Organic fouling control through magnetic ion exchange-nanofiltration (MIEX-NF) in water treatment,” *J. Memb. Sci.*, vol. 549, no. December, pp. 474–485, 2018, doi: 10.1016/j.memsci.2017.12.041.

[33] J. Luo and Y. Wan, “Effects of pH and salt on nanofiltration-a critical review,” *J. Memb. Sci.*, vol. 438, pp. 18–28, 2013, doi: 10.1016/j.memsci.2013.03.029.

S3 Supplementary information

S3.1 Ion composition

Table S3.1: The ion composition of pre-treated manure digestate measured with ion chromatography.

Cations	Concentration [g/L]	Anions	Concentration [g/L]
Na^+	1.5	Cl^-	2.0
K^+	3.2	NO_2^-	1.0
NH_4^+	3.7	SO_4^{2-}	1.5
Mg^{2+}	0.9		
Ca^{2+}	0.1		

S3.2 Membrane characteristics

Table S3.2: Membranes characteristics based on the manufacturer data sheets [1]-[4].

Membrane	NF270	NF90	RO BW	RO SW
Material selective layer	Polyamide thin film composite	Polyamide thin film composite	Thin film nano-composite	Thin film nano-composite
Maximum pressure	41 bar	41 bar	41 bar	83 bar
Maximum temperature	45 °C	45 °C	45 °C	45 °C
Maximum pH feed solution	10	11	11	11
Salt retention	>97.0%	>98.7%	99.8%	99.8%
*Conditions**				
Concentration	*2 g/L $MgSO_4$*	*2 g/L $MgSO_4$*	*2 g/L NaCl*	*32 g/L NaCl*
pH	-	-	*7*	*8*
Pressure	*4.8 bar*	*4.8 bar*	*15.5 bar*	*55 bar*
Recovery	15%	15%	15%	8%

**At 25 °C*

S3.3 Experimental systems

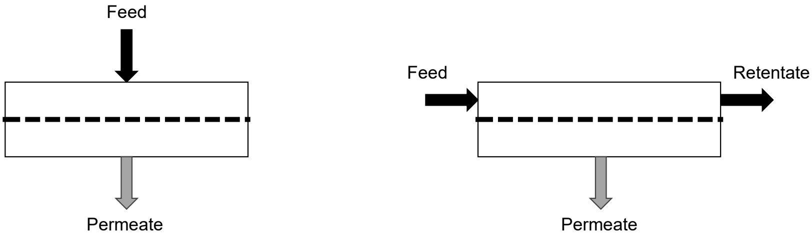

Fig. S3.1: Illustrations of dead-end (left) and cross flow (right) filtration systems according to the definitions as described above.

Dead-end filtration is a system where the feed flow pattern in a membrane module is through the membrane which is the only outlet for the feed resulting in a batch process.

Crossflow filtration is a system where the feed flow pattern is parallel to the membrane surface providing an outlet for the feed as retentate whereas the permeate moves through the membrane out of the system resulting in a continuous process.

S3.4 Zeta potential of membrane surface

Table S3.3: The zeta potential values of the membranes measured in 5 mM KCl at pH 6.

Membrane	NF 270	NF 90	RO BW	RO SW
Zeta potential [mV]	-29	-17	-32	-3.4

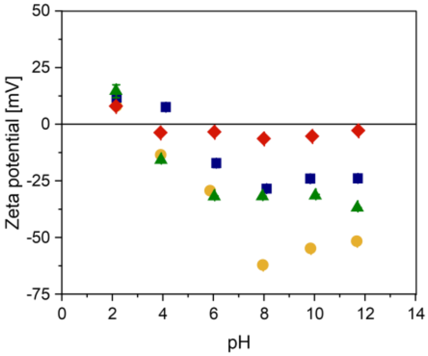

Fig. S3.2: The apparent zeta potential [mV] measured over a pH range for the NF270 (yellow circle), NF90 (blue square), RO BW (green triangle) and RO SW (red diamond) membranes.

S3.5 Membrane performance

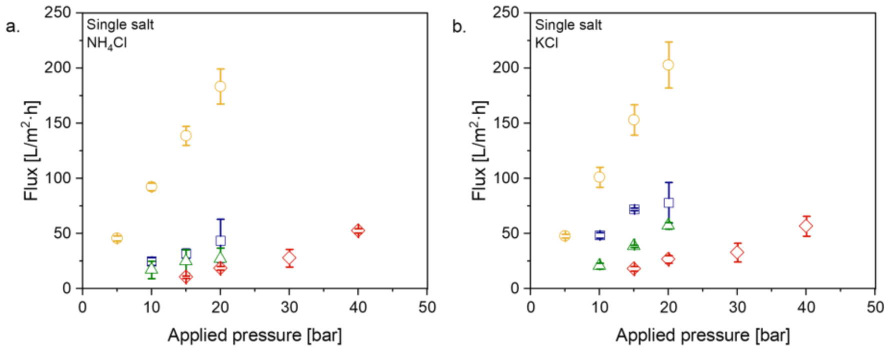

Fig. S3.3: The flux [L/m^2·h] against the pressure [bar] for measurements using single salt solutions containing a. NH_4Cl (10.4 g/L) and b. KCl (6.7 g/L) at a pH of 5-5.5 NF270 (yellow circle), NF90 (blue square), RO BW (green triangle) and RO SW (red diamond) membranes.

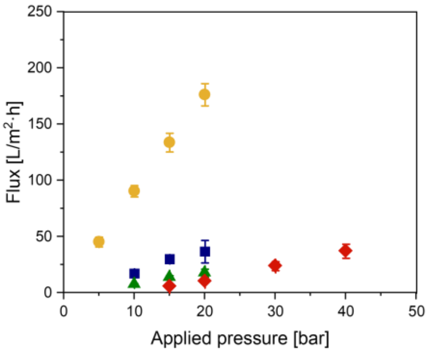

Fig. S3.4: The flux [L/m^2·h] against the pressure [bar] for measurements using a mixture containing NH_4Cl and KCl (10.4 and 6.7 g/L) at a pH of 5.2 for NF270 (yellow circle), NF90 (blue square), RO BW (green triangle) and RO SW (red diamond).

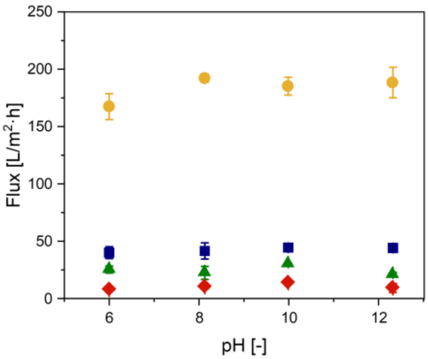

Fig. S3.5: The flux [L/m^2·h] against the pH for the NF270 (yellow circle), NF90 (blue square), RO BW (green triangle) and RO SW (red diamond) membranes measured with a mixture of NH_4Cl and KCl (10.4 and 6.7 g/L) at 20 bar in the dead-end filtration set-up.

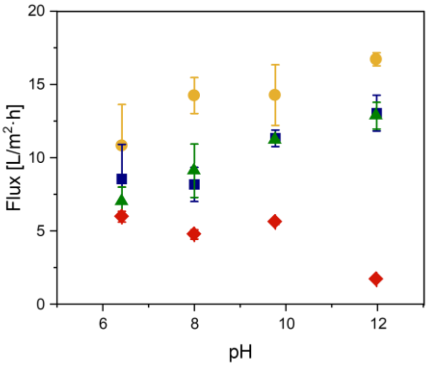

Fig. S3.6: The flux [L/m^2·h] against the pH using pre-treated manure digestate for the NF270 (yellow circle), NF90 (blue square), RO BW (green triangle) and RO SW (red diamond) membranes measured at 20 bar in the dead-end filtration set-up.

S3.6 References

[1] DOW FILMTEC^{TM}, “FILMTEC^{TM} Membranes: FILMTEC^{TM} NF270-4040 Nanofiltration Element,” 2020. https://www.lenntech.com/Data-sheets/DuPont-FilmTec-NF270-2540-4040-L.pdf.

[2] DOW FILMTEC^{TM}, “FILMTEC^{TM} NF90-4040 membranes,” 2020. https://www.lenntech.com/Data-sheets/DuPont-FilmTec-NF90-2540-4040-L.pdf.

[3] LG Chem, “Data sheet: Brackish water Reverse Osmosis (RO) Membranes LG BW 400 R G2,” 2007. https://www.lenntech.com/Data-sheets/LG-Chem-LG-BW-400-R-G2-L.pdf.

[4] LG Chem, “Data sheet: Seawater Reverse Osmosis (RO) memranes LG SW 400 R G2,” 2006. https://www.lenntech.com/Data-sheets/LG-Chem-LG-SW-400-R-G2-L.pdf.

CHAPTER 4

Membrane modification for nutrient separation in manure treatment

Abstract

An emerging application for a more sustainable future is the separation of N and K nutrients from pretreated manure digestate to allow tailored fertilization with recycled functional manure minerals. Reverse osmosis (RO) membranes, traditionally employed in manure treatment, offer efficient water-ion separation but lack ion specificity. To enhance this specificity, membrane modification has emerged as a promising strategy. This chapter investigates a three-step modification approach of an ultrafiltration (UF) polyacrylonitrile (PAN) membrane support to establish ion specific separation. Hydrolysis of the PAN membrane support introduces charged carboxylic acid groups enabling Donnan exclusion with a significant decrease in water flux due to pore swelling. The subsequently applied polyelectrolyte multilayers add size exclusion to the Donnan-exclusion by pore-covering increasing the retention of monovalent and multivalent ions. This size exclusion can be further enhanced by crosslinking although at some expense of the water flux through the rigid polymer network. The NH_4^+/K^+ separation benefits from this, despite the NH_4^+ and K^+ ions having similar native size and charge they differ in dehydration energy. This difference in dehydration energy results in a difference in mobility and thus permeation selectivity through the crosslinked PE layers on the hydrolyzed membranes. Next, the separation of these nutrients can be further improved by increasing the pH of the manure digestate above the pKa value of the NH_4^+/NH_3 equilibrium, which converts NH_4^+ to neutral NH_3. NH_3 molecules are uncharged, and smaller than NH_4^+ ions, making them not susceptible to Donnan exclusion, resulting in an improved N/K separation.

This chapter was submitted as:

M. van der Wal, A. Kinik, M. van Maris, Z. Borneman, K. Nijmeijer, Membrane modification for nutrient separation in manure treatment, **2025**

4.1 Introduction

The agricultural sector contributes to the societal challenges of limiting nitrogen and CO_2 emissions into the atmosphere. In addition, it aims for the valorization of manure into separate nutrient-rich fractions for tailored fertilization to customize the nutrient ratio per crop and season. The liquid fraction remaining after co-digestion of manure contains nitrogen (N) and potassium (K), where the N is mainly present in the form of ammonium (NH_4^+). This stream is further treated with reverse osmosis (RO) to create a mineral concentrate containing both nutrients, N and K, in the same ratio. In this process NH_4^+ and K^+ are thus not separated from each other and both end up in the concentrate stream [1], [2]. Commonly used RO membranes do not provide selectivity between NH_4^+ and K^+ due to the identical size and charge of these ions [3]. The experimentally observed small difference in rejection between NH_4^+ and K^+ is based on the slightly lower dehydration energy of NH_4^+ resulting in a slightly lower retention in comparison to K^+.

The previous chapter showed that the pH is a suitable tool to tune the NH_4^+ retention. Under alkaline conditions NH_4^+ is converted to NH_3, which permeates the membrane more easily because of its smaller size and charge neutrality, while K^+ remains charged and is thus retained by the membrane resulting in nutrient separation [3].

As a next step, this chapter investigates how membrane modification can be used as a tool for N/K separation. Here a systematic multistep membrane modification is performed to fabricate membranes with tailored ion retentions. A three-step modification is conducted with a polyacrylonitrile (PAN) ultrafiltration (UF) membrane as support and starting material. This support is known for its high water flux but, due to its porous nature, lacks retention of any salt ion. The investigated modification starts with hydrolysis of the nitrile groups of this PAN support into carboxylate groups to create negatively charged ionic entities on the support that contribute to Donnan exclusion. Second, polyelectrolyte (PE) multilayers of polyethyleneimine (PEI) and polystyrene sulfonate (PSS) are applied using layer-by-layer (LbL) assembly. The PE layers close off pores with a charged, thin but dense layer inducing a significant decrease in ion permeation by Donnan and size exclusion. The PEI was chosen as it forms dense layers in combination with PSS resulting in a higher monovalent salt retention of 70% when compared to for example the strong polyelectrolyte poly(diallyldimethylammonium chloride) reaching a retention of

10% [4], [5]. Moreover, PEI contains functional groups suitable for crosslinking. Lastly, this crosslinking capability of the PEI layers in the LbL assembly is used by crosslinking with glutaraldehyde (GA) forming a more rigid selective layer that is less susceptible to swelling and that further increases the permeation resistance and retention.

This chapter provides unprecedented insights into how membrane design and optimization affects membrane performance and ion specific retention by quantifying the impact of the successive modification steps on the flux and the salt retention. In line with the above, the performance and subsequent exclusion mechanisms of the membranes are investigated after each modification step to show the concentration and separation potential of nutrients from manure digestate. The research proves that when using carefully selected materials, the combination of these three different approaches together has a complementary effect on ion selectivity. The fundamental information obtained regarding the additional contribution of each modification leads to insights into parameter tuning to fabricate an optimal membrane for a specific application.

4.1.1 Theoretical background

4.1.1.1 Hydrolysis

The neutral nitrile groups in a UF PAN membrane can be hydrolyzed using a strong alkaline medium at elevated temperatures, forming negatively charged carboxylic acid groups. This procedure has been widely used to produce membranes with charged functional groups suitable for UF, pervaporation and desalination applications and as substrate for the assembly of PE multilayers [6]–[9]. The hydrolysis reaction, see Scheme 4.1, typically is reported as a two-step reaction where first a nucleophilic addition of a hydroxide ion on the partially positive carbon in the nitrile group occurs forming an amide intermediate. This amide intermediate then reacts further with another hydroxide ion into a carboxylate group releasing ammonia [10], [11].

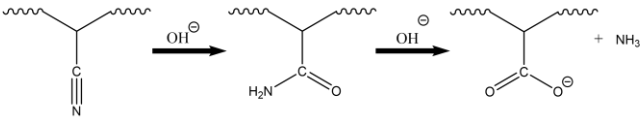

Scheme 4.1: The multistep hydrolysis reaction in alkaline conditions [10].

The amount of conversion depends on the type of base, concentration, temperature, and time. Zhang et al. showed that KOH provides the highest degree of hydrolysis whereas Lohokare et al. shows that higher temperatures and higher concentrations facilitate the hydrolysis reaction [12], [13]. An increased hydrolysis time increases the number of charged groups and thus the impact on ion rejection by Donnan exclusion. Salt retention is facilitated by Donnan exclusion, the electrostatic repulsion between fixed carboxylate groups and solution anions (co-ions). This mechanism dominates when the repulsive force between the fixed charges and anions surpasses the attractive force between the fixed charges and mobile counter-ions. This results in increased salt retention, especially for anions with higher charges, such as multivalent ions [6], [14], [15].

In addition to increasing the charge of the membrane, hydrolysis also increases the hydrophilicity of the membrane, which results in the membrane being more susceptible to swelling. Swelling pushes the pore walls closer together, which not only decreases the pore size but also promotes Donnan exclusion as the charged groups on the pore walls move closer together [13], [14].

The smallest pore radius reported for UF-membranes is typically 0.5 nm, which is still larger than the size of Mg^{2+} with a hydrated radius of 0.428 nm [16], [17]. Ferry and Renkin modeled the rejection of ions (R_{obs}) in such pores using pore radius (r_{pore}), solute radius (r_{solute}), and the fluidic motion of the solvent, resulting in Eq. 4.1 [18], [19].

$$R_{obs} = \left(1 - 2\left(1 - \frac{r_{solute}}{r_{pore}}\right)^2 + \left(1 - \frac{r_{solute}}{r_{pore}}\right)^4\right) \cdot 100\% \qquad \textit{Eq. 4.1}$$

This equation shows that pores larger than the target ion can provide rejection, e.g. a pore with a radius of 0.5 nm pore radius shows a high Mg^{2+} retention of 96%, even without considering the effect of membrane charge. However, larger pores are more common hence a lower rejection of ions is expected for UF. Thus, Eq. 4.1 shows that membranes with a pore radius of 5 nm or greater provides no rejection for the relatively large hydrated Mg^{2+} ion. Hence, it is expected that size exclusion is limited and that therefore Donnan exclusion, driven by the charge carboxylic acid groups, is dominant. However, as mentioned before, these charged groups also induce swelling of the polymer matrix resulting in a reduced pore size which can ultimately result in some retention by size exclusion. Overall, this results in some permeation of cations such as Mg^{2+} as they are attracted by the membrane charge while rejection by size is limited. On the other hand, anions like SO_4^{2-} and Cl^- are rejected by the charge repulsion. Moreover, the contribution of dielectric exclusion, the dehydration of ions to pass a pore, is small if there is limited size-based exclusion.

4.1.1.2 Polyelectrolyte multilayers

The complexation of PE multilayers on top of charged UF membranes has been widely studied as it grants a variety of parameters to tune membrane properties to provide the desired retention and flux [20], [21]. The adsorption of a polycation on a negatively charged substrate (e.g. hydrolyzed PAN) results in strong intrinsic charge compensation between the negative groups of the support and the positive groups of the PE in solution creating a so-called half bilayer (BL) [22]. The then positively charged membrane forms the substrate for the electrostatic adsorption of a subsequent polyanion layer, with the two applied layers now forming one BL. The PE layer provides surface charge resulting in Donnan exclusion while the coverage of pores induces size exclusion and contributes to dielectric exclusion. This approach can be repeated, using similar or even different PEs, until the desired membrane performance is reached [23].

The most versatile tuning opportunities of LbL assembly consist of the PE type, concentration, supporting salt concentration and pH. PSS is an example of a frequently used strong anionic PE, see Fig. 4.1a, which provides a stable negative terminating layer independent of pH. The branched polycation PEI, see Fig. 4.1b and c, is a weak cationic PE known to form dense layers and in addition PEI contains amine groups suitable for crosslinking. Moreover, its charge density depends on the pH, for example PEI shows 100% charge density at a pH of 4 whereas at a pH of 10 the charge density becomes approximately 15% [4].

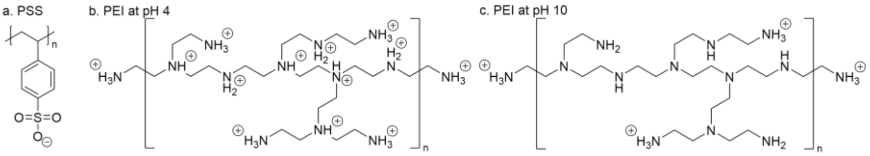

Fig. 4.1: Schematic drawings of a. PSS, b. PEI at pH 4 and c. PEI at pH 10.

Scheepers et al. showed that a PEI solution at pH 4 provides the densest layer resulting in significant monovalent NaCl salt retention reaching 70%, while LbL coated membranes based on other PE couples often fail to retain monovalent ions [4]. However, to separate K^+ from NH_3, a pH of 10 is required to shift the NH_4^+/NH_3 equilibrium towards 90% NH_3, and at this pH, PEI is charged for only 15%. However, the combination of size exclusion by the LbL layers and Donnan exclusion by the negatively charged groups in the PSS terminating layer of the LbL assembly may still result in significant rejection of monovalent salts, such as KCl [24].

Moreover, the PE concentration can be employed to increase the rejection with a higher PE concentration giving a higher adsorption leading to a thicker layer with higher charge densities [5]. Additional tuning can be achieved by adding salt to the PE coating solution, causing less intrinsic (between oppositely PEs) but more extrinsic (between PE and oppositely charged mobile salt ions) charge compensation of the PE functional groups, thereby increasing the charge density of the formed selective layer. The concentration and type (kosmotropic or chaotropic) of salt used during LbL deposition provides different membrane properties [25]. In general, the tunability of LbL assembly offers the opportunity of creating membranes with specific properties.

To provide significant exclusion of monovalent ions with an LbL selective layer a dense layer with a high charge density is required. The charges present provide Donnan exclusion, while the denseness of the LbL layers contribute to size exclusion in combination with dielectric exclusion [20]. Donnan exclusion is the rejection of ions based on charges that are similar to the charges from the membrane surface. Whereas dielectric exclusion is an energy barrier of both cations and anions represented by the difference in solvation energy between the dielectric constant in the bulk and the solvent in the membrane, which is also known as dehydration energy [26]. Generally, the combination of size and charge-based exclusion leads to a higher retention of ions. The highest retentions are typically observed for multivalent salt ions with higher charge density and thus dehydration energy. Nevertheless, greater size and dielectric exclusion also leads to increased monovalent ion retention which are smaller and have a lower charge density compared to multivalent ions [20], [27].

4.1.1.3 Crosslinking

Crosslinking of polymers typically provides more mechanical and chemical strength in terms of reduced swelling and pH resistance [28]. In addition, crosslinking can also be used to increase membrane rejection. The aldehyde entity of GA is well-known for its ability to crosslink primary amine groups forming a crosslinked polymer network and water, see Scheme 4.2. In the case of e.g. PEI, this results in covalent imine bonding between the PEI polymer chains, diminishing swelling and creating a more rigid structure [7].

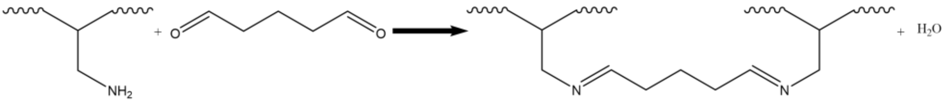

Scheme 4.2: The crosslinking between the amine and aldehyde groups resulting in imine bonds [7].

The denser and more rigid crosslinked polymer structure has narrower paths and the polymer chains are less mobile. The ions thus have more restricted pathways, increasing the permeation resistance in terms of size exclusion [28]. In addition, narrow paths lead to an increase in dielectric exclusion as dehydration is required for the ions to permeate. Hence, the ions with a lower dehydration energy can more easily permeate through a rigid polymer structure compared to ions with a higher dehydration energy [17]. Therefore, the dielectric exclusion and thus the difference in dehydration energy can also attribute to a difference in retention between monovalent ions like NH_4^+ and K^+ with the same stokes radius, see Table S4.1.

4.2 Materials and methods

4.2.1 Chemicals and materials

UF PAN support with a pore size of ±10nm was kindly provided by GMT Membrantechnik GmbH (Germany). Ethanol was purchased from VWR (France). KOH pallets with 85% purity were retrieved from Sigma Aldrich (Germany). PE solutions of 50 wt% polyethyleneimine (PEI) 750 kDa was purchased from Merck (Germany) and 20.4 wt% poly(sodium 4-styrene sulfonate) (PSS) 500-700 kDa from Tosoh Organic Chemical Co. LTD (Japan). Sodium chloride (Sanal® P, pharmaceutical grade) was provided by Akzonobel (currently Nouryon) (the Netherlands). Glutaraldehyde (GA) with a concentration of 50 wt% was purchased at Sigma Aldrich (Germany). Magnesium chloride hexahydrate was purchased from VWR chemicals (Belgium), Sodium sulphate decahydrate with a purity of 99+% from Thermo

Scientific (Spain) and anhydrous magnesium sulphate with a purity of 98+% from Merck (Germany). Polyethylene glycol (PEG) of 1 and 10 kDa were retrieved from Sigma Aldrich (Germany). The ammonium chloride (>98%) and potassium chloride (>99%) were retrieved from Thermo Scientific. All solutions were made with demineralized water. Manure digestate pre-treated with a sieve belt, dissolved air flotation and 80 µm paper filter was kindly supplied by Duurzaam Landleven Bernheze (the Netherlands). For pH adjustment 6 M and 1 M hydrochloric acid VWR chemicals (the Netherlands) and Honeywell Fluka (USA), 1 M and 50% sodium hydroxide and 5 M sulfuric acid were retrieved from Merck (Germany).

4.2.2 Membrane modification

The UF PAN membrane support was pre-treated by soaking it overnight in a 1:1 water ethanol solution. After that it was used as starting material for the membrane modification sequence as shown in Fig. 4.2.

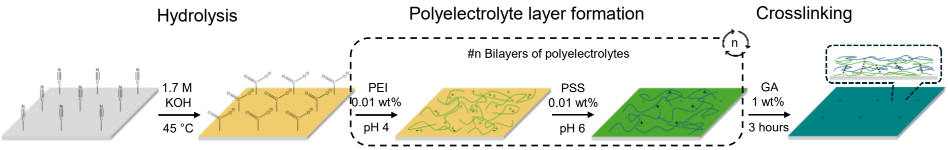

Fig. 4.2: An overview of the membrane modification starting with hydrolyzation of the PAN support using in 1.7 M KOH at 45 °C, followed by the formation of n BLs by subsequent dip coating in 0.01 wt% PEI solution with 50 mM NaCl at a pH of 4 and 0.01 wt% PSS solution with 50 mM NaCl at a pH of 6 interrupted by a rinsing step with 50 mM NaCl and crosslinking for 3 hours in a 1 wt% GA solution as final step.

The substrate was hydrolyzed with 1.7 M KOH solution at 45 °C for 2, 4 and 6 hours on a shaker from IKA-Werke GmbH (Germany) at 60 rpm. For further modification the 4 hours hydrolyzed PAN membranes were used as support for the application of PE layers. The application of the layers was started with the immersion of the 4 hours hydrolyzed PAN support in a solution containing 0.01 wt% PEI in 50 mM NaCl at pH 4 for 15 min on a shaker at 60 rpm, followed by three rinsing steps of 5 min each with fresh salt solution of 50 mM NaCl without pH adjustment. The BLs were finished similarly in a solution of 0.01 wt% PSS in 50 mM NaCl at pH 7 for 15 min with the same subsequent rinsing steps. In this chapter, 2 and 4 BLs were prepared always with a negative terminating layer. For performance comparison a 4 BLs coated membrane was crosslinked using a 1 wt% GA solution, the membrane was immersed for

3 hours and rinsed three times in water for 30 min. All membranes were stored in demineralized water before the measurements.

4.2.3 Membrane surface characterization

The surface composition after hydrolysis was determined with Fourier-Transform Infra-Red (FTIR) spectroscopy, X-ray Photoelectron Spectroscopy (XPS) and zeta potential measurements. The morphology was studied with Field Emission Scanning Electron Microscopy (FESEM).

The functional groups were identified with FTIR spectra using a Varian-cary 3100 FT-IR spectrometer (USA) with a golden gate attenuated total reflectance using a resolution of 4 cm^{-1} and 50 scans at room temperature.

For the elemental composition of the surface the K-alpha XPS from Thermo Scientific (the Netherlands) with a monochromatic small-spot X-ray source and a 180° double focusing hemispherical analyzer with a 128 channel detector was used. The spectra were measured with an aluminum anode source operating at 72 W and a spot size of 400 µm at a constant pass energy of 200 eV and region scans at 50 eV. The ratio of oxygen and nitrogen to carbon (O/C and N/C) was calculated from the elemental analysis.

An electrokinetic analyzer SurPASS^{TM}3 from Anton Paar (Austria) was used to measure the streaming potential using 5 mM KCl over a pH range of 2 to 12 with a cylindrical cell. The Hemholtz-Smoluchowski equation was used to calculate the apparent zeta potential providing an indication of the membrane surface charge.

A Gemini 460 FEG-SEM from Zeiss (Germany) was used to provide detailed images of the selective layer of the membranes after different times of hydrolysis. A ~6 nm platinum coating (as verified by AFM and FESEM on a SI-wafer) was applied to the membrane surface using a JFC-2300HR sputter coater from JEOL (Japan) to improve the electrical conductivity. This coating also served to protect the membranes from electron beam damage and loss of resolution due to surface charging. The membranes were measured with SE in-lens detection using 5 kV acceleration voltage and 42 pA probe current at a working distance of ~3mm.

4.2.4 Membrane performance

For the filtration measurements a HP4750X stirred dead-end filtration cell from Sterlitech (USA) was used. The system was pressurized with nitrogen gas and adjusted using a pressure regulator from Emerson (USA). The solution in the cell was stirred continuously at 500 rpm with the magnetic stirrer insert and a stirring plate from Velp scientific (Italy). The membranes in the cell had an active area of $1.5 \cdot 10^{-3}$ m^2. Measurements were performed in duplicate at room temperature after a stabilization time of at least 1 minute or after at least 1 g of permeate was collected.

4.2.4.1 Pure water permeability

The PWP measurements, using 200 ml of demineralized water, were performed at 5 bar applied pressure until at least 3 g of permeate was collected or permeate was collected for 10 minutes. The collected permeate was used to calculate the *PWP* in L/m^2·h·bar using Eq. 4.2 with the weight of the permeate, W_P, in g, the density ρ of water (997 g/L), the effective membrane area A in m^2, time t in h and the pressure P applied in bar.

$$PWP = \frac{W_P/\rho}{A \cdot t \cdot P} \qquad \text{Eq. 4.2}$$

4.2.4.2 Retention measurements

The retention of various solutions was measured at various pressures with 200 ml of feed solution until at least 3 g of permeate was collected or for 10 minutes. The permeate was weighed (W_p in g) to define the *flux* in L/m^2·h using Eq. 4.3 with the density ρ of water (997 g/L), membrane area A in m^2 and the time t in h.

$$Flux = \frac{W_P/\rho}{A \cdot t} \qquad \text{Eq. 4.3}$$

The retentions (R_{obs}) of different species from various solutions were calculated with Eq. 4.4.

$$R_{obs} = \left(1 - \frac{C_P}{C_{F,avg}}\right) \cdot 100\% \qquad \text{Eq. 4.4}$$

For the single salt solutions, the concentrations of the species in the permeate and on average in the feed, C_P and $C_{F,avg}$, were based on the conductivity of the respective solutions measured in mS/cm. For ion specific retentions (mixed salt solutions and pre-treated manure digestate) the C_P and $C_{F,avg}$ were based on the ion concentrations in g/L measured with ion chromatography (IC) after appropriate dilutions. For the ion concentration analysis, the Aquion (for cations) and Integrion IC (for anions) systems from Thermo Fisher (the

Netherlands) were used with the Ionpac CS12A cation and Dionex Ionpac AS11 anion columns, and methyl sulfonic acid and KOH eluents. The composition of the salt solutions can be found in Table 4.1 including the measured osmotic pressure in bar based on the osmolality (in mOsmol/kg) of the solutions determined with the Osmomat 3000 from Gonotec (Germany).

Table 4.1: An overview of the salt concentration and measured osmotic pressure based on the determined osmolality [mOsmol/kg] of the solution for the solutions used for membrane performance measurements.

Solution	Salt concentration [g/L]	Measured osmotic pressure [bar]
NaCl	1.0	0.8
NaCl	5.0	3.8
$MgCl_2$	1.0	0.7
Na_2SO_4	0.8	0.3
$MgSO_4$	1.0	0.4
NaCl & $MgSO_4$	0.6 & 0.6	0.7
NH_4Cl & KCl	6.7 & 10.4	12.6
Manure digestate	-	23.1

The PEG retention was determined with 1 g/L solutions of PEG with molecular weight values of approximately 1 kDa and 10 kDa. The retention calculations were calculated with Eq. 4.4 based on the concentrations measured with a Gel Permeation Chromatograph (GPC) LC-2050 3D from Shimadzu (Japan). The analysis was performed with a OHpak SB-803 HQ column from Shodex (the Netherlands) and ultrapure water as eluent with a flow rate of 1 ml/min. The size of PEG with a molecular weight of 10 kDa is measured to be approximately 4.5 nm whereas the size of 1 KDa is 1.5 nm based on dynamic light scattering measurements using an Anton Paar Litesizer 500 with an angle of 175 °, 12 to 30 runs at 20 °C.

The selectivity between total ammonia nitrogen (TAN) and K retention was determined with an artificial NH_4Cl and KCl solution of which the pH was adjusted to 8 and 10 with 1 M NaOH. To prevent evaporation of the NH_3 present in the permeate, the permeate was collected in an acid solution containing a known amount of 1 M HCl. For the pre-treated manure digestate the pH was increased to 10 with a 50% NaOH solution to minimize the effect of dilution and NH_3 evaporation was prevented with a known amount of 1 M H_2SO_4 as this provides 2 mol of H^+ for 1 mol of SO_4 instead of 1 to 1 for HCl to keep the chloride peak and conductivity withing the boundaries for IC analysis. Based on the osmotic pressure of these solutions, an applied pressure of 20 bar was used for the artificial solutions and 30 bar for the pre-treated manure digestate to have similar effective pressure values and thus driving force in both cases. Similar as previously described, the experiments were run until at least 3 g of permeate was collected or for 10 minutes starting with 200 ml of feed solution. The flux was calculated with the weight of the permeate using Eq. 4.3. The retention was calculated based on the concentration of the species measured with IC using Eq. 4.4.

4.3 Results and discussion

4.3.1 Effect of hydrolysis time

4.3.1.1 Surface characterization of hydrolyzed membranes

The degree of hydrolysis of the porous PAN support was monitored with FTIR analysis, see Fig. 4.3a, and showed that with increasing hydrolysis time a decrease in the nitrile bond -C≡N peaks at 2245 and 1452 cm^{-1} was observed. In contrast, peaks corresponding to the intermediate amide -C=N bond appeared upon hydrolysis and were observed at 1675 cm^{-1}. Moreover, an increase in the peak height at 1560 cm^{-1} shows the formation of the $-CONH_2$ amide and $-COO^-$ carboxylate bonds. Also, the peak at 1400 cm^{-1} of the $-COO^-$ bond increased in height with increasing hydrolysis time. These results thus confirm the successful hydrolysis of the porous PAN support.

In Fig. 4.3b, the XPS results also confirm that the hydrolysis reaction, visualized by the amount of oxygen to carbon ratio (O/C) within the PAN support, increases with increasing hydrolysis time. Moreover, at the same time the amount of nitrogen in comparison to carbon (N/C) decreases indicating that nitrile groups react away. The increase and decrease of the O/C and N/C ratios between 2 and 6 hours hydrolyzed samples shows that the conversion is time dependent. The reference sample at 0 hours of hydrolysis was not chemically treated hence a different composition is observed where oxygen and nitrogen show similar ratios. Moreover, the offset might be increased by the presence of a preservative or pore stabilizers in the porous structure which are later washed out during the hydrolysis reaction.

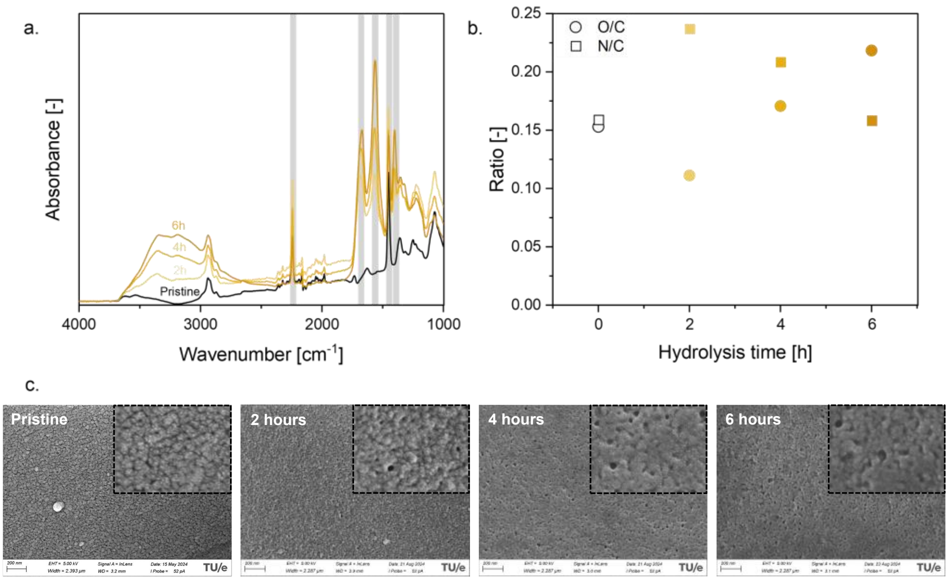

Fig. 4.3: a. The FTIR spectra of the selective layer of the pristine (0), 2, 4 and 6 hours hydrolyzed membranes. b. The O/C (circles) and N/C (squares) ratio based on XPS elemental analysis versus the hydrolysis time [hours]. c. FESEM images of the hydrolyzed surface of the 0 (pristine), 2, 4 and 6 hours hydrolyzed membranes. The insert is a three times magnification.

The advancing hydrolysis reaction is also confirmed by the surface charge of the porous PAN support, measured as zeta potential, plotted in Fig. S4.1. A decrease in zeta potential (i.e. more negative value) with hydrolysis time means the formation of an increasing amount of carboxylate groups over time with after 4 hours a significant decrease in the conversion reaction rate. The pristine sample also showed a negative value which is typically for neutral surfaces as hydroxide ions preferentially adsorb at the surface generating a negative response of the zeta potential [29]. This negative value despite the neutral surface was experimentally confirmed by the absence of an isoelectric point pristine PAN is zero. On the other hand, the isoelectric point was observed for the hydrolyzed samples.

The FESEM pictures of the dried hydrolyzed PAN support in Fig. 4.3c show a morphology change with hydrolysis time showing that the top surface roughness starts to smoothen out. From these images of dry samples, it looks that the number of pores decreases and that their size increases. However, the observed morphology does not represent the actual morphology during water permeation. This is also visible during any performance characterization using aqueous solutions: wetting of the material in that case results in swelling of the membrane thus altering its morphology i.e. lowering its pore size, as investigated by Lohokare [13], [14]. Moreover, the use of a platinum coating results in partial coverage of the pores hence no clear indication of the pore size is provided.

4.3.1.2 Performance with various feed streams

The hydrolysis reaction has a significant effect on the water permeability and the salt retention of the PAN support membrane (Fig. 4.4). The PWP, Fig. 4.4a, drastically drops when the pristine PAN, with a PWP of approximately 200 L/m²·h·bar, is compared with the 2 hours hydrolyzed PAN that reaches only 20 L/m²·h·bar. The PWP keeps declining with the hydrolysis time: the higher amount of nitrile groups converted to carboxylic acid with increasing hydrolysis time makes the membrane more sensitive to swelling. This increased swelling is due to its increased charge and hydrophilicity of the polymer membrane matrix [13]. The higher swelling subsequently results in a higher pore size reduction and thus a decrease in PWP. The PWP of the 4 hours hydrolyzed PAN decreased significantly to values comparable to tight NF or loose RO membranes, implying a performance loss in terms of production capacity [3].

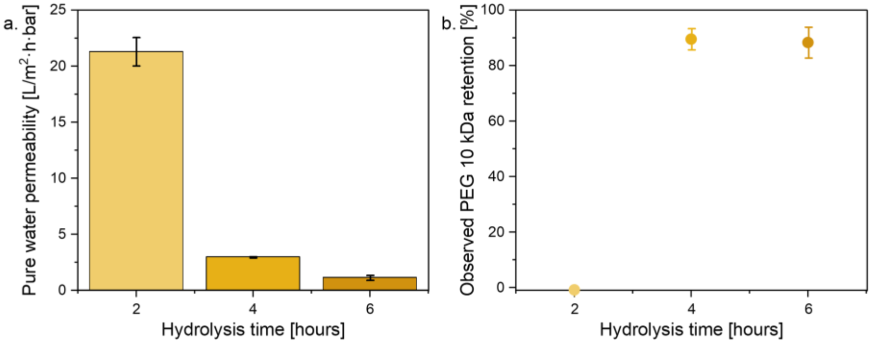

Fig. 4.4: a. The pure water permeability (PWP) [L/m²·h·bar] versus the hydrolysis time [hours] measured at 5 bar applied pressure and b. the observed PEG 10 kDA retention [%] versus the hydrolysis time [hours] measured at 10 bar applied pressure.

Moreover, Fig. 4.4b shows the retention of PEG with a molecular weight of 10 kDa and a size of 4.5 nm. The 2 hours hydrolyzed membrane has the highest PWP, but does not possess retention for PEG 10 kDa due to a too large pore size. Due to swelling the pore size decreases significantly after four hours of hydrolysis, increasing the retention of PEG 10 kDa to 90% for the 4 hours hydrolyzed membrane.

The NaCl rejection (Fig. 4.5) was investigated to understand the effect of the charged groups formed and the associated swelling pore size reduction on the exclusion mechanisms.

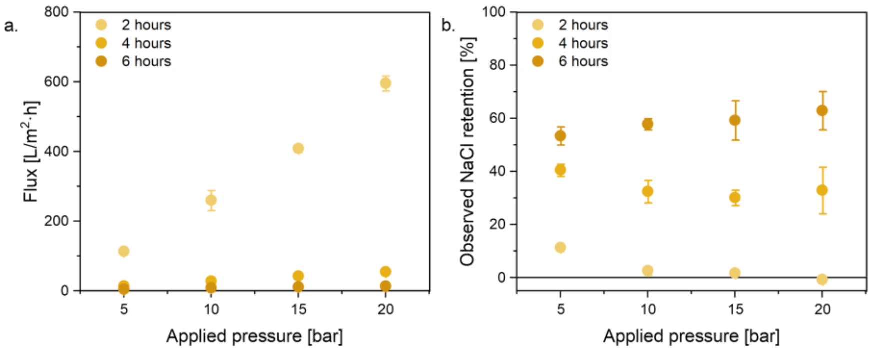

Fig. 4.5: a. The flux [L/m^2·h] and b. The observed NaCl retention [%] versus the applied pressure [bar] for membranes hydrolyzed for 2, 4, and 6 hours using a 1 g/L NaCl feed solution.

First, in Fig. 4.5a, we observe that the flux increases linearly with the applied pressure as the water permeation is convective. The flux for the 2 hours hydrolyzed membrane is much higher due to its more open structure, less pore narrowing by swelling, in comparison to the 4 and 6 hours hydrolyzed membranes. In Fig. 4.5b, the effect of hydrolysis time and applied pressure on the NaCl retention is presented. As the hydrolysis time increases also the NaCl retention increases due to the larger amount of charged groups and thus an increased membrane charge density. This charge causes repulsion and therefore Donnan exclusion between the negatively charged carboxyl groups of the membrane and the negatively charged Cl^- ions of the salt. To maintain electroneutrality, the associated positively charged Na^+ ion is retained as well by the membrane. Moreover, also here the reduced pore size due to swelling can contribute to the increasing retention by size exclusion. For the 2 hours hydrolyzed membranes the NaCl retention slightly decreases at higher pressure. This is attributed to the still more open, pore structure of that membrane, inducing convective salt transport (in contrast to diffusion-controlled transport) which is pressure controlled [17]. A drop in NaCl retention with increasing pressure, although less strong, is also still observed for the 4 hours hydrolyzed sample. Only after 6 hours of hydrolysis, when a significant pore size reduction is reached, the NaCl retention improves slightly with increasing pressure. Here the salt flux becomes more diffusion controlled and thus pressure independent whereas the water flux remains convective as shown in Fig. 4.5a, ultimately resulting in an increase in NaCl retention with pressure.

To provide insight into the impact of charge exclusion, the retention of various salt solutions is presented in Fig. 4.6a and b.

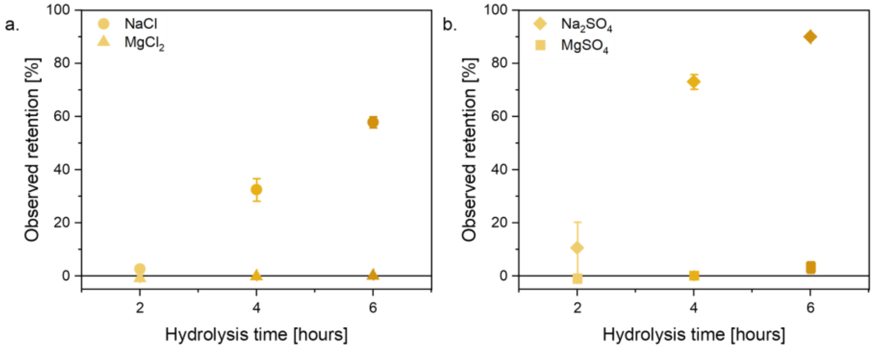

Fig. 4.6: a. The observed retention [%] of NaCl (circles) and $MgCl_2$ (triangles) and b. of Na_2SO_4 (diamonds) and $MgSO_4$ (squares) versus the hydrolysis time [hours] measured at 10 bar applied pressure using feed solutions of approximately 1 g/L.

An increase in NaCl retention with increasing hydrolysis time is observed. However, $MgCl_2$ does not show any retention at all, independent of the hydrolysis time and associated with that the membrane surface charge and pore size. As Mg^{2+} is a multivalent cation, it has a high charge density that induces a significant attraction of Mg^{2+} towards the negative charges of the selective layer, whereas the anion Cl^- provides little rejection due to its small size and single charge and thus lower charge density. Hence, Mg^{2+} ions drag Cl^- ions along through the membrane to keep electroneutrality. Oppositely, as Na^+ has a lower charge density, less attraction between the membrane surface and the Na^+ ions occurs resulting in a rejection that is dominated by the Cl^- ion. Moreover, it can be assumed that size exclusion is not dominant for these membranes as the bigger Mg^{2+} ion (hydrated radius) permeates faster in comparison to the smaller Na^+ ion, see Table S4.1. This is further confirmed in Fig. 4.6b, where the rejection of Mg^{2+} in combination with the multivalent anion

SO_4^{2-} is very low and only slight improvements are visible when a significant reduction in pore size is achieved after 6 hours of hydrolysis. In the case of Na^+ as cation, having a lower attraction to the selective layer, the rejection of SO_4^{2-} is dominant as indicated by the increasing retention with increasing hydrolysis time. This proves that Donnan exclusion is the main rejection mechanism of hydrolyzed PAN membranes, which is induced by the carboxylate groups.

4.3.2 Polyelectrolyte layer formation

Additional modification by PE multilayer formation using LbL assembly on top of the porous hydrolyzed PAN support can further tune flux and retention behavior. Upon coating, the pores of the porous support are covered with PE chains increasing size and dielectric exclusion. Simultaneously, charge exclusion is not compromised as also the PE layers contain charged groups. Pore coverage upon coating is confirmed by the reduction in PWP with increasing number of layers, shown in Fig. 4.7a. The PE layers applied on top of 4 hours hydrolyzed PAN support increase the mass transport resistance and thereby lower the PWP to approximately 2.0 L/m^2·h·bar.

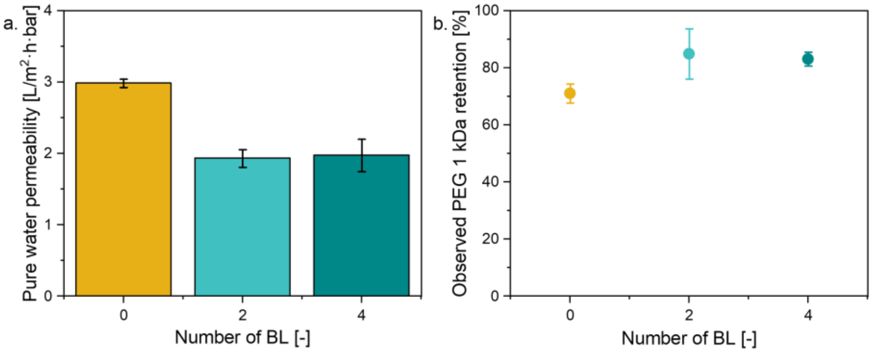

Fig. 4.7: a. The pure water permeability (PWP) [L/m^2·h·bar] versus the number of BL [-] applied on a 4 hours hydrolyzed PAN substrate measured at 5 bar applied pressure and b. the observed PEG 1 kDA retention [%] versus the number of BL [-] applied on a 4 hours hydrolyzed PAN substrate measured at 10 bar applied pressure.

Following the flux-retention trade off, the decrease in flux comes with an increased PEG 1 kDa retention. The increased retention of these smaller sized PEG molecules with a hydrodynamic radius of approximately 1.5 nm indicates that the PE coating enhances size exclusion.

In Fig. 4.8a, the water flux for all membranes increases linearly with the applied pressure confirming that the membranes are pressure stable and that the water flux is convective. Moreover, the addition of PE layers increases the resistance to water permeation which is illustrated by the decreasing water flux with the numbers of BLs applied.

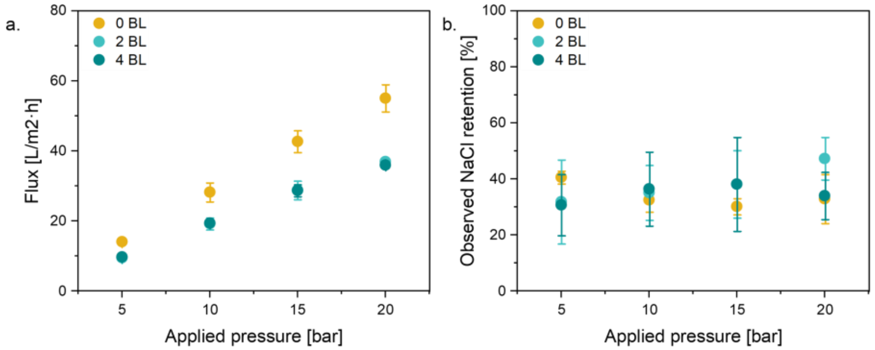

Fig. 4.8: a. The flux [L/m^2·h] and b. The observed NaCl retention [%] versus the applied pressure [bar] for membranes with 0, 2 and 4 BL applied on a 4 hours hydrolyzed PAN substrate using a 1 g/L NaCl feed solution.

Fig. 4.8b shows that the NaCl retention is almost independent of the number of LbL coating layers. The LbL coating creates an approximately constant retention value of 35%. In Fig. 4.9, the retention of various single salt solutions is shown for the different number of BLs. Unlike the retention of monovalent ions, NaCl, the number of LBL coating layers does affect the retention of the divalent ions such as Mg^{2+}, where a significant retention increase is observed with increasing number of BLs. This increase in retention is attributed to the additional effect of size-exclusion originating from the denser LBL coating that amplifies the Donnan exclusion caused by the charge of the support and the final applied PSS PE layer. This additional size exclusion does not show any increase in the Na_2SO_4 retention. This shows that the Donnan exclusion provides a similar amount of rejection as the size exclusion as we observe that regardless of the charge of the cation the amount of rejection reaches similar values for 2 and 4 BLs.

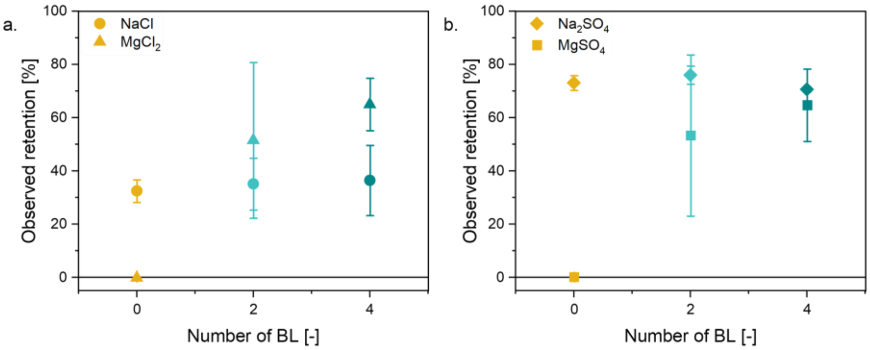

Fig. 4.9: a. The observed retention [%] of NaCl (circles) and $MgCl_2$ (triangles) and b. of Na_2SO_4 (diamonds) and $MgSO_4$ (squares) versus the number of BL [-] applied on 4 hours hydrolyzed PAN substrate measured at 10 bar applied pressure using feed solutions of approximately 1 g/L.

It rarely occurs that a process fluid only consists of one salt type, hence the retention of a mixture of NaCl and $MgSO_4$ is investigated to identify the retention of the specific ions and the effect of ions on each other. Fig. 4.10 shows the observed retention of individual ions in the feed mixture for the uncoated and PE-coated hydrolyzed PAN substrate.

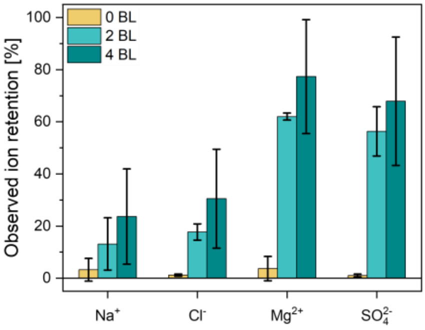

Fig. 4.10: The observed retention [%] of Na^+, Cl^-, Mg^{2+} and SO_4^{2-} ions from a mixture of NaCl and $MgSO_4$ (0.6 and 0.6 g/L respectively) for 0, 2 and 4 BLs applied on a 4 hours hydrolyzed PAN substrate at 10 bar applied pressure.

It is clear that the uncoated membrane (0 BL) does not show any retention for monovalent ions in the salt mixture. This is in contrast to the retentions found for monovalent ions present in a single salt solution, Fig. 6a. This is attributed to the permeation of Mg^{2+} which is attracted to the negative charge of the membrane. This results in ”counter-ion competition”, described by Guo et al. The Mg^{2+} presence in the electrical double layer near the negative membrane surface compensates the charges of the membrane surface and subsequently lowers the charge repulsion for Cl^- and SO_4^{2-} [30]. The PE-coated membranes (2 and 4 BL) do have a higher retention for all ions compared to the uncoated membrane. Here, the highest retention is observed for the multivalent ions when compared to monovalent ions. This is attributed to both size and Donnan exclusion caused by the application of the PE layers. These exclusion mechanisms affect the monovalent ions less due to their smaller size and lower charge density [30]. Moreover, dielectric exclusion, the exclusion based on the required energy for dehydration of an ion, is more relevant for the multivalent ions because their electrostatic interaction with water molecules is greater, resulting in a denser solvation and thus higher dehydration energy that further increases the permeation resistance [27]. Overall, the addition of PE layers on the PAN support results in the formation of an NF membrane with a high multivalent ion retention and limited monovalent ion retention.

4.3.3 ***Crosslinking with glutaraldehyde***

4.3.3.1 Improving retention

Subsequent crosslinking of the PEI layers from the LbL assembly increases the NaCl retention as shown in Fig. 4.11a. This significant doubling in retention towards 70% for low salt concentrations is comparable to that of tight NF or loose RO membranes. As the salt concentration of the feed is increased, the difference in chemical potential between the feed and permeate increases resulting in a higher salt transport. At the same time the water flux decreases due to the higher osmotic pressure difference. These effects reinforce each other resulting in a decrease in retention. Nevertheless, the retention of the crosslinked membrane is still about high compared to the non-crosslinked membrane.

In Fig. 4.11b the retention of specific ions in a mixed solution of NaCl and $MgSO_4$ is presented for the non-crosslinked and crosslinked membranes. Higher retentions are observed for all ions for the crosslinked membrane. The significant increase in retention is a result of more size, dielectric and Donnan exclusion as crosslinking effectively increases polymer network rigidity, reduces swelling and increases charge density, thus increasing exclusion. The retention improved mainly for the monovalent ions in comparison to the multivalent ions as for the monovalent ions the effect of dielectric exclusion is enhanced by the narrower pathways.

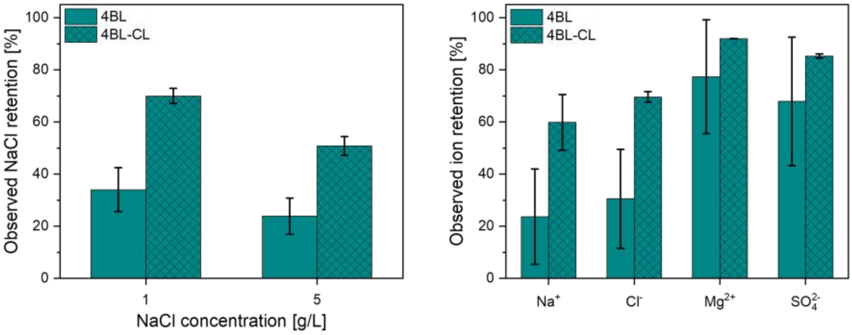

Fig. 4.11: a. The observed NaCl retention [%] for 4 BL and 4 BL-CL (crosslinked) of 1 g/L and 5 g/L NaCl solution at 10 bar applied pressure for membranes with BLs applied on a 4 hours hydrolyzed PAN substrate. b. The observed retention [%] of Na^+, Cl^-, Mg^{2+} and SO_4^{2-} ions from a mixture of NaCl and $MgSO_4$ (0.6 and 0.6 g/L respectively) for for 4 BL and 4 BL-CL (crosslinked). The measurements were performed at 10 bar applied pressure.

Similarly, the rigid PE network increases the resistance for water permeation. This behavior is observed after crosslinking the 4-hour hydrolyzed PAN with four BLs: crosslinking reduces the PWP with 25% to 1.5 L/m^2·h·bar (Fig. S4.2). The crosslinked PE network on the hydrolyzed PAN support results in the best performance of approximately 50% NaCl retention with a corresponding flux of 17.5 L/m^2·h with a 5 g/L NaCl feed solution.

4.3.3.2 Contribution to nutrient separation

Crosslinking the PE layers results in more restricted pathways that increases the permeation resistance and plays an important role in selectivity performance between NH_4^+ and K^+. As addressed in the introduction, the separation of NH_4^+ and K^+ is challenging due to the similarity in size and charge of these two ions. Nevertheless, it is an important separation for applying tailored fertilization what is necessary to create a more sustainable agricultural sector. We investigated the application of a 4 BL crosslinked PE coated hydrolyzed PAN support for the separation of TAN and K, as the three-step modified support provides several exclusion mechanisms.

The left side of Fig. 4.12 shows the retention of TAN and K for an artificial feed at different pH values. These pH values were chosen based on the NH_4^+/NH_3

equilibrium as within this range the equilibrium moves from NH_4^+ to NH_3 [3]. The last two bars of Fig. 4.12 show the separation of N and K using pre-treated real manure digestate at pH 10.

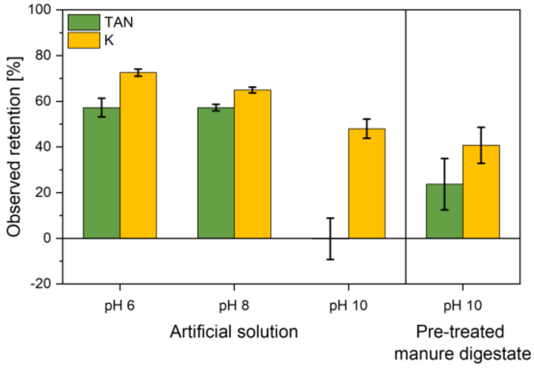

Fig. 4.12: The retention [%] of TAN and K for a mixed salt solution at different pH values measured at an applied pressure of 20 bar and pre-treated manure digestate at pH 10 measured at an applied pressure of 30 bar for the membrane with 4 crosslinked BLs applied on a 4 hours hydrolyzed PAN substrate.

At pH 6 approximately all TAN is present as NH_4^+ while also PEI is at its maximum charge. At that pH, both species, TAN and K are present as monovalent cations and have the same size (Table S4.1). Although the ions have the same size and charge, a lower retention of TAN is observed compared to K^+ which is attributed to the difference in dehydration energy, the energy needed to remove the water molecules from the solvated ions. As the dehydration energy of NH_4^+ is slightly lower than that of K^+ [31], NH_4^+ preferentially permeates the membrane. The difference in retention between NH_4^+ and K^+ reaches 16%, which is higher than observed for RO membranes proving that crosslinked PE layers can provide some selectivity based on the dehydration energy differences and thus dielectric exclusion [3]. At pH 8 merely 5% of the TAN is converted to NH_3 while the PEI charge density drops to 75%. Here the retention of TAN seems unaffected while the retention of K drops slightly due to lower charge density in the selective PE layers, thus lowering the contribution of Donnan exclusion. At pH 10, 85% of the TAN is present as NH_3 whereas the charge density of PEI drops drastically to only 15%. The shift in NH_4^+/NH_3 equilibrium results in a drop in TAN retention as NH_3 can more easily permeate the membrane due to its smaller size and lack of charge and thus lack of Donnan exclusion. Due to the also lower charge density of PEI at this pH, the contribution of the Donnan exclusion decreases even further resulting in a lower K retention in comparison to the lower pH values. Nevertheless, the retention of K remains relatively high, which combined with lack of retention for TAN results in higher separation at pH 10 compared to pH 6.

On the right side of Fig. 4.12, the TAN and K retention at pH 10 for real pre-treated manure digestate are presented. Also, here 85% of the TAN is present as neutral NH_3, and the charge density of PEI is 15%. Contrary to the artificial stream, the real digestate contains next to TAN and K also other species like multivalent ions and organic matter, which influences the retentions significantly. During permeation, organic matter accumulates on top of the crosslinked LbL coated layer creating an additional resistance against mass transfer. This leads to an increase in TAN retention in comparison to the retentions observed for the artificial stream at pH 10. This increased permeation resistance is confirmed by the drop in flux from 17.3 for the artificial solution to 14.3 $L/m^2 \cdot h$ for the manure digestate. On the other hand, the K retention is slightly lower compared to the use of artificial feed, which can be attributed to the interaction of the ionic species present in manure with the charges in the PE layer. This leads to compensation of the membrane charges resulting in a lower charge density of the membrane and associated Donnan exclusion and thus a drop in retention, as seen before when the charge density of PEI is changed by changing the pH of the solution. For real manure digestate this translates into separation of the monovalent ions K and N but at a lower value than obtained for artificial streams, as also found for conventional RO membranes [3].

4.4 Conclusion

The investigation of different modifications of an UF PAN membrane has led to further understanding of the exclusion mechanisms and corresponding rejection of specific ions. PAN hydrolysis increases the charge density of the membrane and thereby induces Donnan exclusion, causing NaCl rejection. The negative charge of the selective layer also attracts multivalent cations, such as Mg^{2+}, causing charge compensation that, in a complex ionic mixture, results in reduced retention due to a decrease in Donnan exclusion while the pores are too large to establish separation by size exclusion. The application of PE layers on top of the porous PAN support provide size exclusion in addition to Donnan exclusion because the pores are covered with PE layers increasing retention, especially for multivalent ions like Mg^{2+}. Additional crosslinking of these PE layers makes the selective layer more rigid and the overall membrane less susceptible to swelling. This crosslinking increases ion retention due to an increased permeation resistance of the ions through the membrane. In general, this leads to an enhanced selective permeation based on ion dehydration energy for ions with similar size and charge such as NH_4^+ and K^+. The separation of NH_4^+ and K^+, essential fertilizers present in manure digestate, is further enhanced when operating in alkaline conditions above the pKa of NH_4^+, where the NH_4^+/NH_3 equilibrium shifts towards NH_3. This allows the separation of the small and neutral NH_3 molecule from the larger and charged K^+ ion with the latter experiencing a higher mass transfer resistance for permeating through the hydrolyzed crosslinked PE membrane. The proposed membrane modifications together with customized process conditions allow the separation of manure digestate nutrients in both a K-enriched and an N-enriched fraction which increases the applicability of animal fertilizers while tailored fertilization made possible does not burden the environment with leaching out and emissions of nutrients.

4.5 References

[1] G.L. Velthof, “Mineral concentrate from processed manure as fertiliser,” 2015, Available: https://edepot.wur.nl/352930.

[2] P. Hoeksma and F.E. de Buisonjé, “Production of mineral concentrates from animal manure using reverse osmosis,” 2015. [Online]. Available: https://edepot.wur.nl/364053.

[3] M. van der Wal, J. van Alphen, K. Nijmeijer, and Z. Borneman, “Dynamic ammonium retention for nutrient separation from manure digestate,” *Waste Manag.*, vol. 190, no. October, pp. 644–653, 2024, doi: 10.1016/j.wasman.2024.10.034.

[4] D. Scheepers, J. De Keizer, Z. Borneman, and K. Nijmeijer, “The pH as a tool to tailor the performance of symmetric and asymmetric layer-by-layer nanofiltration membranes,” *J. Memb. Sci.*, vol. 670, no. October, 2023, doi: 10.1016/j.memsci.2022.121320.

[5] D. Scheepers, Z. Borneman, and K. Nijmeijer, “Nanofiltration membrane performance of layer-by-layer membranes with different polyelectrolyte concentrations,” *Desalination*, vol. 574, no. July, 2024, doi: 10.1016/j.desal.2023.117246.

[6] H.F.M. Austria *et al.*, “Investigation of salt penetration mechanism in hydrolyzed polyacrylonitrile asymmetric membranes for pervaporation desalination,” *Desalination*, vol. 463, no. March, pp. 32–39, 2019, doi: 10.1016/j.desal.2019.04.012.

[7] P.H.H. Duong, J. Zuo, and T. Chung, “Highly crosslinked layer-by-layer polyelectrolyte FO membranes : Understanding effects of salt concentration and deposition time on FO performance,” *J. Memb. Sci.*, vol. 427, pp. 411–421, 2013, doi: 10.1016/j.memsci.2012.10.014.

[8] C. Qiu, S. Qi, and C. Y. Tang, “Synthesis of high flux forward osmosis membranes by chemically crosslinked layer-by-layer polyelectrolytes,” *J. Memb. Sci.*, vol. 381, no. 1–2, pp. 74–80, 2011, doi: 10.1016/j.memsci.2011.07.013.

[9] Y. Guo, H. Zhang, X. Zhang, X. Hu, C. Wang, and Y. Yang, “Study on properties of ultrafiltration membrane prepared by hydrolyzed polyacrylonitrile,” *Desalin. Water Treat.*, vol. 207, pp. 10–19, 2020, doi:

10.5004/dwt.2020.26368.

[10] P.Á. Leyre, L. Ruiz-rubio, I. Moreno, and J.L. Vilas-vilela, “Characterization and Optimization of the Alkaline Hydrolysis of Polyacrylonitrile Membranes,” pp. 1–11, 2019, doi:10.3390/polym11111843.

[11] P.R. Sruthi and S. Anas, “An overview of synthetic modification of nitrile group in polymers and applications,” *J. Polym. Sci.*, vol. 58, no. 8, pp. 1039–1061, 2020, doi: 10.1002/pol.20190190.

[12] G. Zhang, H. Meng, and S. Ji, “Hydrolysis differences of polyacrylonitrile support membrane and its influences on polyacrylonitrile-based membrane performance,” *Desalination*, vol. 242, no. 1–3, pp. 313–324, 2009, doi: 10.1016/j.desal.2008.05.010.

[13] H.R. Lohokare, S.C. Kumbharkar, Y.S. Bhole, and U.K. Kharul, “Surface Modification of Polyacrylonitrile Based Ultrafiltration Membrane,” no. July, 2005, doi: 10.1002/app.23917.

[14] H.R. Lohokare, M.R. Muthu, G.P. Agarwal, and U.K. Kharul, “Effective arsenic removal using polyacrylonitrile-based ultrafiltration (UF) membrane,” *J. Memb. Sci.*, vol. 320, no. 1–2, pp. 159–166, 2008, doi: 10.1016/j.memsci.2008.03.068.

[15] K.D. Collins, “Charge density-dependent strength of hydration and biological structure,” *Biophys. J.*, vol. 72, no. 1, pp. 65–76, 1997, doi: 10.1016/S0006-3495(97)78647-8.

[16] E.R. Nightingale, “Phenomenological theory of ion solvation. Effective radii of hydrated ions,” *J. Phys. Chem.*, vol. 63, no. 9, pp. 1381–1387, 1959, doi: 10.1021/j150579a011.

[17] R.W. Baker, *MEMBRANE TECHNOLOGY*, 2th ed. John Wiley & Sons, Ltd., 2004.

[18] R.W. Baker and H. Strathmann, “Ultrafiltration of Macromolecular Solutions with High-Flux Membranes,” *J. Appl. Polym. Sci.*, vol. 14, pp. 1197–1214, 1970.

[19] E.M. Renkin, “Filtration, diffusion, and molecular sieving through porous cellulose membranes.,” *J. Gen. Physiol.*, vol. 38, no. 2, pp. 225–243,

1954.

[20] J.A. Regenspurg, W.A. Jonkers, M.A. Junker, I. Achterhuis, E. Brinke, and W.M. de Vos, “Polyelectrolyte multilayer membranes : An experimental review,” *Desalination*, vol. 583, no. January, 2024, doi: 10.1016/j.desal.2024.117693.

[21] E.N. Durmaz, S. Sahin, E. Virga, S. De Beer, L.C.P.M. de Smet, and W.M. de Vos, “Polyelectrolytes as Building Blocks for Next-Generation Membranes with Advanced Functionalities,” *ACS Appl. Polym. Mater.*, vol. 3, no. 9, pp. 4347–4374, 2021, doi: 10.1021/acsapm.1c00654.

[22] J. Kamp, S. Emonds, M. Seidenfaden, P. Papenheim, M. Kryschewski, J. Rubner and M. Wessling, “Tuning the excess charge and inverting the salt rejection hierarchy of polyelectrolyte multilayer membranes,” *J. Memb. Sci.*, vol. 639, no. March, 2021, doi: 10.1016/j.memsci.2021.119636.

[23] D. Scheepers, B. Chatillon, K. Nijmeijer, and Z. Borneman, “Asymmetric layer-by-layer polyelectrolyte nanofiltration membranes with tunable retention,” *J. Polym. Sci.*, no. April, pp. 1293–1304, 2021, doi: 10.1002/pol.20210166.

[24] D.M. Reurink, J.D. Willott, H.D.W. Roesink, and W.M. De Vos, “Role of Polycation and Cross-Linking in Polyelectrolyte Multilayer Membranes,” *ACS Appl. Polym. Mater*., vol. 2, pp. 5278-5289, 2020, doi: 10.1021/acsapm.0c00992.

[25] A. Casimiro, C. Weijers, Z. Borneman, and K. Nijmeijer, “Kosmotropes and chaotropes : Specific ion effects to tailor layer-by-layer membrane characteristics and performances,” vol. 672, no. February, 2023, doi: 10.1016/j.memsci.2023.121446.

[26] O.A. Kazi, W. Chen, J.G. Eatman, F. Gao, Y. Liu, Y. Wang, Z. Zia and S.B. Darling, “Material Design Strategies for Recovery of Critical Resources from Water,” *Adv. Mater.*, vol. 35, no. 36, pp. 1–34, 2023, doi: 10.1002/adma.202300913.

[27] R. Epsztein, E. Shaulsky, N. Dizge, D.M. Warsinger, and M. Elimelech, “Role of Ionic Charge Density in Donnan Exclusion of Monovalent Anions by Nanofiltration,” *Environ. Sci. Technol.*, vol. 52, no. 7, pp.

4108–4116, 2018, doi: 10.1021/acs.est.7b06400.

[28] Y. Liu, G.Q. Chen, X. Yang, and H. Deng, “Preparation of layer-by-layer nanofiltration membranes by dynamic deposition and crosslinking,” *Membranes (Basel).*, vol. 9, no. 2, 2019, doi: 10.3390/membranes9020020.

[29] R. Zimmermann, U. Freudenberg, R. Schweiß, D. Küttner, and C. Werner, “Hydroxide and hydronium ion adsorption - A survey,” *Curr. Opin. Colloid Interface Sci.*, vol. 15, no. 3, pp. 196–202, 2010, doi: 10.1016/j.cocis.2010.01.002.

[30] H. Guo, X. Gao, K. Yu, X. Wang, and S. Liu, “Ion adsorption on nanofiltration membrane surface and its effect on rejection of charged solutes : A zeta potential approach,” *Sep. Purif. Technol.*, vol. 326, no. July, 2023, doi: 10.1016/j.seppur.2023.124830.

[31] K.P.S. Piash, R. Anwar, C. Shingleton, R. Erwin, L.S. Lin, and O. Sanyal, “Integrating chemical precipitation and membrane separation for phosphorus and ammonia recovery from anaerobic digestate,” *AIChE J.*, no. August, pp. 1–13, 2022, doi: 10.1002/aic.17869.

[32] Y. Marcus, “Thermodynamics of Solvation of Ions,” *J. Chem. Soc., Faraday Trans.*, vol. 89, no. 4, pp. 713–718, 1993.

S4 Supplementary information

S4.1 Ion characteristics

Table S4.1: The stokes radius [nm], hydrated radius [nm], valency [-] and hydration energy [kJ/mol] of the various ions investigated.

Ion	Stokes radius[a] [nm]	Hydrated radius[a] [nm]	Valency [-]	Hydration energy[b] [kJ/mol]
Sodium	0.184	0.358	+1	-365
Chloride	0.121	0.332	-1	-340
Magnesium	0.347	0.428	+2	-1830
Sulphate	0.230	0.379	-2	-1080
Potassium	0.125	0.331	+1	-295
Ammonium	0.125	0.331	+1	-285

[a] Nightingale et al. [1], [b] Marcus et al.[2]

S4.2 Zeta potential

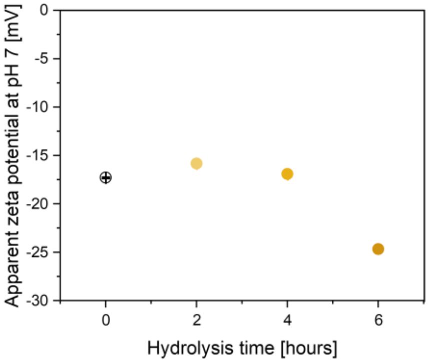

Fig. S4.1: The apparent zeta potential [mV] at pH 7 versus the hydrolysis time [h].

S4.3 Influence of PE layers and crosslinking on pure water permeability

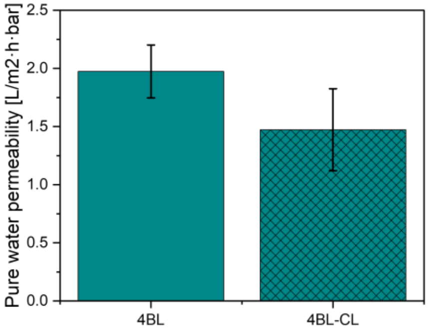

Fig. S4.2: The pure water permeability (PWP) [L/m^2·h·bar] for the 4 hours hydrolyzed PAN substrate with 4 BL measured at 5 bar applied pressure and the 4 hours hydrolyzed PAN substrate with 4 BL crosslinked measured at 10 bar applied pressure

S4.4 References

[1] E.R. Nightingale, “Phenomenological theory of ion solvation. Effective radii of hydrated ions,” *J. Phys. Chem.*, vol. 63, no. 9, pp. 1381–1387, 1959, doi: 10.1021/j150579a011.

[2] Y. Marcus, “Thermodynamics of Solvation of Ions,” *J. Chem. Soc., Faraday Trans.*, vol. 89, no. 4, pp. 713–718, 1993.

CHAPTER 5

Bipolar membrane electrodialysis enhanced nutrient separation in manure treatment

Abstract:

To improve circularity in the agricultural sector, the nutrients nitrogen (N) and potassium (K) present in manure must be separated. This can be achieved by reverse osmosis (RO) under alkaline conditions where NH_4^+ is converted to neutral NH_3 for selective permeation while K^+ is retained by the membrane. The NH_3 in the collected permeate can be concentrated after acidification, where the NH_3 is converted back to NH_4^+, in a second RO step to produce valuable liquid N-fertilizer. In this chapter, the OH^- and H^+ required for the separation of the nutrients is produced in-situ by bipolar membranes, known for their high water dissociation rate. The process becomes more sustainable by saving on transportation, storage and dilution by adding aqueous alkali and acid. For system validation, first a water dissociation experiment was performed in a membrane stack with three compartments fed with a NaCl solution. Follow-up experiments were done with artificial model solutions and co-digested manure digestate. It was found that the NaCl feed and the artificial feed stream showed similar performance for both the OH^- and H^+ compartments. On the other hand, the real co-digested manure showed an effective OH^- production for the conversion of NH_4^+ to NH_3 that was half of the effective production of the acid compartment. This lower efficiency of the base compartment is due to the presence of other components in the manure digestate. The surplus in H^+ production can be used as acid for other processes in the manure treatment.

This chapter was submitted as:

M. van der Wal, R. Rovai, K. Nijmeijer, Z. Borneman, Bipolar membrane electrodialysis enhanced nutrient separation in manure treatment, **2025**

5.1 Introduction

To meet the environmental directives of the EU, the agricultural sector puts significant efforts to contribute to the societal challenges of limiting nitrogen and (climate driven) CO_2 emissions into the environment. To minimize emissions to air and leaching of nutrients to ground and surface water, manure fractionating is a valuable approach to achieve a balanced crop fertilization strategy. Relevant in this context is the separation of the liquid manure digestate stream in a nitrogen (N) and a potassium (K) rich fraction. Controlled use of both fractions enhances tailored fertilization and local circularity as the nutrients can be used as substitute for artificial fertilizer [1]. These N and K nutrients are, after digestion, present in the liquid fraction as ammonium ions (NH_4^+) and potassium ions (K^+). Due to the similarity in their size and charge, separation of NH_4^+ and K^+ through membrane filtration is challenging as nanofiltration and reverse osmosis (RO) provide separation based on size and/or charge exclusion [2]. A distinct difference between both components though, is their sensitivity to pH. The previous chapters shows that alkaline conditions can be employed to push the acid-base equilibrium from NH_4^+ to NH_3 (Fig. S5.1), after which the uncharged NH_3 can be separated from the charged K^+ ions by selective permeation through an RO membrane [3].

This RO separation is effective at pH values above 10 where at least 85% of the nitrogen is present as NH_3. This separation leads to a permeate that is enriched in N and a concentrated retentate that is enriched in K [3]. The permeate is a clean diluted stream with a low osmotic pressure that can be easily concentrated with an additional, second RO step. This increases its value as land application becomes more efficient and meanwhile transportation costs are reduced. To shift the equilibrium and ensure that all N is present as NH_4^+ and thus retained by the second RO concentrating step, acidification of the permeate is required towards approximately pH 6 for the best performance [3], [4]. Separation and concentration of nutrients with RO thus requires a two-step process with in the first step an increase in pH of the liquid manure digestate to separate the N from K while simultaneously concentrating the K in the digestate, and acidification in the second step necessary to concentrate the diluted N in the RO permeate [3]. These two significant pH adjustments require corrosive aqueous chemicals that must be stored on-site and when used result in dilution of the mineral streams while the aim is to prepare the opposite, i.e., mineral concentrates by water removal.

Bipolar membrane electrodialysis (BMED) is a very elegant method for the local production of base and acid and offers an opportunity to circumvent the afore mentioned disadvantages when integrated into the described nutrient separation and concentration process [5]. The hydroxide ions (OH^-) produced in the BMED system can be used to convert NH_4^+ to NH_3 that allows separation of NH_3 from K^+ in the first RO step, whereas the produced H^+ in the acid compartment can be used to convert NH_3 back to NH_4^+ that allows concentration in the second RO step (Fig. 5.1).

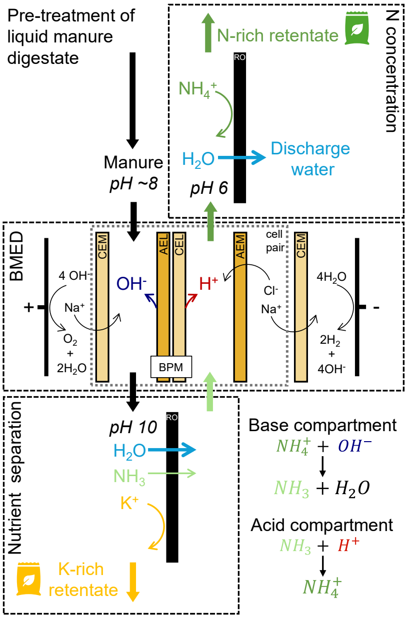

Fig. 5.1: Schematic overview of a three-compartment BMED system (middle square) combined with the respective RO steps (top and bottom squares) for the formation of a K-rich retentate and an N-rich retentate.

In Fig. 5.1, the BMED system is shown with the conversion of an electrical current, which can be supplied from renewable energy, into an ionic current via redox reactions, for example hydrogen and oxygen evolution, at the electrodes. The produced ionic current is selectively carried through ion exchange membranes, cation exchange membranes (CEM) and anion exchange membranes (AEM), whereas the bipolar membrane (BPM) dissociates water into hydroxide ions (OH^-) and protons (H^+) at the interface between the cation and anion exchange layers (CEL and AEL). The OH^- migrates to the compartment on the anode side creating a basic solution while the H^+ migrates to the compartment on the cathode side creating an acid solution. The BPM dissociates water more than a million times faster than in aqueous solutions due to the combination of a strong electrical field and protonation-deprotonation reactions at the thin junction between the AEL and CEL [6], [7]. In addition, the BPM water dissociation is energy efficient when compared to traditional methods and is environmentally friendly because it uses less harsh chemicals and minimizes waste [8].

The most useful configuration is a three-compartment configuration adding next to the base and acid compartment a salt compartment to maintain electroneutrality and to ensure higher quality of the base and acid streams [6]. The efficiency and quality of the base and acid streams depend on the amount of ion leakage that passes through the membranes. This ion leakage, i.e., crossover, is related to the so-called permselectivity of the membranes. The permselectivity is a measure of the fraction of the current that is transported through the membrane by the desired counter-ion transport and how much current is lost via diffusion or migration of the co-ions [9]. Moreover, specifically the presence of neutral NH_3 can lead to additional leakage through the BPM and the other membranes [10]. The permselectivity affects the overall concentration of OH^- and H^+ and thus the current efficiency and energy consumption.

Earlier studies have shown that electrodialysis (ED) can facilitate the removal of NH_4^+ from an anaerobic digester stream, containing amongst others K^+, NH_4^+, Na^+ and Cl^-, by selective transport of NH_4^+ through a CEM resulting in an N-enriched receiving compartment [11]. This method has been combined with stripping and RO to subsequently increase the N concentration. However, in this approach, the NH_4^+/NH_3 equilibrium shift towards NH_3 resulting in evaporation and thus losses of N [12], [13]. Other previous studies already utilized the BMED system to treat N-containing wastewater streams with lower N losses [10], [14]–[17]. In these studies, the NH_4^+/NH_3 equilibrium is used as an advantage. Due to the migration of ions in the electrical field, the NH_4^+ moves towards the base compartment through a CEM where the conversion to NH_3 occurs due to the reaction with OH^- that is produced in the BPM junction. Next, this N-rich stream is treated in a stripper or membrane contactor, to capture the NH_3 in an acid solution [10], [14]–[17].

Opposite to the work described above, in this chapter the BMED system is used for the integrated production of OH^- and H^+ for the required shift in the NH_3/NH_4^+

equilibrium for the separation and concentration of N and K with RO. This reduces the transport and storage of corrosive base and acids at the manure treatment site. In addition, the production of the base and acid when achieved with renewable energy further decreases the environmental impact of the agricultural sector. The bycatch of the coupled BMED with RO process is the production of high-quality water, free of discharge costs. Moreover, here the BMED feed streams directly originating from the manure treatment process, the OH^- and H^+ produced can react immediately with the total ammonium nitrogen (TAN) present. As a result, no additional water is added in contrast to external dosing of base and acid solutions where inherent dilution decreases the efficiency of the concentration process. In this chapter, a batch process was chosen to demonstrate the principle with a three-compartment system with one cell pair, consisting of an AEM, CEM and BPM, and with sodium sulphate as electrolyte, to gain insight into the production rate and associated conversion. First, this is done for artificial model solutions and based on the obtained results, to complement the work, also a real digestate stream is used. On a large scale, the production rate requires to be coupled with the conversion of a certain TAN concentration and volume. Alignment can be reached with a suitable process type like batch, feed and bleed or a continuous modus [9].

5.2 Materials and methods

5.2.1 Chemicals and materials

The sodium chloride Sanal® P (pharmaceutical grade) was kindly supplied by Akzonobel (currently Nouryon), the Netherlands. Ammonium chloride (98+%), potassium chloride (99+%), and sodium sulphate decahydrate (99+%) were purchased at Thermo Scientific, the Netherlands. Sodium hydroxide solution (50%) was purchased from Merck, Germany. The 1 M hydrochloric acid solution was retrieved from Honeywell Fluka, USA.

5.2.2 Stack assembly

The BMED stack, REDstack B.V., the Netherlands, was built as a three compartment system, see BMED part in Fig. 5.1, using a BPM, two CEM shielding membranes for the electrolyte compartments and an AEM. All membranes were purchased from Fumatech, Germany and the characteristics are given in Table S5.1.

The electrolyte compartments were closed with CEM, the BPM was placed with the AEL towards the anode and the CEL towards the cathode. Next to the CEL an AEM was used to close the acid compartment and form a salt compartment. The compartments consisted of woven gasket integrated spacers (Deukum GmbH, Germany) with approximately 80% porosity, a thickness of 0.048 cm and an area of 10 x 10 cm^2. The endplates had embedded platinized titanium mesh electrodes (MAGNETO Special Anodes BV, the Netherlands) with each an active area of $9.8 \times 9.8\,cm^2$ to convert the electric current into an ionic current. Different current densities were applied (1, 5 and 10 mA/cm^2) with an ES 030-5 power supply (Delta Elektronika, the Netherlands). The corresponding voltage was measured with a XDM2041 digital multimeter (Owon, China). For the current conversion, an electrolyte solution of 1 L of 0.5 M Na_2SO_4 solution was used. The salt compartment was filled with 0.5 L of 0.5 M (29.22 g/L) NaCl solution. For the acid and base compartments various solutions, NaCl, artificial and real manure digestate, were applied in different configurations as presented in Table S5.2.

The acid and base production rate of the system was determined using a 0.5 M NaCl solution as starting solution in the base and acid compartments. Next, the conversion of TAN in the BMED system was investigated with artificial solutions. The concentrations of the artificial solutions in the base and acid compartments were mimicking the real digestate and the permeate concentrations obtained during the process, without BMED [3]. All concentrations and pHs used in this research are listed in Table 5.2. Lastly, pre-treated real liquid manure digestate (kindly provided by Duurzaam Landleven Bernheze, the Netherlands) was used as starting solution in the base compartment next to the artificial solution in the acid compartment. The solutions were pumped with two peristaltic pumps with double pump heads (Masterflex, the Netherlands). The base, acid and salt solutions were recirculated with a linear flow velocity of 1 cm/s.

5.2.3 Water dissociation with model system

The stack with the three-compartment configuration was evaluated with NaCl solution to investigate the production of OH^- and H^+ in duplo. The system ran for 30 minutes during which the voltage was recorded every 5 minutes and samples of 2 mL were taken. The pH of the samples was determined with an EC600 pH probe (Extech instruments, USA) where for the base samples acid titration was used. The effective production of OH^- and H^+, Δn (mmol), in time was determined using the logarithmic correlation between the measured pH and concentration of OH^- and H^+. The difference in concentration resulted in the production per time step after taking into account a stabilization time of 5 minutes after initial production, as shown in Eq. 5.1 and Eq. 5.2 using the *pH* (-) and the volume *V* (L) corrected for the sampling at the respective time step.

$$\Delta n_{OH^-} = (10^{-(14-pH_{(t+1)})} \cdot V_{t+1} - 10^{-(14-pH_{(t)})} \cdot V_t) \cdot 10^3 \qquad \textit{Eq. 5.1}$$

$$\Delta n_{H^+} = (10^{-pH_{(t+1)}} \cdot V_{t+1} - 10^{-pH_{(t)}} \cdot V_t) \cdot 10^3 \qquad \textit{Eq. 5.2}$$

The current efficiency and energy consumption were based on the production rate $\dot{n}_i$ (mmol/min) that followed from the slope of the effective production divided by 60 to convert to mmol/s. The current efficiency η_i (-) was calculated as shown in Eq. 5.3. Here the *I* is the applied current (A) and *F* is the Faradaic constant (96485 C/mol), the subscript *i* represents either H^+ or OH^-.

$$\eta_i = \frac{\dot{n}_i/60}{I/(F \cdot 10^{-3})} \qquad \textit{Eq. 5.3}$$

The energy consumption for H^+ and OH^- (Wh/mol) is calculated using Eq. 5.4 with the stack potential *E* (V), the current *I* (A) and the production rate $\dot{n}_i$ (mmol/min) corrected to convert to mol, the subscript *i* represents either H^+ or OH^-. The value of 60 is required to correct for the time.

$$Energy\ consumption_i = \frac{E \cdot I \cdot 60}{\dot{n}_i \cdot 10^{-3}} \qquad \textit{Eq. 5.4}$$

5.2.4 TAN conversion in BMED system

The BMED system was evaluated with artificial solutions with KCl and NH_4Cl in the base and NH_4Cl in the acid compartment. In addition, the system was used in the same way but now with manure digestate in the base compartment. For the real manure digestate, the volume of the feed recirculated in the base compartment was half of the volume in the acid compartment, Table S5.2, to provide a more balanced system in terms of required OH^- and H^+ production. The aim was to achieve a pH of 10 in the base compartment and 6 or lower in the acid compartment so that appropriate TAN conversion takes place to separate the nutrients K^+ and NH_3 with RO in the base stream and to concentrate NH_4^+ in the acid stream. During the production of OH^- and H^+, the equilibrium of TAN was shifted as a result of the reactions between the produced ions and respective TAN form. Therefore, the effective production of OH^- and H^+ is defined as the sum of the pH change and the amount of OH^- or H^+ used for TAN conversion. Here, the *pH* and the *pKa*, 9.25 for the NH_4^+/NH_3 equilibrium, was used as tool to determine the amount of conversion using the rewritten Henderson-Hasselbach equations shown in Eq. 5.5 and Eq. 5.6, and simultaneously for the contribution of the produced OH^- and H^+ to the pH change as previously described in Eq. 5.1 and Eq. 5.2.

$$[NH_3] = \frac{[TAN]}{\left(1 + \frac{10^{-pH}}{10^{-pKa}}\right)} \qquad \textit{Eq. 5.5}$$

$$[NH_4{}^+] = [TAN] - \frac{[TAN]}{\left(1 + \frac{10^{-pH}}{10^{-pKa}}\right)} \qquad \textit{Eq. 5.6}$$

To determine the conversion of the total amount of TAN, the concentration of the ions, including Na^+ and K^+, was monitored using ion chromatography (Aquion system with a Ionpac CS12A cation column with methyl sulfonic acid eluent (Thermo Fisher, the Netherlands)). Hence, 2 mL samples were taken at specific time intervals to measure the pH and ion concentrations. From these samples the production of OH^- and H^+ per unit of time was determined as the sum of the OH^- or H^+ attributed to pH change and conversion of TAN. This leads to the production rate which is equal to the slope of the production versus the time. Similar as previously discussed, this information was used to calculate the current efficiency (Eq. 5.3) and energy consumption (Eq. 5.4).

5.3 Results and discussion

5.3.1 Producing acid and base in model system

The production of OH^- and H^+ with 0.5 M NaCl as starting solution was monitored over time as shown in Fig. 5.2. The production of both OH^- and H^+ shows a linear trend correlating to a constant production rate indicating a stable operation in time. The linear trend follows from the constant efficiency of the process in which a set number of the electrons, delivered by the external power source, per unit time is used for water dissociation. However, the production observed in the system is lower than the theoretical production calculated based on the number of electrons (i.e., current) supplied. Hence, not all electrons are used for the dissociation and/or some of the produced OH^- and H^+ products leak away through crossover phenomena because of not 100% permselective membranes. This difference between the theoretical maximum and the measured effective production results mainly from migration and diffusion through the membranes. The unwanted migration of co-ions increases with increasing ion transport and thus with increasing current density, while the contribution of diffusion remains constant because it is independence of the current density [10], [18]. Hence, the difference between the theoretical and measured effective production is larger at the lowest current density of 1 mA/cm^2 as here the contribution of diffusion is relatively the highest. The CEM used in this chapter has a permselectivity for K^+ over Cl^- of 97% and the Cl^- over K^+ permselectivity of the AEM is 92%. Considering that OH^- and H^+ have a higher ion mobility than Cl^- and K^+ respectively, OH^- and H^+ leakage is typically higher than indicated by the standard permselectivity values reported for the CEM and AEM [19]. Moreover, the difference observed between OH^- and H^+ at this low current density is the result of measurement sensitivity.

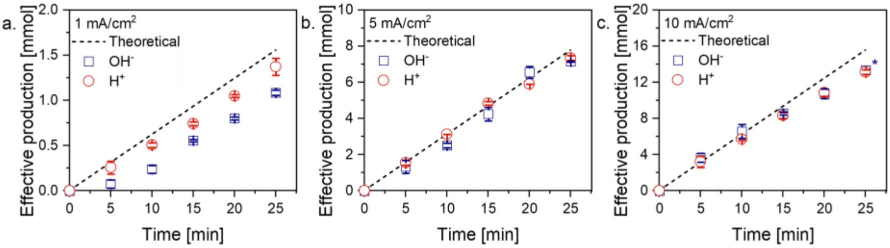

Fig. 5.2: Effective production of OH^- (squares, blue) and H^+ (circles, red) [mmol] versus the time [min] for a current density of a. 1 mA/cm^2, b. 5 mA/cm^2 and c. 10 mA/cm^2 in the system starting with 0.5 M NaCl as feed. All experiments were done in duplicate with the standard deviation presented by the error bars (indicates a point based on a single measurement). The dashed lines represent the theoretical maximum production for the respective current densities.*

The production rates that follow from the production in time, amongst other performance parameters, are shown in Table 5.1. The production rate, the slope of the production over time, increases linearly with the current density. The production rates vary between 73 and 98% of the theoretical values of 0.06, 0.31 and 0.62 mmol/min for 1, 5 and 10 mA/cm^2 respectively. This difference between theory and practical application is often observed for BMED systems and as discussed attributed to OH^- leakage through the CEM and H^+ leakage through the AEM [10]. As mentioned before, the diffusion is independent of the current density while migration is dependent hence the lowest efficiencies are found for 1 mA/cm^2.

Table 5.1: Performance results of the system with 0.5 M NaCl as feed for different current densities.

Current density [mA/cm²]	**Applied current [A]**	**Stack potential [V]**	**Production rate [mmol/min]**		**Current efficiency [%]**		**Energy consumption [Wh/mol]**	
			OH^-	*H^+*	*OH^-*	*H^+*	*OH^-*	*H^+*
1	0.10	3.21	0.05	0.05	73	87	118	99
5	0.50	3.81	0.30	0.29	98	95	104	108
10	1.00	4.30	0.51	0.52	83	84	139	137

To validate whether the redox reactions in the electrolyte compartment may play a role in the lower efficiency, the same experiment with an iron couple as electrolyte ($FeCl_2$/$FeCl_3$) was performed, showing identical behavior in terms of production over time. This redox couple was chosen as compared to Na_2SO_4 this couple does not produce gas and OH^-, next to this it has a lower standard electrode potential which lowers the overall energy consumption. The results indicate that different redox reactions do not alter the efficiency (Fig. S5.2 and Table S5.3).

The current efficiency in Table 5.1 is calculated as the ratio of the measured and theoretical production rate. This shows that 100% efficiency is not reached, which is attributed to leakage and inefficient conversion of the electric current to the ionic current. Typically, the efficiency should improve with increasing current density as the attribution of diffusive ion leakage becomes less. Nevertheless, no clear trend is observed and the found difference between the efficiency values can be attributed to the standard deviation found for the experimental procedure. Table 5.1 also shows a difference between the energy consumption for OH^- and H^+ at a current density of 1 mA/cm^2 due to the slight difference in production rate. At 5 mA/cm^2, we observe lower energy consumptions than for the highest current density which is linked to the difference in efficiency and thus lays within the deviation of the experimental procedure. The energy consumption as listed in Table 5.1, is on the high side compared to what is observed in other BMED systems for acid and base production, where the energy consumption ranges from 15 to 125 Wh/mol from laboratory scale to industrial pilots [9], [18], [20], [21]. Considering the energy price in 2022 in the Netherlands of approximately 0.15 €/kWh for industry, the costs become approximately 0.02 €/mol of OH^-/H^+ [22], which is slightly higher than the price for commercially available HCl and NaOH of approximately 0.013

and 0.017 €/mol for bulk amounts excluding transport, which is not necessary in the case of on-site production with BMED [23], [24]. Moreover, using renewable energy to produce the acid and base without transportation costs is a green alternative to external supply. In addition, a large-scale BMED system with an increased number of cell pairs and thus production has a reduced energy consumption per mole by more than 50% (see Fig. S5.3). This reduced energy consumption follows from the negligible voltage and thus resistance contribution of the electrolyte compartments when comparing a single cell pair to a 100 or more. The energy consumption is calculated based on the measured voltage over the electrolyte compartment (with one CEM) and the single cell pair (CEM, BPM and AEM). The specific voltage attribution of each can be determined by measuring the voltage response of the electrolyte compartments separately. With this information the energy consumption for multiple cell pairs is determined by the sum of the voltage of the electrolyte compartments and cell pairs together with the increasing production with increasing number of cell pairs. Moreover, the system can be used for the integrated approach, as shown in Fig. 5.1, to further lower the costs in terms of water removal with RO as the respective streams are provided with solely the required OH^- and H^+ and their counter ions from the adjacent compartments whereas general base and acid dosage often includes water.

5.3.2 Conversion in integrated system with artificial feed

The previous results show the typical performance of a single BMED system. In this paragraph, the BMED system is integrated with the feed solutions for a first RO step for the separation of N and K and a second RO step for the concentration of N. As such, the feed streams for the two RO separations are first fed to the BMED to increase the pH (first RO step) or decrease the pH (second RO step), as schematically presented in Fig. 5.1. This implies that in the base compartment of the BMED, NH_4^+ consumes part of the OH^- produced for the conversion into NH_3. Vice versa, in the acid compartment part of the H^+ is used to convert NH_3 into NH_4^+. Moreover, part of the produced OH^- and H^+ ions contributes to the change in pH of the respective solutions. The sum of the produced OH^- or H^+ used for conversion and for pH change thus describes the effective production in the BMED system. This time-dependent effective production in this integrated system is shown in Fig. 5.3.

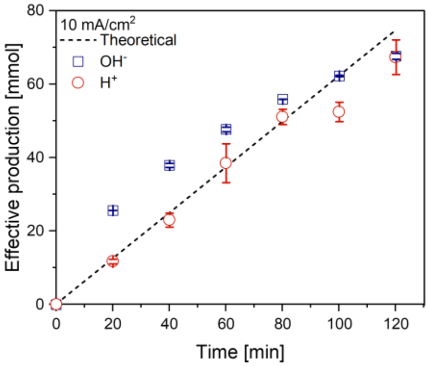

Fig. 5.3: Effective production of OH^- (squares, blue) and H^+ (circles, red) [mmol] versus the time [min] for a current density of 10 mA/cm^2 in the system with artificial manure as feed solutions with a NH_4Cl/KCl ratio of 10.37/6.67 g/L and a starting pH of 6.4 in the base compartment and NH_4Cl (4.28 g/L) with a starting pH of 11.5 in the acid compartment The dashed line represents the theoretical maximum production of OH^- or H^+ for the used current density. The experiment is done in duplicate with the standard deviation presented by the error bars.

The effective production over time increases reasonably linear with time. The OH^- production is slightly higher than the H^+ production especially at the start, which results from an overestimation of the OH^- production originating from the calculation of the TAN conversion. This follows from the higher concentration of TAN (NH_4Cl) in the base compartment compared to the acid compartment (Table S5.2), leading to a higher deviation in the base compartment compared to the acid.

Table 5.2: Performance results of the system with artificial solutions of NH_4Cl/KCl (10.37/6.67 g/L) with a starting pH of 6.4 in the base compartment and NH_4Cl (4.28 g/L) with a starting pH of 11.5 in the acid compartment for a current density of 10 mA/cm^2.

Current density [mA/cm²]	**Applied current [A]**	**Stack potential [V]**	**Production rate [mmol/min]**		**Current efficiency [%]**		**Energy consumption [Wh/mol]**	
			OH^-	*H^+*	*OH^-*	*H^+*	*OH^-*	*H^+*
10	1.00	4.36	0.42	0.54	67	87	175	134

Moreover, the H^+ production rate (Table 5.2) aligns with the theoretical total production rate of 0.62 mmol/min as well as the NaCl case, showing that the system performs similarly when integrated in comparison to the stand-alone

NaCl case. The OH^- production rate is slightly lower compared to the H^+ rate, which is linked to the overestimation of its value due to a difference in TAN concentration between the base and acid compartment for the effective production and thus altering the slope. This leads to a lower efficiency for OH^- of 67% in comparison to the 87% found for H^+ and consequently a difference in calculated energy consumption based on OH^- or H^+. The energy consumption for H^+ is similar to the value found in the NaCl case and that shows that integrating the feed streams in the BMED system does not necessarily increase costs in terms of performance of the BMED system.

The concentration of TAN and NH_3 in the base (Fig. 5.4a) and TAN and NH_4^+ in the acid (Fig. 5.4b) compartment was monitored over time to provide insight in the performance of the integrated BMED manure treatment system. In Fig. 5.4 also the pH of the respective solutions is provided with the base compartment having a starting pH of 6.4 and the acid compartment starting with a pH of 11.5.

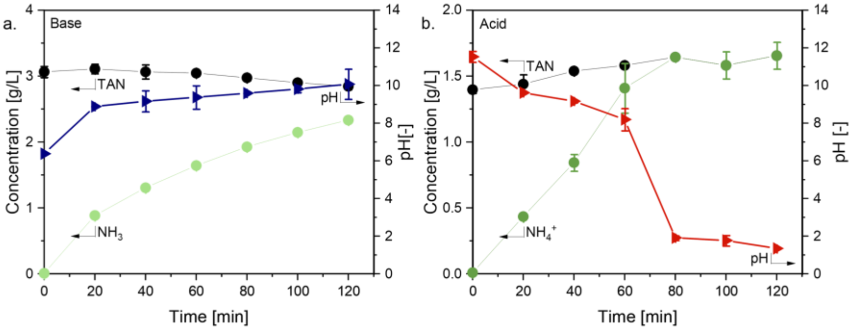

Fig. 5.4: a. TAN (black circles) and NH_3 (light green circles) concentrations [g/L] and pH (blue triangles) [-] in the base compartment versus time [min] and b. TAN (black circles) and NH_4^+ (dark green circles) concentrations [g/L] and pH (red triangles) [-] in the acid compartment versus time [min] for a current density of 10 mA/cm^2 and artificial solutions of NH_4Cl/KCl (10.37/6.67 g/L) at a feed pH starting at 6.4 in the base compartment and NH_4Cl (4.28 g/L) at a feed pH starting at 11.5 in the acid compartment. All experiments are done in duplicate with the standard deviation presented by the error bars.

A strong increase in NH_3 concentration in the base compartment in time is observed following the increase of the pH in time. When a pH of 10 is reached, after 120 minutes of operation, 85% of NH_4^+ is converted to NH_3. At the same time, in the acid compartment a pH of 2 is reached, which results according to the NH_4^+/NH_3 equilibrium in 100% conversion of NH_3 to NH_4^+, even though the same amount of OH^- and H^+ are produced in the base and the acid compartment respectively. Also here, the difference in conversion is a result of the relatively higher TAN concentration in the base compartment compared to that in the acid compartment. Because of that, a higher amount of base is needed to convert all NH_4^+ than the amount of acid needed to convert all NH_3. Also, as soon as all TAN is converted to NH_4^+ in the acid compartment the production of additional H^+ immediately results in a decrease in pH, relatively quickly reaching a value of 2. However, for effective integration, a decrease to a pH of only 6 at 100% TAN conversion is already sufficient for the integration with the second RO step to further concentrate TAN. Any additional production of H^+ (which is now used to decrease the pH below 6) is a bycatch and can in a real application thus be used for other purposes, resulting in additional savings.

In the base compartment NH_4^+ is converted into NH_3, hence the NH_3 concentration increases over time. NH_3 is a neutral species able to diffuse through ion exchange membranes. Here, the NH_3 flux through the BPM, based on the change in TAN concentration in the base compartment and only considering leakage through the BPM, is 6 $g/h \cdot m^2$. This is in line with the flux found by Ali et al. for a 17 g/L NH_3 feed solution and measured under slightly different conditions with membranes from several different manufacturers [10]. This leakage of nitrogen species explains the small decrease in TAN concentration in the base compartment with time. Similarly, the concentration of TAN in the acid compartment slightly increases over time with approximately the same rate. This diffusion increases the overall efficiency of the process as it contributes to the main aim of the integrated BMED-RO system: the removal of TAN from the digestate stream (base compartment) and the concentration of TAN in the N-rich permeate stream (acid compartment).

Moreover, other ionic species (Na^+ and Cl^-) migrate in the BMED system as shown in Fig. 5.1. This migration alters the final composition of the streams and thus the produced fertilizer. For example, a high concentration of Na^+ in comparison to K^+ can lead to the inhibited uptake of K [25]. Moreover, the amount of K^+ in the base compartment remains stable overtime as required for nutrient separation (see Fig. S5.4).

5.3.3 Integrated system performance with real feed

To validate the proposed BMED concept, we also performed experiments with real pretreated manure digestate as feed in the base compartment. The acid compartment was still fed with artificial N-rich permeate at a pH of 11.9 as this stream is not yet produced at sufficient scale. Fig. 5.5 shows the effective OH^- and H^+ production in time in the base and acid compartment, respectively.

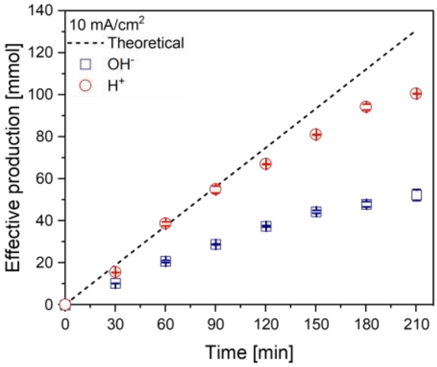

Fig. 5.5: Effective production of OH^- (squares, blue) and H^+ (circles, red) [mmol] versus time [min] for a current density of 10 mA/cm^2 using pre-treated liquid manure digestate at pH 8.4 as feed in the base compartment and an artificial solution of NH_4Cl (4.28 g/L) at a pH of 11.9 as feed in the acid compartment. The experiment is performed in duplicate with the standard deviation presented by the error bars. The dashed line represents the theoretical maximum production of OH^- or H^+ for the used current density.

The measured H^+ production in the acid compartment is similar to the artificial case as expected due to the use of an identical feed solution. Conversely, in the base compartment the measured effective OH^- production is much lower than the H^+ production and the OH^- production obtained with artificial feed. Moreover, it highly deviates from the theoretical values being about half the theoretical maximum. Fig. 5.5 shows only the fraction of the total OH^- produced that is effectively utilized for the conversion of TAN and the pH change. However, opposite to artificial feed streams, real manure digestate contains multiple other ions and components like carbonates, calcium and magnesium that can interact with the OH^- [26]. Hence, the strong deviation of the OH^- production in Fig. 5.5 from the theoretical value is attributed to the presence of the other components in the digestate that consume about 50% of the total amount of OH^- produced. This matrix effect creates a difference between the total productivity and the amount of OH- and H+ effectively used (i.e. produced) for the conversion of TAN. The resulting performance parameters are summarized in Table 5.3.

Table 5.3: Performance results of the system with pre-treated liquid manure digestate at pH 8.4 in the base compartment and an artificial solution of NH_4Cl (4.28 g/L) at a pH of 11.9 in the acid compartment for a current density of 10 mA/cm^2.

Current density [mA/cm²]	**Applied current [A]**	**Stack potential [V]**	**Production rate [mmol/min]**		**Current efficiency [%]**		**Energy consumption [Wh/mol]**	
			OH^-	*H^+*	*OH^-*	*H^+*	*OH^-*	*H^+*
10	1.00	4.59	0.25	0.49	40	79	304	156

The effective production rate of 0.49 mmol/min for H^+ is comparable to the production rate when NaCl or an artificial feed are used, while the effective production rate of 0.25 mmol/min for OH^- is half as low when compared to the other two cases. Due to the mentioned matrix effects, less OH^- is effectively available for the conversion of TAN, and relatively more OH^- has to be produced. Hence, in the base compartment, longer residence times are required for the aimed TAN conversion in the liquid manure digestate compared to the residence times required in the acid compartment to achieve the required conversion. Consequently, the current efficiency and energy consumption calculated based on the OH^- production are lower and higher respectively when compared to the values calculated based on the H^+ production. By definition, OH^- and H^+ are produced at the same amount and rate, the consequence of the above is an overproduction of acid that can be used for other purposes, e.g. for back neutralization of digestate, membrane cleaning, regeneration of ion exchangers or gas scrubbers. Additionally, with external addition of base, this matrix effect must be compensated for, and thus the amount of base needed for the integrated system is equal to that required with external base addition.

Fig. 5.6 shows the concentration of TAN, NH_3 and NH_4^+ and the pH change in time for the base and acid compartments. Due to the matrix effect of the real digestate, more time and thus OH^- is required to achieve 85% NH_4^+ to NH_3 conversion at pH 10, as shown in Fig. 5.6a, compared to the artificial case. Due to the longer OH^- production time required to reach pH 10, there is slightly more crossover of OH^- and H^+ between the compartments which means a small decrease in efficiency when compared to the artificial case. Similarly, also more

Na^+ migrates from the electrolyte compartment into the base compartment to neutralize the OH^- and Cl^- present, as shown in Fig. S5.5.

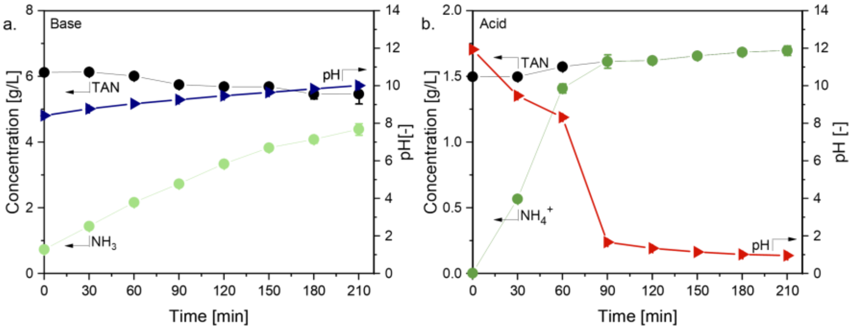

Fig. 5.6: a. the TAN (black circles) and NH_3 (light green circles) concentration [g/L] and pH (blue triangles) [-] in the base compartment versus time [min] and b. the TAN (black circles) and NH_4^+ (dark green circles) concentration [g/L] and pH (red triangles) [-] versus time [min] in the acid compartment for a current density of 10 mA/cm^2 and with pre-treated liquid manure digestate at pH 8.4 as feed in the base compartment and an artificial solution of NH_4Cl (4.28 g/L) at a pH of 11.9 as feed in the acid compartment. All experiments are done in duplicate with the standard deviation presented by the error bars.

Fig. 5.6b shows an increase in TAN concentration in the acid compartment, this is attributed to the diffusion of NH_3 from the base compartment to the acid compartment. Moreover, in the acid compartment the production of H^+ leads to 100% conversion of NH_3 into NH_4^+ within 90 minutes. After this point all produced H^+ results in a decrease in pH reaching a pH of approximately 1 at the end of the experiment, whereas a pH of 6 would already be sufficient for a second RO step as mentioned before.

5.3.3.1 Segmented production with BMED

The disbalance in use and with that the relative overproduction of H^+ compared to OH^- further indicates the necessity of tuning of the BMED system in terms of operating configuration with for example a segmented process. In a segmented process the N-rich permeate can be acidified until the required TAN conversion is reached at pH 6 while in the remaining time HCl can be produced. The HCl is suitable for digestate neutralization, membrane cleaning, regeneration of ion exchangers or for gas scrubbers. For example, in the time that 1 m^3 manure digestate is treated in the base compartment to reach a pH of 10, the acid compartment can be used to acidify 0.18 m^3 of the N-rich permeate to a pH of 6 and to produce 0.82 m^3 HCl acid solution with a concentration of 30 mM when the same flow rates are used. This segmented process can be further finetuned in terms of flow rate and recycle loops to find a suitable operation that results in the required conversion in the manure digestate and N-rich permeate and the production of a concentrated HCl solution.

5.4 Conclusion

In this research, the application of a BMED system is investigated for the production of base and acid on manure treatment sites to enhance N/K separation with RO utilizing the NH_4^+/NH_3 equilibrium. The integration of the BMED system shows efficient conversion of NH_4^+ into NH_3 in the base compartment and vice versa in the acidic compartment for artificial TAN-containing streams. Real pre-treated manure digestate required larger amounts of OH^- for TAN conversion due to matrix effects. Moreover, integration of the BMED system increases the RO efficiency as pH adjustment is achieved without addition of water. Overall, the BMED system allows high production rates of OH^- and H^+ from NaCl solutions with efficiencies reaching up to 98%. Moreover, the use of renewable energy and the absence of chemical storage and transport result in environmental benefits.

5.5 References

[1] A. Zarebska, D. Romero Nieto, K.V. Christensen, L. Fjerbæk Søtoft, and B. Norddahl, “Ammonium fertilizers production from manure: A critical review,” *Crit. Rev. Environ. Sci. Technol.*, vol. 45, no. 14, pp. 1469–1521, 2015, doi: 10.1080/10643389.2014.955630.

[2] R.W. Baker, *MEMBRANE TECHNOLOGY*, 2th ed. John Wiley & Sons, Ltd., 2004.

[3] M. van der Wal, J. van Alphen, K. Nijmeijer, and Z. Borneman, “Dynamic ammonium retention for nutrient separation from manure digestate,” *Waste Manag.*, vol. 190, no. October, pp. 644–653, 2024, doi: 10.1016/j.wasman.2024.10.034.

[4] L. Masse, D.I. Massé, and Y. Pellerin, “The effect of pH on the separation of manure nutrients with reverse osmosis membranes,” *J. Memb. Sci.*, vol. 325, no. 2, pp. 914–919, 2008, doi: 10.1016/j.memsci.2008.09.017.

[5] A. Filingeri, M. Herrero-Gonzalez, J. O’Sullivan, J. López Rodriguez, A. Culcasi, A. Tamburini, A. Cipollina, R. Ibañez, M.C. Ferrari, J.L. Cortina and G. Micale, “Acid/Base Production via Bipolar Membrane Electrodialysis: Brine Feed Streams to Reduce Fresh Water Consumption,” *Ind. Eng. Chem. Res.*, vol. 63, pp. 3198-3210, 2024, doi: 10.1021/acs.iecr.3c03553.

[6] R. Pärnamäe, S. Mareev, V. Nikonenko, S. Melnikov, N. Sheldeshov, V. Zabolotskii, H.V.M. Hamelers and M. Tedesco, “Bipolar membranes: A review on principles, latest developments, and applications,” *J. Memb. Sci.*, vol. 617, 2021, doi: 10.1016/j.memsci.2020.118538.

[7] H. Strathmann, J.J. Krol, H.J. Rapp, and G. Eigenberger, “Limiting current density and water dissociation in bipolar membranes,” *J. Memb. Sci.*, vol. 125, no. 1, pp. 123–142, 1997, doi: 10.1016/S0376-7388(96)00185-8.

[8] R. Fu, H. Wang, J. Yan, R. Li, C. Jiang, Y. Wang and T. Xu, “Asymmetric bipolar membrane electrodialysis for acid and base production,” *AIChE J.*, vol. 69, no. 3, pp. 15–18, 2023, doi: 10.1002/aic.17957.

[9] G. Pourcelly, “Electrodialysis with bipolar membranes: principles,

optimization, and applications,” *Russ. J. Electrochem.*, vol. 38, no. 8, pp. 1026-1033, 2001, doi: 10.1201/9780203747223-10.

[10] M.A. Ben Ali, M. Rakib, S. Laborie, P. Viers, and G. Durand, “Coupling of bipolar membrane electrodialysis and ammonia stripping for direct treatment of wastewaters containing ammonium nitrate,” vol. 244, pp. 89–96, 2004, doi: 10.1016/j.memsci.2004.07.007.

[11] A.J. Ward, K. Arola, E. Thompson, C.M. Mehta, and D.J. Batstone, “Nutrient recovery from wastewater through pilot scale electrodialysis,” *Water Res.*, vol. 135, pp. 57–65, 2018, doi: 10.1016/j.watres.2018.02.021.

[12] D. Ippersiel, M. Mondor, F. Lamarche, F. Tremblay, J. Dubreuil, and L. Masse, “Nitrogen potential recovery and concentration of ammonia from swine manure using electrodialysis coupled with air stripping,” *J. Environ. Manage.*, vol. 95, pp. S165–S169, 2012, doi: 10.1016/j.jenvman.2011.05.026.

[13] M. Mondor, L. Masse, D. Ippersiel, F. Lamarche and D.I. Massé, “Use of electrodialysis and reverse osmosis for the recovery and concentration of ammonia from swine manure,” vol. 99, pp. 7363–7368, 2008, doi: 10.1016/j.biortech.2006.12.039.

[14] D. Saabas and J. Lee, “Recovery of ammonia from simulated membrane contactor effluent using bipolar membrane electrodialysis,” *J. Memb. Sci.*, vol. 644, no. August 2021, 2022, doi: 10.1016/j.memsci.2021.120081.

[15] F. Ferrari, M. Pijuan, S. Molenaar, N. Duinsleager, T. Sleutels, P. Kunte and J. Radjenovic, “Ammonia recovery from anaerobic digester centrate using onsite pilot scale bipolar membrane electrodialysis coupled to membrane stripping,” *Water Res.*, vol. 218, no. April, 2022, doi: 10.1016/j.watres.2022.118504.

[16] M. Rodrigues, T.T. de Mattos, T. Sleutels, A. ter Heijne, H.V.M. Hamelers, C.J.N. Buisman and P. Kunte, “Minimal Bipolar Membrane Cell Configuration for Scaling Up Ammonium Recovery,” *ACS Sustainable Chem. Eng.*, vol. 8, pp. 17359-17367, 2020, doi: 10.1021/acssuschemeng.0c05043.

[17] M. Rodrigues, A. Paradkar, T. Sleutels, A. ter Heijne, C.J.N. Buisman, H.V.M. Hamelers and P. Kunte, “Donnan Dialysis for scaling mitigation during electrochemical ammonium recovery from complex wastewater,” *Water Res.*, vol. 201, no. February, 2021, doi: 10.1016/j.watres.2021.117260.

[18] J. Shen, J. Huang, L. Liu, W. Ye, J. Lin, and B. Van Der Bruggen, “The use of BMED for glyphosate recovery from glyphosate neutralization liquor in view of zero discharge,” *J. Hazard. Mater.*, vol. 260, pp. 660–667, 2013, doi: 10.1016/j.jhazmat.2013.06.028.

[19] T. Luo, S. Abdu, and M. Wessling, “Selectivity of ion exchange membranes : A review,” *J. Memb. Sci.*, vol. 555, no. December 2017, pp. 429–454, 2018, doi: 10.1016/j.memsci.2018.03.051.

[20] C. Huang and T. Xu, “Electrodialysis with Bipolar Membranes for Sustainable Development,” vol. 40, no. 17, pp. 5233–5243, 2006, doi:10.1021/es060039p.

[21] Y. Luo, Y. Liu, J. Shen, and B. Van der Bruggen, “Application of Bipolar Membrane Electrodialysis in Environmental Protection and Resource Recovery: A Review,” *Membranes*, vol. 12, no. 9, 2022, doi: 10.3390/membranes12090829.

[22] Eurostat, “Prices of electricity for non-household consumers in the Netherlands from 2008-2022,” 2024. https://www.statista.com/statistics/596254/electricity-non-household-price-netherlands/, Accessed November 2024.

[23] Chemanalyst, “Hydrochloric acid price trend and forecast,” 2023. https://www.chemanalyst.com/Pricing-data/hydrochloric-acid-61, Accessed November 2024.

[24] Chemanalyst, “Caustic soda price trend and forecast,” 2023. https://www.chemanalyst.com/Pricing-data/caustic-soda-3, Accessed November 2024.

[25] H. Nadian, B. Nateghzadeh, and S. Jafari, “Effects of salinity and nitrogen fertilizer on some quantity and quality parameters of sugar cane,” *J. Food, Agric. Environ.*, vol. 10, no. 1, pp. 470–474, 2012.

[26] P. Hoeksma, H. Schmitt, H.P. Komleh, and P. Ehlert, “Composition of mineral concentrates,” 2020. doi: https://doi.org/10.18174/541577.

S5 Supplementary information

S5.1 Ammonium equilibrium

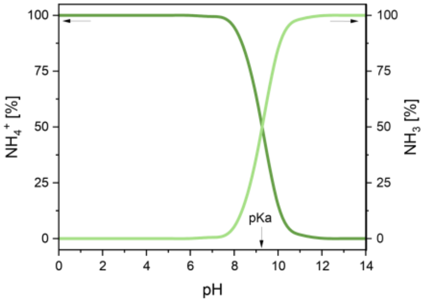

Fig. S5.1: The NH_4^+/NH_3 equilibrium in terms of percentage versus the pH at 25ºC [1].

S5.2 Materials and methods

Table S5.1: Membrane specifications from technical data sheets [2]-[4].

Membrane	**Type Fumasep®**	**Thickness [µm]**	**Resistance [Ω cm²]**	**Perm selectivity (KCl) [%]**	**pH range [-]**
BPM	FBM	110-160	-	-	-
CEM	FKB-PK-75	60-90	<2.5	>97	0-14
AEM	FAB-PK-75	60-90	<4	>92	1-14

Table S5.2: An overview regarding the different configurations and corresponding salt concentrations and pH values, mimicking the composition of the real streams for the starting solutions in the base and acid compartments [1].

Configuration	**Base compartment**			**Acid compartment**		
	Salt	pH	Volume	Salt	pH	Volume
Model	29.22 g/L NaCl	5.4	0.50 L	29.22 g/L NaCl	5.2	0.50 L
Artificial	10.37 g/L NH_4Cl 6.67 g/L KCl	6.4	0.50 L	4.28 g/L NH_4Cl	11.5	0.50 L
Real/artificial	Real manure digestate	8.4	0.25 L	4.28 g/L NH_4Cl	11.9	0.25 L

S5.3 Iron couple as electrolyte

To validate the use of Na_2SO_4, iron(II)chloride/iron(III)chloride ($FeCl_2$/$FeCl_3$) in acidic media was used as electrolyte, which has a reversible cell potential of 0.77 V. The corresponding redox reactions are shown in Scheme S5.1 and Scheme S5.2 [5].

Anode $$Fe^{3+}{}_{(aq)} + e^{-} \rightarrow Fe^{2+}{}_{(aq)}$$ *Scheme S5.1*

Cathode $$Fe^{2+}{}_{(aq)} \rightarrow Fe^{3+}{}_{(aq)} + e^{-}$$ *Scheme S5.2*

An acidic 0.25/0.25 M $FeCl_2$/$FeCl_3$ solution at pH 1 was used as electrolyte. The solution was made with iron(II) chloride and iron(III) chloride (98+%) (Sigma-Aldrich, Germany) and 1 M hydrogen chloride solution (Honeywell Fluka, USA). The total production, production rate, current efficiency and energy consumption were determined as explained in the materials and methods section.

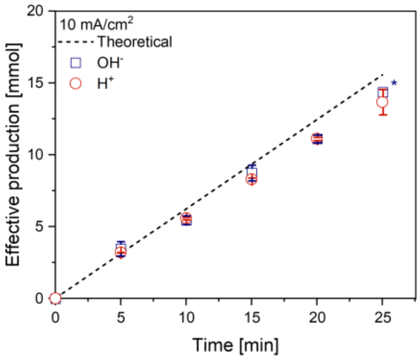

Fig. S5.2: a. Effective production of OH^- (squares, blue) and H^+ (circles, red) [mmol] versus the time [min] for a current density of 10 mA/cm^2 in the system starting with 0.5 M NaCl with $FeCl_2$/$FeCl_3$ (0.25/0.25 M) electrolyte (This measurement point is based on a single measurement). The dashed line represents the theoretical maximum production of OH^- and H^+ for the used current density. This experiment is done in duplicate with the standard deviation presented by the error bars.*

Table S5.3: The performance results of the system with 0.5 M NaCl with $FeCl_2$/$FeCl_3$ (0.25/0.25 M) electrolyte for a current density of 10 mA/cm^2.

Current density [mA/cm^2]	Applied current [A]	Stack potential [V]	Production rate [mmol/min]		Current efficiency [%]		Energy consumption [Wh/mol]	
			OH^-	*H^+*	*OH^-*	*H^+*	*OH^-*	*H^+*
10	1.00	1.60	0.56	0.54	90	87	48	49

S5.4 Effect of cell pairs on performance with NaCl

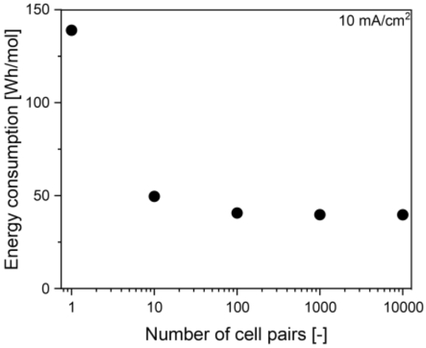

Fig. S5.3: Energy consumption [Wh/mol] versus the number of cell pairs calculated for a current density of 10 mA/cm^2 in the system starting with 0.5 M NaCl based on a measured voltage for the electrolyte compartments including one CEM of ~3.1 V and corrected for the increased voltage and production with increasing number of cell pairs.

S5.5 Production with artificial feed

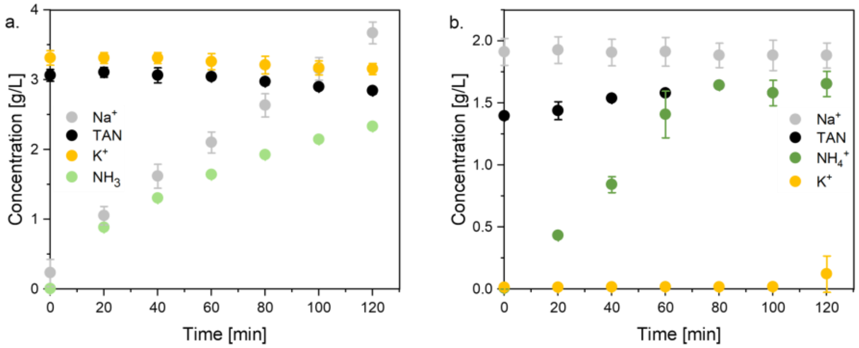

Fig. S5.4: The TAN (black circles), NH_4^+ (dark green circles), NH_3 (light green circles), K^+ (yellow circles) and Na^+ (grey circles) concentration [g/L] versus time [min] in the a. the base compartment and b. the acid compartment for a current density of 10 mA/cm^2 and artificial feed solutions of NH_4Cl/KCl (10.37/6.67 g/L) at a pH of 6.4 in the base compartment and NH_4Cl (4.28 g/L) at a pH of 11.5 in the acid compartment. All experiments are done in duplicate with the standard deviation presented by the error bars.

S5.6 Production with real manure digestate feed stream

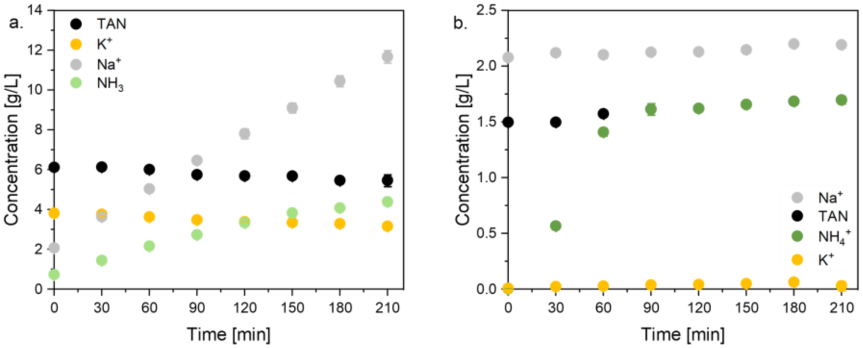

Fig. S5.5: The TAN (black circles), NH_4^+ (dark green circles), NH_3 (light green circles), K^+ (yellow circles) and Na^+ (grey circles) concentration [g/L] versus time [min] in the a. the base compartment and b. the acid compartment for a current density of 10 mA/cm^2 and with pre-treated liquid manure digestate at pH 8.4 in the base compartment and an artificial feed solution of NH_4Cl (4.28 g/L) at a pH of 11.9 in the acid compartment. All experiments are done in duplicate with the standard deviation presented by the error bars.

S5.7 References

[1] M. van der Wal, J. van Alphen, K. Nijmeijer, and Z. Borneman, “Dynamic ammonium retention for nutrient separation from manure digestate,” *Waste Manag.*, vol. 190, no. October, pp. 644–653, 2024, doi: 10.1016/j.wasman.2024.10.034.

[2] Fumatech, “Technical data sheet - fumasep FAB-PK-75,” 2021.

[3] Fumatech, “Technical data sheet - fumasep FKB-PK-75,” no. 0, 2021.

[4] Fumatech, “Technical data sheet - fumasep FBM,” no. 0, 2021.

[5] O. Scialdone, C. Guarisco, S. Grispo, A.D. Angelo, and A. Galia, “Investigation of electrode material - Redox couple systems for reverse electrodialysis processes. Part I: Iron redox couples,” *J. Electroanal. Chem.*, vol. 681, pp. 66–75, 2012, doi: 10.1016/j.jelechem.2012.05.

CHAPTER 6

Conclusion, implementation and future research directions

This chapter starts with summarizing the main conclusions. This is followed by a description of the implementation of this dissertation. Finally, it concludes with an outlook on future research directions to further improve the manure treatment in order to enhance circularity by the formation of separate nutrient fraction for tailored fertilization.

6.1 Conclusions

The emission of greenhouse gases from energy production, industry, transport, waste management and agriculture has led to climate change. Moreover, the release of ammonia results in pollution of nature and water bodies all leading to risks for biodiversity. Hence, strict regulations have been enforced in order to reduce the environmental impact of ammonia emissions. In the agricultural sector in the Netherlands this leads to a growing manure surplus, putting pressure on farmers as well as the manure treatment facilities. This dissertation provides insights on aspects to improve different manure treatment processes in order to enhance the valorization of manure and increase circularity.

In **Chapter 2** various flocculants for the improvement of solid-liquid separation were investigated to determine which type and dosage is most suitable for the separation of the solid and liquid fractions originating from manure digestate. The flocculant efficiency, based on the turbidity removal in the liquid fraction, indicated that flocculants that establish hydrophobic interactions and hydrogen bonding provide the highest organic matter removal. Moreover, a linear high molecular weight flocculant with a low negative charge density gives superior removal with a low flocculant dosage. Efficient use of flocculants leads to a reduction in chemical use and costs in terms of chemicals and membrane cleaning and replacement.

Chapter 3 shows the potential of pH tuning for the separation of nitrogen (N) and potassium (K) from liquid manure digestate with reverse osmosis (RO). An increase in pH lowers the retention of N as this nutrient is mainly present in the form of ammonium (NH_4^+) that due to its acid-base equilibrium is converted to neutral ammonia (NH_3) which permeates the membrane more easily. Meanwhile potassium ions (K^+) are retained by the membrane resulting in separation of N and K. The membranes investigated do not show separation of N and K at a pH of 6 as both ions are charged at this pH whereas at a pH higher than 10 high amounts of N permeate due to the lack of charge of NH_3 while the K retention remains constant, thus separating both nutrients. As a pH of 12 exceeds the maximum pH for long-term operation of the selected membranes, a pH of 10 is recommended. At a pH of 10 the selected brackish water RO membrane shows an N/K selectivity of 3 with a flux of 11 L/m^2·h in a dead-end filtration set-up with real pre-treated manure digestate. This leads to a permeate stream containing 1.4 g/L of N which can be further concentrated with a subsequent RO step at a pH of 6. Moreover, in a crossflow system but with an artificial solution an even higher N/K selectivity of 35 can be established. Overall, the pH tuning proofs suitable for N and K separation from liquid manure digestate and given the configuration and already used chemicals, can be relatively easily implemented in existing RO processes in manure treatment plants.

The research in **Chapter 4** focuses on the modification of ultrafiltration polyacrylonitrile (PAN) membranes using subsequent hydrolysis, polyelectrolyte layer formation and crosslinking to investigate the retention of various salt solutions including artificial and real manure digestate. The results show that only hydrolysis and thus the formation of negatively charged carboxylic acid groups on the native PAN membrane results in Donnan exclusion which is not sufficient to retain a mixture mono- and multivalent salt ions. Subsequent coating of the hydrolyzed PAN membrane with polyelectrolyte layers forming a layer-by-layer assembly covers the pores of the PAN membrane providing additional size exclusion next to Donnan exclusion. This leads to higher retentions reaching 60% for multivalent ions and 20% for monovalent ions in a mixture. Crosslinking of the polyelectrolyte layers further increases the retention of mono and multivalent ions by the formation of a more rigid and less swollen polymer structure. This leads to a retention difference between NH_4^+ and K^+ due to their small difference in dehydration energy. The separation is further enhanced at alkaline conditions following the approach described in **Chapter 3**.

In **Chapter 5**, the integration of a bipolar membrane electrodialysis system (BMED) with nutrient separation using RO is investigated. With the BMED system hydroxide ions (OH^-) and protons (H^+) are produced on-site. The OH^- converts NH_4^+ in the liquid fraction of manure digestate to NH_3 that then permeates the RO membrane, while K^+ is retained, resulting in separation of N and K as described in **Chapter 3**. H^+, also generated in the BMED system, is then used to convert NH_3 in the RO permeate back into NH_4^+, followed by an RO concentrating step generating an N-rich stream. Using artificial solutions, a proof of concept is obtained. Experiments with real manure digestate confirm the applicability for real streams but also show that half of the OH^- is consumed by other species than NH_4^+, present in real manure digestate. Nevertheless, the total required amount of OH^-, taking into account both NH_4^+ conversion as well as interactions with other species, is comparable to the required amount from an external obtained aqueous base solution. Moreover, the process configuration (active membrane area, flow rates, etc.) must be chosen such that the amount of OH^- produced aligns with the amount of OH^- needed. This results in an overproduction of H^+ that can be utilized elsewhere in the treatment process. Overall, this process is a sustainable option as it can utilize renewable electricity, minimizing the water added to the RO feed streams and reducing storage and transportation of corrosive chemicals.

6.2 Implementation of this dissertation

6.2.1 Flocculation improvement

Fouling of membranes is directly correlated to the presence of, amongst others, organic matter. Monitoring the solid-liquid separation treatment can be done by continuous measuring of the turbidity of the respective liquid. This can lead to the early discovery of problems like high organic matter concentrations in the liquid streams in the manure (digestate) treatment process, allowing early detection and responses to facilitate proper operation in the downstream process (e.g. RO). The flocculation efficiency can be improved by determining which (bio-)flocculant reaches the highest turbidity removal. This can be accomplished with the screening method proposed in **Chapter 2**, see Fig. 6.1. Moreover, this method can provide an indication of the optimal dosage for the respective flocculant to reduce costs and chemical consumption.

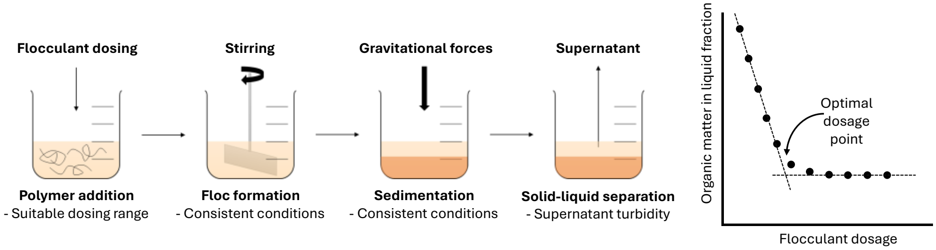

Fig. 6.1: Schematic overview of screening method for flocculant type and optimal dosage determination.

The implementation of this method to establish which flocculant type is most suitable to reach a high organic matter removal improves the separation and quality of the liquid stream for subsequent treatment (e.g. with RO) resulting in less frequently required membrane cleaning and replacement. Moreover, establishing the optimal dosage can significantly reduce the amount of chemicals used and improves the quality of the solid stream next to lower operation costs further improving the treatment.

6.2.2 Separation of N and K with reverse osmosis

In **Chapter 3**, the separation of N and K with RO is accomplished at a pH of 10 and higher. This is presented as an alternative to stripping-scrubbing (currently regularly employed) for the production of ammonium salt fertilizer. The overall treatment process then includes solid-liquid separation to produce a phosphorus (P)-rich solid fraction and a liquid fraction containing N and K present in ionic form (NH_4^+ and K^+). After conversion of NH_4^+ into NH_3 at pH 10, the nutrients in the liquid fraction are then separated by RO. Here the retentate stream is concentrated in K, while water and NH_3 permeate. The permeate stream is further concentrated by the permeation of water in an additional RO step at pH 6 to ensure the retention of N in the form of NH_4^+. In Fig. 6.2, a mass balance for the total mass as well as the inorganic nutrients is presented for the above-described membrane-based process. The estimated balances are calculated based on the dry matter content of samples collected from the Duurzaam Landleven Bernheze (the Netherlands) manure treatment plant. Moreover, it is assumed that all dry matter is retained in the first RO step as this is a dense membrane used to retain species as small as monovalent ions. In both balances only inorganic P, N and K are considered with the assumption that in this case all P goes to the solid-fraction as PO_4^{2-} precipitates with other ions present like Ca^{2+} and Mg^{2+} resulting in collection with the dry matter [1]. Based on this, the amount of P that might remain in the liquid fraction is little. Moreover, for these calculations it is assumed that all N and K go to the liquid fraction, however in practice some N and K might be collected in the solid fraction. The concentrations of N and K in the liquid fraction are obtained from **Chapter 3**. For the RO steps, the retention values are obtained from the same chapter from the separation of N and K with the brackish water RO membranes at pH 10 and 6. Moreover, the concentration factor in the first RO step was set to a value of 3.0. The concentration factor for the second RO step was set to 7.4, to reach an overall water recovery of 50% comparable to values found in literature [1], [2]. These values are chosen as this corresponds to osmotic pressure differences, based on the N and K concentrations, which remain within the maximum pressure of 41 bar for the brackish water RO membrane with an effective membrane pressure that remains above 5 bar [3]. Nevertheless, the concentration factor used in the second RO step is high and might be an overestimation.

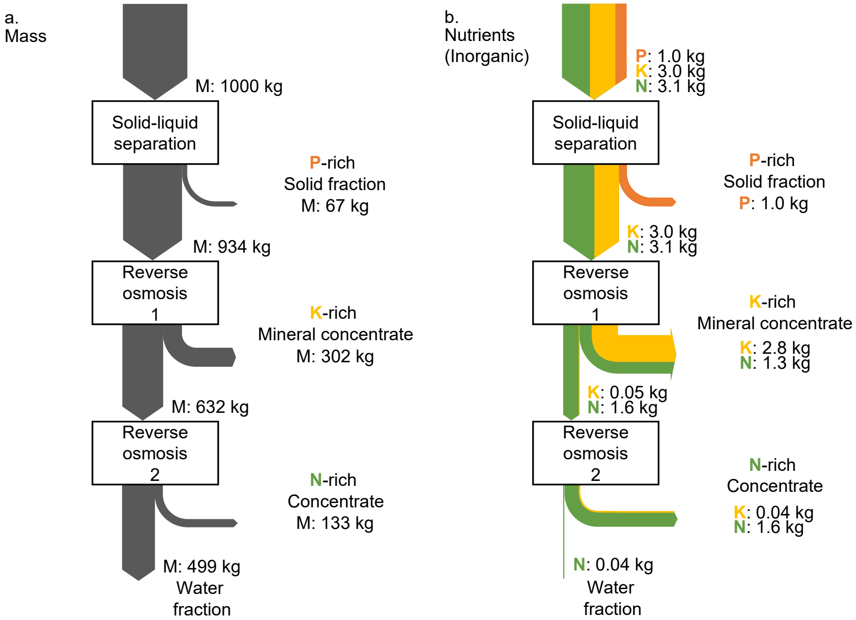

Fig. 6.2: Mass balances of a. the overall mass and b. inorganic nutrients N (in the form of TAN), K and P (PO_4^{2-}). The balances were estimated for a system with a solid-liquid separation pre-treatment with two subsequent RO steps for the separation (N/K separation) and concentration of nutrients (N-concentrate) resulting in a P-rich solid fraction, K-rich mineral concentrate, N-rich concentrate and water.

From the estimated overall mass balance, Fig. 6.2a, it can be observed that only a small solid fraction is retrieved. Based on the samples obtained from Duurzaam Landleven, it was established that approximately 78% of the dry matter originally present is collected in the solid fraction. The removal of dry matter can be further increased by optimization of the solid-liquid separation which can also reduce fouling problems in the subsequent RO steps. Moreover, the calculation shows that it is possible to recover separate K and N rich streams, next to the recovery of approximately 50% water of the original stream.

Moreover, the mass balance of the inorganic nutrients, Fig. 6.2b, provides information regarding the nutrient content in the different fractions. The solid fraction contains all P, resulting in a concentration of approximately 29 g/kg based on the amount of P and the mass of the solid stream. The liquid fraction contains N and K in a ratio of approximately 1:1 before treatment with RO, based on ion chromatography measurements of the samples collected as shown in **Chapter 3**. In the first RO step (N/K separation), a significant amount of N permeates at alkaline conditions whereas the K is retained, resulting in a so-called K-enriched mineral concentrate. This mineral concentrate has a K concentration of 9.3 g/L and N concentration of only 4.3 g/L when considering the amount of N and K in the fraction and the overall mass of the fraction. The second RO step concentrates the N in the permeate stream originating from the first RO step to a concentration of 12.1 g/L, resulting in a clean N-rich concentrate stream as product, comparable to the ammonium salt product from a stripping-scrubbing process. Moreover, the permeate stream of the second RO step contains only a small amount of N.

The separate nutrient streams can replace artificial fertilizer and are suitable for tailored fertilization as the nutrient ratio can be easily adjusted. Typically, these products are still considered to be manure and are therefore not allowed as fertilizer products outside of the nutrient limits set for manure. The introduction of new European legislation Renure, REcovered Nitrogen from ManURE, changes this perspective and allows N containing products from manure treatment above the set limits. The Renure status is granted if the stream complies with the certain characteristics (Table 6.1).

Table 6.1: The final product criteria for the artificial manure replacement Renure [4].

Category	**Criteria**
Technology	Physical, chemical and/or biological process step
Nitrogen ratio	Nitrogen : Total Nitrogen ≥90% or Total Organic Carbon : Total Nitrogen ≤3 Corrected for N not originating from manure
Metals	Cu ≤300 mg / kg dry matter Zn ≤800 mg / kg dry matter
Micro-organisms	Salmonella spp. 0 colony forming units (CFU) in 25 ml Escherichia coli or Enterococcaceae ≤1 000 CFU in 1 ml

In terms of Renure status, the N-rich concentrate stream complies with the Renure status as it is produced with RO and is a clean stream due to treatment with the dense RO membrane in the first RO step resulting in the removal of organic carbon, copper, zinc and bacteria. The quality of the N-rich concentrate containing ammonium salt is comparable to the Renure product produced with stripping and scrubbing, as both are clean NH_3 containing streams in which the N is captured in an acidic solution.

The mineral concentrate, typically produced in manure treatment plants containing both N and K in equal amounts, is considered to meet the Renure criteria [5]. The mineral concentrate enriched in K in the N/K separation at alkaline conditions is produced in the same way. Hence, this K-rich mineral concentrate has a similar composition and is thus expected to meet the Renure criteria. Nevertheless, the bacteria and copper and zinc that might be present in the liquid fraction of the manure digestate are concentrated in the first RO step. Depending on the initial concentration and concentration factor this might exceed the criteria values introducing an issue for both the mineral concentrate and K-rich mineral concentrate. Moreover, the Renure products require a TOC to N ratio below a value of 3. Due to the removal of the of N and the concentration of the TOC present, the TOC to N ratio becomes lower for the K-rich mineral concentrate from the N/K separation in comparison to the typical mineral concentrate retaining both N and K. Nevertheless, this stream shows to have potential to also meet the Renure requirements.

The main N containing product produced with the two-step RO process is as mentioned before comparable to the ammonium salt produced with a stripping-scrubbing process. The stripping-scrubbing process utilizes the NH_4^+/NH_3 equilibrium to physically transfer NH_3 from the aqueous to gas phase and back. The liquid fraction enters the stripping column that contains a basic solution. Due to the basic conditions, NH_4^+ is converted into NH_3 and removed from the stripper as NH_3-rich gas. The NH_3 is converted back into NH_4^+ in the scrubber with an acidic solution resulting in the recovery of an ammonium salt. The stripping tower is typically operated at a pH >9.5 and temperatures between 60-70 ˚C [1]. Both systems produce an ammonium salt that can be considered a Renure product as shown in Fig. 6.3. The systems use base and acid as driving force to utilize the NH_4^+/NH_3 equilibrium whereas RO using pressure to enhance separation while stripping-scrubbing uses heat.

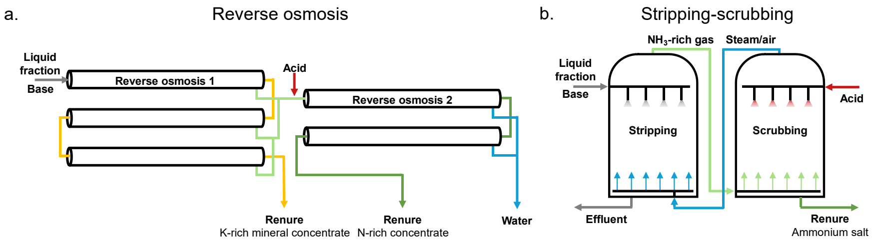

Fig. 6.3: Schematic drawings of nutrient separation from manure digestate. a. A two-step reverse osmosis system for the production of K-rich mineral concentrate, N-rich concentrate consisting of an ammonium salt and clean water and b. A stripping-scrubbing process for the production of an ammonium salt and an N-depleted effluent. Both systems utilize base and acid to produce the respective streams.

Currently, the main reasoning of using an RO system is the recovery of water which can reach values up to 50% relative to the initial digestate stream as also established in the mass balance (Fig. 6.2) [1]. Water recovery is not possible with scrubbing-stripping installations. However, several studies have shown that RO gives higher total estimated costs per m^3 digestate in comparison to stripping-scrubbing. [1], [6], [7]. Bolzonella et al. calculated the capital and operational costs for a membrane and a stripping-scrubbing installation for the treatment of manure with the RO producing a mineral concentrate containing 41% of the initial N and the stripping-scrubbing producing an ammonium salt containing 17% of the initial N. The feed for the RO originates from two different digestates, cow and pig manure, with flow rates of 42 and 60 ton per day whereas the stripping-scrubbing digestate came from combined cow and pig manure with a flowrate of 130 ton per day. Both processes have pretreatment steps for the removal of organic matter, the RO system a screw press followed by decanter and ultrafiltration with flocculant addition and the stripping-scrubbing process a screw press followed by a lamella settler for sedimentation. The capital costs are depreciated over a period of 10 years with an interest of 3% to be able to include the capital costs in the total estimated costs. For the chemical costs for the RO process the chemicals are the flocculant for the pre-treatment and membrane cleaning agents and for the stripping-scrubbing the lime to reach a pH above 9 and sulfuric acid to recover the ammonium. In Table 6.2, the capital costs and operational costs estimated by Bolzonella et al. are presented which does not include the value of the products [1].

Table 6.2: Estimated capital and operational costs for a two-step RO system for the production of a mineral concentrate and water and for a stripping-scrubbing installation for the production of an ammonium salt with adapted energy costs to current energy prices from Bolzonella et al. [1]. The energy costs are based on an energy price of 0.15 €/kWh for non-household consumers in the Netherlands in 2024 [8].

Cost item	**Two-step RO (mineral concentrate)**	**Stripping-scrubbing**
Capital cost [€]	1 000 000	750 000
Depreciation [€/m^3]	2.74	1.58
Energy [kWh/m^3]	18.5	10.6
Energy cost [€/m^3]	2.78	1.59
Chemicals [€/m^3]	0.33	1.50
Labor/service [€/m^3]	1.05	0.30
Estimated operational cost [€/m^3]	4.16	3.39
Total estimated cost [€/m^3] (including depreciation)	6.90	4.97

The capital cost for the RO system is approximately 33% higher compared to the stripping-scrubbing system. Also, the operational costs are higher for RO as a result of the required amount of energy and the more expensive expertise for labor/service [1]. Moreover, the chemicals costs of the RO system are low compared to stripping-scrubbing. However, these costs would increase when the separation of N and K in RO step 1 is considered as base and acid are required in this step next to the other chemicals, the amount of base and acid required for N and K separation is comparable to stripping-scrubbing. Overall, the operational cost for the RO system is approximately 20% higher than for the stripping-scrubbing system. However, this does not consider the difference in the profit that can be made with the produced fertilizer products and the reduced transportation costs by the recovery of approximately 50% of water with the RO system. Hence, more investigation is required to establish a comparable cost overview with capital costs for the same stream and the inclusion of the profit that can be made with the different streams obtained to couple the benefit of RO to the costs. Moreover, the separation of N and K and thus the production of N fertilizer can be produced within existing RO systems by pH tuning lowering the investment costs.

6.2.3 Integration of BMED

As previously discussed, both RO and stripping-scrubbing require base and acid in the proposed configuration, see Fig. 6.3. The BMED system described in **Chapter 5** can provide this base and acid in an integrated manner resulting in the on-site production of base and acid. As discussed in **Chapter 5**, this results in less transport and storage of chemicals next to comparable costs for the OH^- and H^+ produced with a BMED system compared to the costs for NaOH and HCl in bulk. Table 6.3 presents an overview of the operational parameters of a large scale system able to treat 800 L/h of pre-treated manure digestate to reach a pH of 10 with the production of 320 mol OH^-/h, based on the results obtained in **Chapter 5**, to have a suitable stream for nutrient separation with RO. The flow velocity (1 cm/s), current density (100 A/m^2) and resulting cell performance in terms of efficiency (80%) are based on the parameters used and established in **Chapter 5**. The production of the required amount of OH^- for separation with RO is in here achieved in a single pass for the given membrane area and number of cell pairs.

*Table 6.3: An overview of the BMED operational parameters to produce the required amount of OH^- during the single pas integrated treatment of manure digestate for subsequent N/K nutrient separation with RO based on the performance measurements described in detail in **Chapter 5**.*

Parameter	Value
Flow rate [L/h]	800
Flow velocity [cm/s]	1
Number of cell pairs [-]	125
Membrane area [m^2]	0.86
Current density [A/m^2]	100
Current efficiency [%]	80
Energy consumption [kWh/L]	0.016

To reach the required amount of OH^-, 125 cell pairs are required consisting of three membranes, each with an area of 0.86 m^2 corresponding to a width of 0.46 and a length of 1.9 m to provide a fitting residence time for the required OH^- production. Based on the efficiency and the assumption that the energy consumption scales linearly with the membrane area, the expected energy consumption reaches 0.016 kWh/L manure digestate treated and the additional production of an acid stream suitable to treat the N-rich permeate for subsequent concentrating. This leads to operating costs of in terms of energy of 0.002 €/L based on an energy price of 0.15 €/kWh for non-household consumers in the Netherlands in 2024 [8].

The dimensions of the BMED system are used to estimate the capital cost of the system as presented in Table 6.4, based on the costs determined for a first of a kind acid-base flow battery, consisting of the same components as a BMED system [9]. The study of Pärnamäe et al. shows the costs of a 100x upscaled plant in comparison to a pilot scale plant, taking into account the development in technology and using estimated prices between 2021 and 2025. The costs for the BMED system membrane stack are corrected for the amount of cell pairs and area whereas the cost of the electrode assembly is extracted from the power subsystem costs mentioned in the study corrected for the area. It is assumed that the sub- and management systems are comparable to the values estimated in the study.

Table 6.4: An estimation of the total capital cost for the BMED system for the integrated treatment of 800 L/h of manure digestate for subsequent nutrient separation with RO. The numbers are adapted based on cost evaluation of a first of a kind system for an acid-base flow battery consisting of the same components as the described BMED system [9].

Component	Value
Membrane stack [€] ***(Membranes, spacers)***	11 000
Electrode assembly [€] ***(Electrodes, endplates)***	13 000
Subsystem [€] ***(Storage tanks, electrolyte)***	35 000
Management system [€] ***(Computer system, sensors)***	22 000
Estimated total capital cost [€]	81 000

The cost of a membrane triplet for the battery was estimated to reach a value of approximately 100 €/m^2 based on the expectation of lower membrane prices due to the scale and membrane development. This leads to an overall price for the membrane stack of €11 000 which is comparable to the additional electrode assembly cost of approximately €13 000 to complete the BMED stack. The costs of the subsystem and management system are the values estimated for the acid-base flow battery, which are expected to be overestimated. For example, the cost for the subsystem of the BMED might be lower due to a difference in required tank size and number of tanks. Moreover, the management system is expected to be less complex as the BMED system only runs in reverse bias whereas the battery also requires forward bias. Overall, this leads to an estimated capital cost of €81 000 for an on-site BMED system for the production of base and acid. The investment in a BMED system is only 40% of the capital costs estimated for RO and stripping-scrubbing, making the integration of the BMED an interesting option (Table 6.2). Moreover, the integration of the BMED system provides several benefits like less transportation and storage of chemicals and, when implemented with an RO system, less removal of water when compared to the addition of aqueous commercial base and acid. This can lead to a reduction of approximately 1.30 €/day in operational costs for the RO system considering a feed of 800 L/h, a 50% NaOH solution and the operational costs reported in Table 6.2.

6.3 Future challenges and research directions

6.3.1 Solid-liquid separation treatment

6.3.1.1 Silt density index (SDI)

A series of solid-liquid pretreatment processes is required to accommodate RO operation in manure (digestate) treatment, producing the final mineral concentrate. This solid-liquid separation in manure treatment varies tremendously between treatment plants, originating from the different manure types, optional co-products added and varying volumes [2], [10], [11]. It is challenging to find one single solution to efficiently separate the solid particles from the liquid fraction.

A way to determine the quality and suitability of a liquid stream for RO is the silt density index (SDI), which is a standardized method used to determine the membrane fouling tendency of a solution [12]. When a liquid stream has an SDI value below 5, which correlates to a turbidity below 1.0 NTU, it can be treated with seawater RO [3], [13], [14]. Values less than 3 would require cleaning treatments every other month whereas for SDI values between 3 to 5 particulate fouling is expected for which frequent cleaning will be required [13]. This SDI system is mainly used for seawater RO which requires less pre-treatment compared to manure treatment based on the amount of solid matter present. For liquid streams originating from manure treatment, if at all measurable, SDI and NTU values are far beyond the applicable range, even after intensive pretreatment. For example, at the manure treatment plant Duurzaam Landleven Bernheze (the Netherlands), a pre-treatment consisting of a sieve belt, dissolved air flotation, vibrating screen and filter paper with several flocculant additions only reaches a turbidity of 2750 NTU, measured for a sample retrieved after all pretreatment steps with the method described in **Chapter 2**. As in many manure treatment plants, the subsequent RO operates under conditions out of the regular membrane specifications, while intensive cleaning in combination with frequent membrane replacement is required. Nevertheless, based on practical experience, the plant at Bernheze (and many others) has surprisingly been running for several years regardless of the high turbidity and correlated maintenance showing that operation out of specifications and with intensive cleaning works but can be further improved. Hence, a similar system as the SDI values for manure treatment is beneficial as it can provide a more realistic view on the balance between pretreatment costs and membrane lifetime. This method can be based on the SDI method but with a more open filter to reduce the amount of clogging. Another approach is to adjust the interpretation of the SDI values to fit with current treatment systems that can run effectively.

6.3.1.2 Aiming for improved flocculation

Not only does the process configuration contribute to an improved solid-liquid separation. Flocculation (after adding flocculants) of organic matter in the manure digestate is frequently used and further lowers the turbidity and thus the SDI value of the liquid fraction. Fluctuations in the digestate composition due to the use of, for example varying co-products, require flexibility in flocculation type and dose added aligned with the specific (but fluctuating) composition of the to be treated stream. However, currently, there a no methods to effectively determine which flocculants are needed and with which concentration. The relatively straightforward method presented in **Chapter 2** provides an approach to determine the type of flocculants and their optimal dosages. However, this still requires a lot of time while often an immediate response is required to maintain a low turbidity. Control of the turbidity removal can be achieved by monitoring the turbidity throughout the process providing insight into the treatment quality and flocculant dosing requirements.

Moreover, the type of coagulant or flocculant used can alter the quality of the solid fraction as they can be considered toxic if present in high quantity [15]. The potential toxicity can limit the use of the solid fraction as soil improver in agriculture. Replacement of the current additives by biobased and/or biodegradable coagulants and flocculants can limit the toxicity in the final product. Currently, research shows for example the potential of chitosan, alginate, starch, extracellular polymeric substances and polysaccharides for organic matter removal from waste waters [15]–[20]. Some research has been conducted regarding flocculation of manure and digestate [21]–[24]. However, overall limited information is available regarding flocculation of digestate originating from manure [25]–[27]. Hence, more knowledge should be gained to find suitable flocculant types and especially bio-based flocculants.

Moreover, the use of specific additives can lead to additional improvements in the valorization of manure digestate. For example, an iron coagulant can increase removal of phosphorus (P) towards the solid fraction which improves the separation of nutrients in the manure treatment [28]–[30]. The combination of the commercial flocculants and iron(II)sulphate for the removal of phosphate from manure digestate was investigated experimentally, using the methods described in **Chapter 2**, as shown in Fig. 6.4. Different concentrations of iron(II)sulphate were added to manure digestate in combination with the optimal dosage of the commercial flocculants nPAM, 5CL, 12AB and 8 AL (2.79, 0.96, 5.18 and 2.34 mg/g DM) as described in **Chapter 2**. After stirring, a sample was centrifuged in order to remove the liquid fraction to assess the removal of phosphate. The amount of phosphate was measured via ion chromatography whereas the turbidity removal was measured with a turbidity meter.

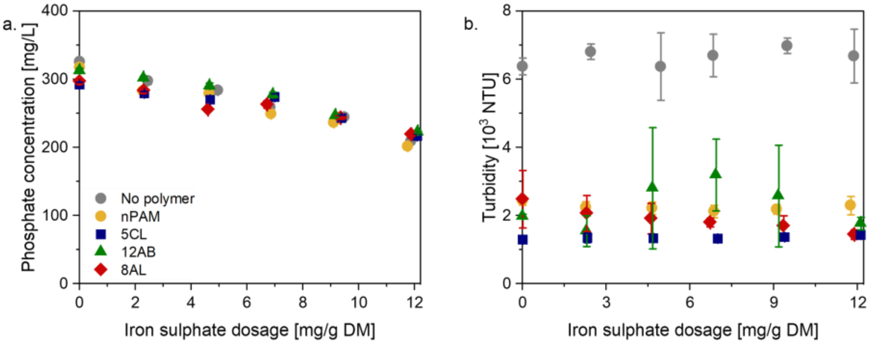

*Fig. 6.4: a. Phosphate concentration [mg/L] and b. the turbidity [10^3 NTU] versus iron sulphate dosage [mg/g DM] in the liquid fraction of manure digestate with no polymer added and combined with the optimal dosages of nPAM, 5CL, 12AB and 8AL as reported in **Chapter 2**.*

Fig. 6.4a shows that the phosphate concentration is lowered with increasing iron sulphate dosage regardless of the commercial flocculant presence indicating that more phosphate is captured in the solid fraction, thus improving the separation of P from N and K that remain in the liquid fraction. Moreover, Fig. 6.4b shows that the addition of iron sulphate in different dosages does not result in additional removal of organic matter which would have been an additional benefit. Similarly, Lin et al. summarized the dosage of the more suitable coagulants Fe^{3+} and Al^{3+} (molar ratio between 2 to 3 of metal to phosphorus) and their corresponding phosphorus removal from digestate streams. The addition of these coagulants leads to phosphorus removals of more than 95% compared to 50% for natural sedimentation [28]. Moreover, this indicates that higher removals can be reached than shown in Fig. 6.4 as ferric salts are more efficient than ferrous salts [28]. Manure treatment processes can benefit from additional research regarding phosphorus removal in combination with organic matter from manure digestate using coagulants improving the nutrient separation. For example, the combination of coagulants and flocculants can lead to increased efficiencies [29]. Moreover, the type of additives should be chosen carefully to ensure that the fertilizer quality of the solid fraction fulfills the requirements for land application and that the nutrients like phosphate remain available for the plants.

6.3.2 Nutrient separation with reverse osmosis

6.3.2.1 The effect of temperature on the NH_4^+/NH_3 equilibrium

The separation of nutrients with RO in this dissertation focused on the presence of N in the form of NH_4^+. The acid-base equilibrium of NH_4^+ and NH_3, Scheme 6.1, is utilized to separate N and K via charge exclusion due to the conversion to neutral NH_3 after which NH_3 permeates the RO membrane while K^+ is retained.

$$NH_4{}^+ + OH^- \leftrightharpoons NH_3 + H_2O \qquad \textit{Scheme 6.1}$$

An equilibrium is typically pushed towards the product side by the addition and removal of respectively reactants and products. In this dissertation, the equilibrium is pushed towards NH_3 due to the production of OH^-, (i.e. a high pH). Moreover, the removal of the product (NH_3) over the length of the membrane in the crossflow system showed improved removal of the total ammonium nitrogen (TAN) compared to a dead-end cell configuration (**Chapter 3**). Another way to push the equilibrium is by influencing the equilibrium constant of the reaction, the pKa. An equilibrium constant is based on the change in Gibs free energy and thus the enthalpy and entropy (Eq. 6.1). The equilibrium constant is thus affected by the temperature [31].

$$K = e^{-\Delta G^{\circ}/RT} = e^{-(\Delta H^{\circ} - T\Delta S^{\circ})/RT} \qquad \textit{Eq. 6.1}$$

In this case, the increase in temperature lowers the pKa value and thus, at the same pH, but higher temperature, more NH_4^+ converts to NH_3 resulting in more permeation of NH_3 through the membrane [32].

Emerson et al. studied the effect of temperature on the *pKa* values of the aqueous ammonia equilibrium [33]. The study provided Eq. 6.2 for the calculation of the pKa value at a specific temperature *T* (°C).

$$pKa = 0.09018 + \frac{2729.92}{T + 273.15} \qquad \textit{Eq. 6.2}$$

The percentage of TAN present as NH_3 can be calculated based on Eq. 6.3 which is the acid-base equilibrium as rewritten Henderson-Hasselbach equation as described in **Chapter 5** with the *pKa* value correlated to a certain temperature.

$$[NH_3] = \frac{[TAN]}{\left(1 + \frac{10^{-pH}}{10^{-pKa}}\right)} \qquad \textit{Eq. 6.3}$$

In Fig. 6.5, the percentage of NH_3 calculated with the above equations is plotted over a pH range at a temperature varying from 10 to 50 ˚C.

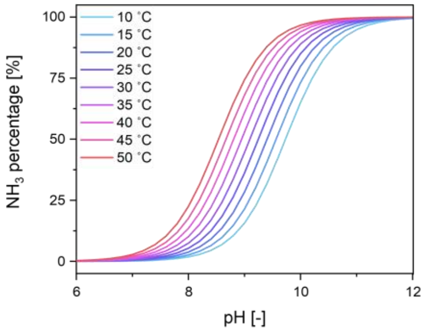

Fig. 6.5: The percentage of NH_3 [%] over a pH range based on the NH_4^+/NH_3 equilibrium at different temperatures [˚C].

A drop in the pKa value from 9.73 to 8.54 is observed when the temperature is increased from 10 to 50 ˚C. This shift means that 65% of the TAN is converted to NH_3 at pH 10 at 10 ˚C whereas at the same pH at 50 ˚C 97% is converted which can lead to more separation of N and K in an RO system. However, considering the membrane in the nutrient separation process, the temperature should not exceed the limit of typically 45 ˚C as this can damage the membrane. Moreover, membranes also have a limited lifetime in alkalinity that exceeds pH 11 [3], [14]. Long-term operation is recommended at a temperature of 40 ˚C at a pH of 10 at which 94% of the TAN is present as NH_3 to maximize the N/K separation. However, adjustment of the temperature increases the operation costs. Hence, the benefit of additional separation over the increased costs should be investigated. For example, in certain cases heat exchange can be utilized to lower the costs.

6.3.2.2 The presence of other N-containing species

The separation of N from K has been mainly focused on the presence of NH_4^+ that at alkaline conditions can be separated from K^+. Risberg et al. showed an elaborate overview of the N content of cow manure, pig slurry, manure digestate with manure as main component for digestion and digestate with organic matter as the main component [34]. In Fig. 6.6, the average of the total N present in the different streams is shown, accompanied by the concentration of organic (carbon) and inorganic (non-carbon) containing N-species. Moreover, the concentration of TAN is shown, which is the majority of the inorganic N and a potential risk to environment hence a by law restrained component for fertilization. It is observed that the total concentration of N is higher for digestate than for manure which is attributed to the addition of N containing organic matter to the digester. Moreover, a large error bar is observed showing the large variation in compositions. For manure this can be the result of the difference in origin whereas for digestate streams this is a combination with the variety of organic co-products that have been added. The organic N in all streams is comparable, whereas the concentration of inorganic N increases for the digestate as during the digestion process organic N is partially converted into inorganic N. The inorganic N present in the streams is almost identical to the concentration of TAN which shows that this is the main N species that requires consideration in manure treatment, especially for separation with RO as the majority of the organic N is removed during the pre-treatment steps.

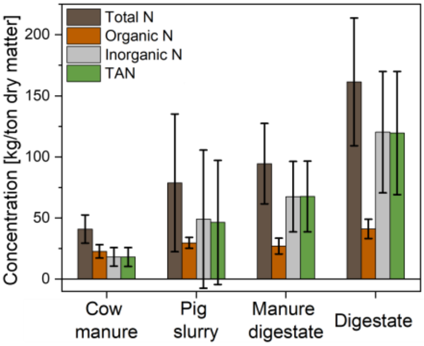

Fig. 6.6: Concentration [kg/ton dry matter] of the total N (taupe), the fractions of this being organic (brown) and inorganic (grey) and of TAN (green) being a fraction of the inorganic N given for cow manure, pig slurry, manure digestate (co-digested with as majority manure) and digestate (with as majority organic matter) as studied by Risberg et al. [34].

As mentioned before, during digestion or even storage, the organic N can be converted into inorganic N. For example, urea, a N containing species found in urine, is hydrolyzed into TAN during storage, catalyzed by the enzyme urease as shown in Scheme 6.2 [32].

$$NH_2(CO)NH_2 + H_2O \xrightarrow{Urease} NH_3 + NH_4^+ + HCO_3^- \qquad \text{Scheme 6.2}$$

Furthermore, urea is typically permeating RO membranes indicating most N from this organic component is pushed towards the N-rich permeate during N and K separation with RO [35].

Other inorganic N that might be present are nitrite and nitrate ions. These ions are typically charged indicating that these ions are retained by the membrane. The presence of these ions can therefore decrease the N and K separation with RO. Hence, further investigation regarding the concentration of these ions in digestate can provide an indication of their impact on the separation of N and K. For example, additional rejection measurements with RO for these N containing species in manure digestate can show if the produced streams have increased N concentrations effecting their value in terms of fertilization potential and for the clean water stream if discharge to the surface water is allowed.

6.3.2.3 Alternative membrane improvements

The stability of thin film composite polyamide RO membranes is a reportedly addressed issue. Studies have shown that incorporation of additives, e.g. graphene oxide, can improve the alkaline stability of nanofiltration membranes [36]. Another benefit of the addition of graphene oxide is that it can increase the permeability of the membrane while a high retention is maintained [37]. This can further improve the separation of N and K as more N-rich permeate is produced. In addition, the permeability of NH_3 might increase due to the hydrophilic pathway. Further investigation regarding improved transport of TAN with additives can lead to superior separation with or without pH tuning. Moreover, research on the formation of a selective layer on top of a porous support with epoxides and biobased polymer chitosan shows excellent alkaline stability [38], [39]. An increased chemical stability of the membrane results in an elongated lifetime in alkaline conditions. Moreover, in that case the separation of nutrients could be achieved at higher alkalinity like for example pH 12 where 100% of the TAN is present as NH_3, in comparison to the currently advised pH 10 where 85% TAN is converted to NH_3. However, this increase in pH requires more OH^- and in a subsequent RO step more acidification is necessary which together will increase the amount of chemicals required which has to be considered to determine the benefit of more N/K separation at pH 12.

Next to the aforementioned alternative membrane modifications, the modification as addressed in this dissertation, with crosslinked polyelectrolyte layers, can be further improved. As the separation of N and K is enhanced at alkaline conditions, the use of strong polyelectrolytes, that remain fully charged regardless of the pH, is recommended. Moreover, the crosslinking of the polyelectrolyte layers improves the separation of N and K. Hence, the presence of a functional group suitable for crosslinking is beneficial. Therefore, improved performance can be achieved by the synthesis of a polyelectrolyte with a strong charged group and a functional group suitable for crosslinking, for example, a combination of a quaternary ammonium group for the charge and an amine group suitable for crosslinking with glutaraldehyde.

6.3.3 Alternative technology for acidification

Typically, organic fertilizers have a high concentration of NH_4^+ and at alkaline conditions this results in emission of NH_3, for example after application on land. Hence, the pH of N fertilizers is often kept around a pH of 5 to limit the NH_3 emission. In many processes the ammonium stream is acidified with sulfuric acid (H_2SO_4) or nitric acid (HNO_3) to reach this pH. While H_2SO_4 is relatively cheap (0.004 €/mol H^+), HNO_3 (0.025 €/mol H^+ or N) has the benefit that it increases the fertilization capacity as its addition leads to an increased N concentration [40], [41]. However, next to the higher costs, HNO_3 is typically produced via the Haber-Bosch nitrogen fixation (Scheme 6.3) followed by the Ostwald process (Scheme 6.4, Scheme 6.5 and Scheme 6.6). This widely applied process is responsible for approximately 1% of the world's energy consumption and results in 1% of the world's CO_2 emission [42].

$$N_2 + 3H_2 \rightarrow 2NH_3 \qquad \textit{Scheme 6.3}$$

$$4NH_3 + 5O_2 \rightarrow 4NO + 6H_2O \qquad \textit{Scheme 6.4}$$

$$2NO + O_2 \rightarrow 2NO_2 \qquad \textit{Scheme 6.5}$$

$$3NO_2 + H_2O \rightarrow 2HNO_3 + NO \qquad \textit{Scheme 6.6}$$

Hence, plasma is an upcoming alternative method to fabricate N fertilizer in the form of ammonium nitrate on-site via nitrogen fixation. The gaseous plasma initiates nitrogen oxidation by a reaction between N_2 and O_2 from the air resulting in nitrogen oxide products (NO and NO_2) via radical intermediates. The produced NO_2 can react with water molecules forming HNO_3 [42], [43].

Plasma treatment can thus also be used for organic waste streams like digestate, leading to its acidification due to the formation of HNO_3. Hence, this method can be used to limit NH_3 emissions from digestate, mineral concentrates and N-rich permeate streams. Manaigo et al. indicates that the energy required for nitrogen fixation at experimental scale lays around 2 MJ/mol N for low yields of around 5% [42]. This leads to a price of 0.08 €/mol N considering an energy price of 0.15 €/kWh for non-household consumers [8]. Hence, plasma induced nitrogen fixation shows potential to replace industrial HNO_3 produced with the Haber-Bosch system/Ostwald process. Moreover, plasma treatment can be installed on-site, reducing transportation costs and storage of chemicals. In addition, the system can use renewable energy. Nevertheless, the explosive nature of ammonium nitrate results in risks that have to be taken into account during production, storage and application.

6.4 References

[1] D. Bolzonella, F. Fatone, M. Gottardo, and N. Frison, “Nutrients recovery from anaerobic digestate of agro-waste: Techno-economic assessment of full scale applications,” *J. Environ. Manage.*, vol. 216, pp. 111–119, 2018, doi: 10.1016/j.jenvman.2017.08.026.

[2] A. Zarebska, D. Romero Nieto, K.V. Christensen, L. Fjerbæk Søtoft, and B. Norddahl, “Ammonium fertilizers production from manure: A critical review,” *Crit. Rev. Environ. Sci. Technol.*, vol. 45, no. 14, pp. 1469–1521, 2015, doi: 10.1080/10643389.2014.955630.

[3] LG Chem, “Data sheet: Brackish water Reverse Osmosis (RO) Membranes LG BW 400 R G2,” 2007. https://www.lenntech.com/Data-sheets/LG-Chem-LG-BW-400-R-G2-L.pdf.

[4] European Commission, *Annex to the comission directive amending council directive 91/676/EEC as regards the use of certain fertilising materials from livestock manure*. 2024.

[5] R. Vingerhoets, M. Spiller, O. Schoumans, S.E. Vlaeminck, J. Buysse, and E. Meers, “Economic potential for nutrient recovery from manure in the European union,” *Resour. Conserv. Recycl.*, vol. 215, 2024, p. 108079, 2025, doi: 10.1016/j.resconrec.2024.108079.

[6] C. Vaneeckhaute, V. Lebuf, E. Michels, E. Belia, P.A. Vanrolleghem, F.M.G. Tack and E. Meers, “Nutrient Recovery from Digestate: Systematic Technology Review and Product Classification,” *Waste and biomass valorization*, pp. 21–40, 2017, doi: 10.1007/s12649-016-9642-x.

[7] J. de Vrieze, G. Colica, C. Pintucci, J. Sarli, C. Pedizzi, G. Willeghems, A. Bral, S. Varga, D. Prat, L. Peng, M. Spiller, J. Buysse, J. Colsen, O. Benito, M. Carballa and S.E. Vlaeminck, “Resource recovery from pig manure via an integrated approach : A technical and economic assessment for full-scale applications,” *Bioresour. Technol.*, vol. 272, pp. 582–593, 2019, doi: 10.1016/j.biortech.2018.10.024.

[8] Eurostat, “Prices of electricity for non-household consumers in the Netherlands from 2008-2022,” 2024. https://www.statista.com/statistics/596254/electricity-non-household-

price-netherlands/, Accessed November 2024.

[9] R. Pärnamäe, L. Gurreri, J. Post, W.J. van Egmond, A. Culcasi, M. Saakes, J. Chen, E. Goosen, A. Tamburini, D.A. Vermaas and M. Tedesco, “The acid–base flow battery: Sustainable energy storage via reversible water dissociation with bipolar membranes,” *Membranes*, vol. 10, no. 12, pp. 1–20, 2020, doi: 10.3390/membranes10120409.

[10] P. Hoeksma and F.E. de Buisonjé, “Production of mineral concentrates from animal manure using reverse osmosis,” 2015. [Online]. Available: https://edepot.wur.nl/364053.

[11] O.F. Schoumans, W.H. Rulkens, O. Oenema, and P.A.I. Ehlert, “Phosphorus recovery from animal manure; Technical opportunities and agro-economical perspectives,” 2010, [Online]. Available: https://edepot.wur.nl/163684.

[12] C. Wei, S. Laborie, R. Ben, and G. Amy, “Full utilization of silt density index (SDI) measurements for seawater,” *J. Memb. Sci.*, vol. 405–406, pp. 212–218, 2012, doi: 10.1016/j.memsci.2012.03.010.

[13] R.W. Baker, *MEMBRANE TECHNOLOGY*, 2th ed. John Wiley & Sons, Ltd., 2004.

[14] LG Chem, “Data sheet: Seawater Reverse Osmosis (RO) memranes LG SW 400 R G2,” 2006. https://www.lenntech.com/Data-sheets/LG-Chem-LG-SW-400-R-G2-L.pdf.

[15] H.N.P. Dayarathne, M.J. Angove, R. Aryal, H. Abuel-Naga, and B. Mainali, “Removal of natural organic matter from source water: Review on coagulants, dual coagulation, alternative coagulants, and mechanisms,” *J. Water Process Eng.*, vol. 40, 2020, p. 101820, 2021, doi: 10.1016/j.jwpe.2020.101820.

[16] F. Renault, B. Sancey, P. M. Badot, and G. Crini, “Chitosan for coagulation/flocculation processes - An eco-friendly approach,” *Eur. Polym. J.*, vol. 45, no. 5, pp. 1337–1348, 2009, doi: 10.1016/j.eurpolymj.2008.12.027.

[17] Q. Wei, F. O. Mcyotto, C. W. K. Chow, Z. Nadeem, Z. Li, and J. Liu, “Eco-friendly decolorization of cationic dyes by coagulation using

natural coagulant Bentonite and biodegradable flocculant Sodium Alginate,” *SDRP J. Earth Sci. Environ. Stud.*, vol. 5, no. 2, pp. 51–60, 2020, doi: 10.25177/jeses.5.2.ra.10648.

[18] D. Sableviciene, R. Klimaviciute, J. Bendoraitiene, and A. Zemaitaitis, “Flocculation properties of high-substituted cationic starches,” *Colloids Surfaces A Physicochem. Eng. Asp.*, vol. 259, no. 1–3, pp. 23–30, 2005, doi: 10.1016/j.colsurfa.2005.02.004.

[19] T.T. More, J.S.S. Yadav, S. Yan, R.D. Tyagi, and R.Y. Surampalli, “Extracellular polymeric substances of bacteria and their potential environmental applications,” *J. Environ. Manage.*, vol. 144, pp. 1–25, 2014, doi: 10.1016/j.jenvman.2014.05.010.

[20] R.P. Singh, S. Pal, and S.A. Ali, “Novel biodegradable polymeric flocculants based on cationic polysaccharides,” *Adv. Mater. Lett.*, vol. 5, no. 1, pp. 24–30, 2014, doi: 10.5185/amlett.2013.6498.

[21] A. Chuda and K. Ziemiński, “Digestate mechanical separation in industrial conditions: Efficiency profiles and fertilising potential,” *Waste Manag.*, vol. 128, pp. 167–178, 2021, doi: 10.1016/j.wasman.2021.04.049.

[22] M.C. Garcia, A.A. Szogi, M.B. Vanotti, J.P. Chastain and P.D. Millner, “Enhanced solid-liquid separation of dairy manure with natural flocculants,” *Bioresour. Technol.*, vol. 100, no. 22, pp. 5417–5423, 2009, doi: 10.1016/j.biortech.2008.11.012.

[23] M. Hjorth, M.L. Christensen, and P.V. Christensen, “Flocculation, coagulation, and precipitation of manure affecting three separation techniques,” *Bioresour. Technol.*, vol. 99, no. 18, pp. 8598–8604, 2008, doi: 10.1016/j.biortech.2008.04.009.

[24] L. Masse and D.I. Massé, “The effect of environmental and process parameters on flocculation treatment of high dry matter swine manure with polymers,” *Bioresour. Technol.*, vol. 101, no. 16, pp. 6304–6308, 2010, doi: 10.1016/j.biortech.2010.03.037.

[25] S. Heviánková, R. Souček, M. Kyncl, and N. Surovcová, “Contribution To The Study Of Flocculation Of Digestate,” *Geosci. Eng.*, vol. 61, no. 3, pp. 37–44, 2018, doi: 10.1515/gse-2015-0021.

[26] O. Popovic and F. Gioelli, “Centrifugation of Digestate : The Effect of Chitosan on Separation Efficiency,” pp. 1–9, 2017, doi: 10.3390/su9122302.

[27] L. Wang, M. Addy, J. Liu, C. Nekich, R. Zhang, P. Peng, Y. Cheng, K. Cobbm Y. Liu, H. Wang and R. Ruan, “Integrated process for anaerobically digested swine manure treatment,” *Bioresour. Technol.*, vol. 273, no. November 2018, pp. 506–514, 2019, doi: 10.1016/j.biortech.2018.11.050.

[28] H. Lin, J. Gan, A. Rajendran, C.E. Rodrigues Reis and B. Hu, “Phosphorus removal and recovery from digestate after biogas production,” in *Biofuels, status and perspective*, 2015, pp. 517–546.

[29] H. Luo, T. Lyu, A. Muhmood, Y. Xue, H. Wu, E. Meers, R. Dong and S. Wu, “Effect of flocculation pre-treatment on membrane nutrient recovery of digested chicken slurry: Mitigating suspended solids and retaining nutrients,” *Chem. Eng. J.*, vol. 352, no. July, pp. 855–862, 2018, doi: 10.1016/j.cej.2018.07.097.

[30] P.H. Hsu, “Comparison of iron(III) and aluminum in precipitation of phosphate from solution,” *Water Res.*, vol. 10, no. 10, pp. 903–907, 1976, doi: 10.1016/0043-1354(76)90026-9.

[31] D.C. Harris, *Quantitive chemical analysis*. New York: W. H. Freeman & Company, 2016.

[32] L. Masse, D.I. Massé, and Y. Pellerin, “The use of membranes for the treatment of manure: a critical literature review,” *Biosyst. Eng.*, vol. 98, no. 4, pp. 371–380, 2007, doi: 10.1016/j.biosystemseng.2007.09.003.

[33] K. Emerson, R.C. Russo, R.E. Lund, and R.V. Thurston, “Aqueous Ammonia Equilibrium Calculations : Effect of pH and Temperature,” *J. Fish. Res.*, pp. 2379–2383, 1975.

[34] K. Risberg, H. Cederlund, M. Pell, V. Arthurson, and A. Schnürer, “Comparative characterization of digestate versus pig slurry and cow manure – Chemical composition and effects on soil microbial activity,” *Waste Manag.*, vol. 61, pp. 529–538, 2017, doi: 10.1016/j.wasman.2016.12.016.

[35] L. Crane, H. Ray, F. Perreault, and T.H. Boyer, “Recovery of Urea from Human Urine Using Nanofiltration and Reverse Osmosis,” *ACS ES&T Water*, 2023, doi: 10.1021/acsestwater.2c00336.

[36] Q. Xie, S. Zhang, Z. Xiao, X. Hu, Z. Hong, R. Yi, W. Shao and Q. Wang, “Preparation and characterization of novel alkali-resistant nano fi ltration membranes with enhanced permeation and antifouling properties: the effects of functionalized graphene nanosheets,” *RSC Adv.*, pp. 18755–18764, 2017, doi: 10.1039/c7ra00928c.

[37] M.E.A. Ali, L. Wang, X. Wang, and X. Feng, “Thin film composite membranes embedded with graphene oxide for water desalination,” *DES*, vol. 386, pp. 67–76, 2016, doi: 10.1016/j.desal.2016.02.034.

[38] R. Verbeke, D.M. Davenport, T. Stassin, S. Eyley, M. Dickmann, A.J. Cruz, P. Dara, C.L. Ritt, C. Bogaerts. W. Egger, R. Ameloot, J. Meersschaut, W. Tielemans, G. Koeckelberghs, M. Elimelech and I.F.J. Vankelecom, “Chlorine-Resistant Epoxide-Based Membranes for Sustainable Water Desalination,” *Environ. Sci. Technol. Lett.*, vol. 8, pp. 818-824, 2021, doi: 10.1021/acs.estlett.1c00515.

[39] T. Yang and R.R. Zall, “Chitosan Membranes for Reverse Osmosis Application,” *Journal of food science*, vol. 49, pp. 91–93, 1984.

[40] Chemanalyst, “Sulphuric acid price trend and forecast,” 2024. https://www.chemanalyst.com/Pricing-data/sulphuric-acid-70, Accessed November 2024.

[41] Chemanalyst, “Nitric acid price trend and forecast,” 2024. https://www.chemanalyst.com/Pricing-data/nitric-acid-1142, Accessed November 2024.

[42] F. Manaigo, K. Rouwenhorst, A. Bogaerts, and R. Snyders, “Feasibility study of a small-scale fertilizer production facility based on plasma nitrogen fixation,” *Energy Convers. Manag.*, vol. 302, no. January, p. 118124, 2024, doi: 10.1016/j.enconman.2024.118124.

[43] D.B. Graves, L.B. Bakken, M.B. Jensen, and R. Ingels, “Plasma Activated Organic Fertilizer,” *Plasma Chem. Plasma Process.*, vol. 39, no. 1, pp. 1–19, 2019, doi: 10.1007/s11090-018-9944-9.

Acknowledgements

Every journey starts somewhere, mine started all the way in the north of the Netherlands with the support of my family and friends. Heit, mem, Dytmer en Sywert tige tank foar jimme support foar en tiidens dit aventoer sûnder jimme hie ik dizze kâns net pakt.

The journey itself was challenging in many aspects. Thanks to the guidance of Kitty and Zandrie I was able to manage on scientific and personal fronts. Thank you both for your confidence in me from start to finish and for your guidance along the way.

Finalizing a PhD is not possible without a committee to asses the dissertation. Prof.dr.ir Erik Meers, prof.dr.ir. Cees Buisman, prof.dr.ir Remco Tuinier and prof.dr.ir John van der Schaaf thank you kindly for accepting the invitation to join the committee and for assessing my work. Also, a special thanks to ir. Richard van Lijssel for the many insightful discussions during my PhD and for your advising role in the committee. Thank you prof.dr. Albert Schenning for chairing my defense ceremony.

De earste nacht fan dit aventoer begûn ek hoe it einiget, samen mei Anna en Boukje op e strún yn it suden. Tige tank foar jimme steun foar, tiidens en oan it ein fan dizze bysûndere ûnderfining. Natuurlik hat de rest fan de keet hjir ek een bydrage oan, elts momint fan ûntspanning en even thús wêze hat holpen.

The PhD journey started of course as a first year who thinks to have an idea about what doing a PhD is but is proven wrong very quickly by the “older generation”. The lovely thing is that they can teach you a lot; in the lab, about life and literally about teaching itself. Anna, Menno, Daniëlle and Maxime thank you for your patience, guidance and all the amazing moments amongst the struggles.

Later on, I found myself in the most amazing office together with Nadia and Woutje, all three of us being at a similar stage and having our own challenges. Thank you both for all the conversations, help and horseback riding along the way. Together the PhD and travel journeys were amazing.

Of course, there were more colleagues which have proven to be amazing both scientifically and outside of work during for example creative sessions. Jadwiga and Aylin, thank you for your support and collaboration throughout the years and I wish you all the best for your own journeys.

At the end of my PhD the roles were reversed and I was able to assist the new candidates. However, also new colleagues can tremendously contribute to your work with their fresh spirit and knowledge. Rebecca thank you for suffering with me on the lab to finalize this thesis with a nice electrochemistry chapter.

There are some colleagues that somehow stay by your side even though their PhD journeys are finished or appear as new friends in time. Remy (and Maria), Emre and Moji (and Marz), thank you for all your advice, help and get to togethers in times of need.

Naturally, thank you to the fellow membrane researchers that have supported me until the very end. Alex, Tao, Sarthak, Thijs, Leong, Cas and Liang-Shin thank you very much for the nice time. Also, a special thanks to the not so membrane researchers from EMS whom I have worked closely with throughout the years, your kindness, knowledge and enthusiasm is much appreciated. Also not to forget, the always supportive technicians Cees, Renate, Jeroen and Niek, thank you for all your help in the past years.

Most important of all, Adrian, thank you for finding me during this special journey. I cherish all the time for sport, extra working hours on the weekend and just time on the couch you have devoted to making sure that each day ended in a joyful manner. Your love and support have been an essential part of my time in the south. Even though I don’t always say it, you are my home wherever we are. I am looking forward to all the time to come after this journey comes to an end.

About the author

Marrit van der Wal was born on July 21st 1998 in Workum the Netherlands. She obtained her bachelor's degree in chemistry at University of Applied Science Van Hall Larenstein in Leeuwarden in 2019. Afterwards, she continued her studies with the master degree Water Technology from Wageningen University and Research, University of Twente and University of Groningen (joint degree) at the Wetsus academy in Leeuwarden. In 2021 she graduated on the fabrication of electrospun bipolar membranes. In the same year she started a PhD project in the research group Membrane Materials and Processes at Eindhoven University of Technology in the Netherlands of which the results are presented in this dissertation.

List of publications

Publications related to this dissertation:

M. van der Wal, J. van Alphen, K. Nijmeijer, Z. Borneman, Dynamic ammonium retention for nutrients separation from manure, *Waste management,* 190, **2024**

M. van der Wal, Z. Borneman, K. Nijmeijer, Optimizing flocculation of digestate to increase circularity in manure treatment, *Bioresource Technology Reports,* 23, **2023**

In preparation:

M. van der Wal, A. Kinik, M. van Maris, Z. Borneman, K. Nijmeijer, Membrane modification for nutrient separation in manure treatment, **2025**

M. van der Wal, R. Rovai, K. Nijmeijer, Z. Borneman, Bipolar membrane electrodialysis enhanced nutrient separation in manure treatment, **2025**

Other publications:

G. J. Doornbusch, M. van der Wal, M. Tedesco, J. W. Post, K. Nijmeijer, Z. Borneman, Multistage electrodialysis for desalination of natural seawater, *Desalination*, 505, **2021**

In preparation:

A. Kinik, M. van der Wal, K. Nijmeijer, Z. Borneman, Enhanced forward osmosis performance with Pluronic® as a draw solution: unraveling the role of interactions between layer-by-layer membranes and Pluronic®, **2025**

List of conference abstracts:

Conference and symposium oral presentations:

M. van der Wal, Z. Borneman, K. Nijmeijer, Tijd voor mest valorisatie (Time for manure valorization), Invited oral presentation at symposium Mest het Bruine Goud (Manure the Brown Gold), Den Bosch, the Netherlands, 2024

M. van der Wal, No time to waste manure, Pitch presentation at Talking Science event Eindhoven University of Technology, Eindhoven, the Netherlands, 2024

M. van der Wal, Z. Borneman, K. Nijmeijer, Dynamic ammonium retention for nutrient separation from manure digestate, Oral presentation at North American Membrane Society conference, Santa Fe, New Mexico, United States, 2024

M. van der Wal, Z. Borneman, K. Nijmeijer, Dynamic ammonia retention for nutrient separation, Oral presentation at the 6th ManuREsource conference, Antwerp, Belgium, 2024

M. van der Wal, Z. Borneman, K. Nijmeijer, Dynamic ammonia retention for nutrient separation, Oral presentation at the 18th Netherlands Process technology Symposium (NPS2023), Enschede, the Netherlands, 2023

Conference and symposium poster presentations:

M. van der Wal, Z. Borneman, K. Nijmeijer, Dynamic ammonium retention for nutrient separation from manure digestate, Poster presentation at the Nederlands Membraan Genootschap (NMG) (Dutch Membrane Society) poster day, Veldhoven, the Netherlands, 2024

M. van der Wal, Z. Borneman, K. Nijmeijer, Dynamic ammonium retention for nutrient separation from manure digestate, Poster presentation at North American Membrane Society conference, Santa Fe, New Mexico, United States, 2024

M. van der Wal, Z. Borneman, K. Nijmeijer, Optimizing flocculation to increase nutrient recovery from manure, Poster presentation at EuroMembrane 2022 to celebrate 40th EMS Anniversary, Sorrento, Italy, 2022

M. van der Wal, Z. Borneman, K. Nijmeijer, Optimizing the flocculation of digestate to increase circularity in the nutrient recovery from manure, Poster presentation at the 17th Netherlands Process technology Symposium (NPS17), Delft, the Netherlands, 20

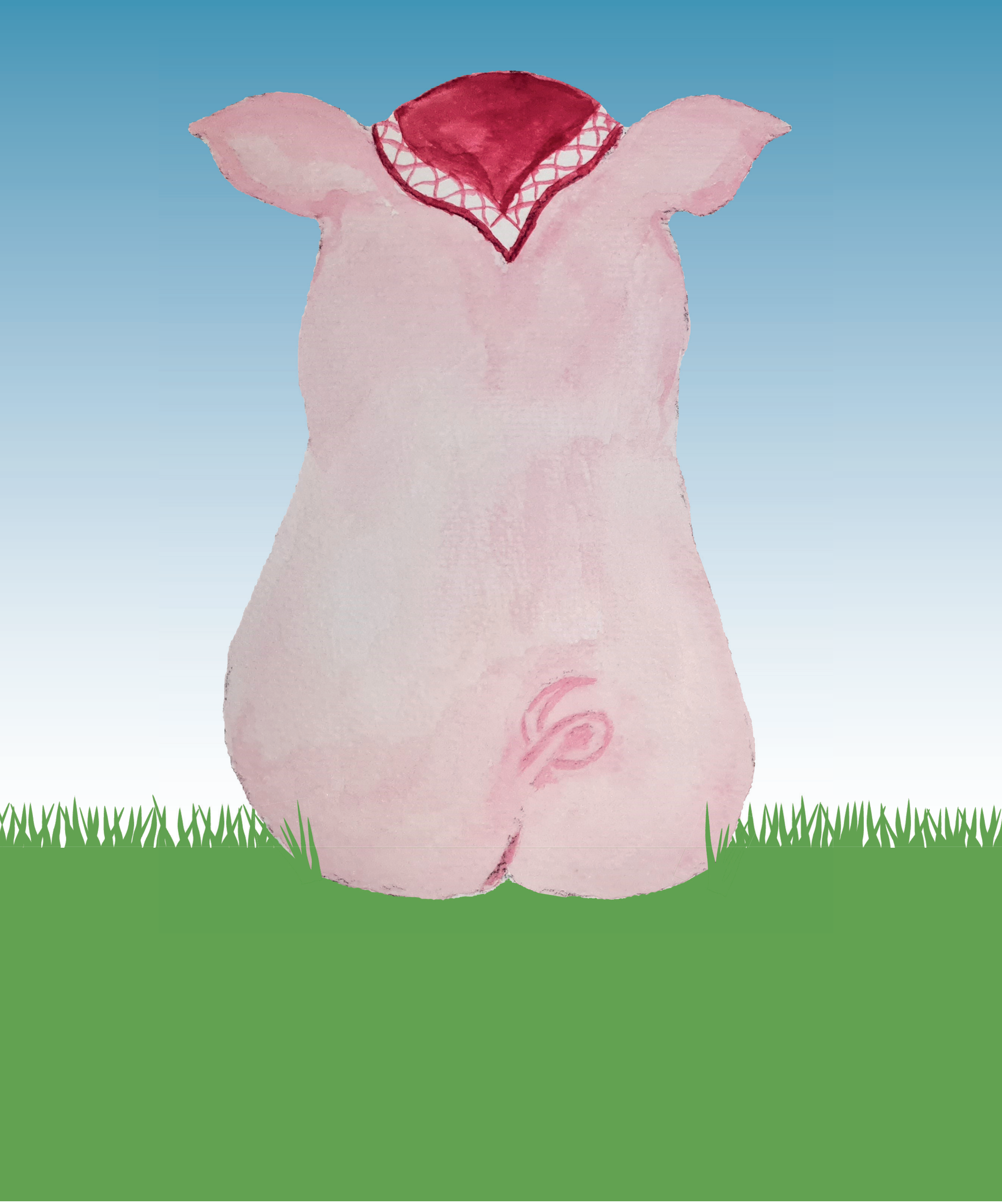

EINDHOVEN
UNIVERSITY OF
TECHNOLOGY